UNIVERSIDADE FEDERAL
DO RIO DE JANEIRO

MODELAGEM DA CIRCULAÇÃO EM EVENTOS SUBINERCIAIS NA BAÍA DE GUANABARA - RJ

Ivenis Italo Capistrano Pita

Dissertação de Mestrado apresentada ao Programa de Pós-graduação em Meteorologia do Instituto de Geociências do Centro de Ciências Matemáticas e da Natureza da Universidade Federal do Rio de Janeiro (PPGM-IGEO-CCMN-UFRJ), como parte dos requisitos necessários à obtenção do título de Mestre em Ciências (área: Meteorologia).

Orientadores: Mauro Cirano
Afonso de Moraes Paiva

Rio de Janeiro
Dezembro de 2019

MODELAGEM DA CIRCULAÇÃO EM EVENTOS SUBINERCIAIS NA BAÍA
DE GUANABARA - RJ

Ivenis Italo Capistrano Pita

DISSERTAÇÃO SUBMETIDA AO CORPO DOCENTE DO INSTITUTO DE
GEOCIÊNCIAS (IGEO) DA UNIVERSIDADE FEDERAL DO RIO DE JANEIRO
COMO PARTE DOS REQUISITOS NECESSÁRIOS PARA A OBTENÇÃO DO
GRAU DE MESTRE EM METEOROLOGIA.

Examinada por:

_____
Prof. Mauro Cirano, Ph.D.

_____
Prof. Afonso de Moraes Paiva, Ph.D.

_____
Prof. Luiz Paulo de Freitas Assad, D.Sc.

_____
Prof. Alexandre Macedo Fernandes, Ph.D.

_____
Prof. Marcos Nicolás Gallo, D.Sc.

RIO DE JANEIRO, RJ – BRASIL
DEZEMBRO DE 2019

Dedico esta dissertação a qualquer pessoa que algum dia pensou que não conseguiria fazer algo. Insista, seja humilde para reconhecer seus erros e corajoso para se erguer e tentar novamente.

Agradecimentos

Agradeço imensamente a todo o suporte que os professores e os alunos do Mestrado em Meteorologia me deram durante esses anos. Foram anos que com toda a certeza vou levar para a vida. Aprendi muito durante esse período e cresci como pessoa e como profissional. Devo um agradecimento em especial a todos os alunos do LOF e do LASA. Compartilhamos muitos cafés (mesmo não bebendo), muitas risadas e muitas sessões de terapia. Agradeço ao meu orientador, Mauro Cirano, por ser muito mais que um orientador, por ser meu amigo e sempre confiar em mim, me motivando e me mostrando que sou capaz. Nossa parceria começou em 2013 e tenho certeza que vai durar muito tempo! Agradeço ao meu co-orientador, Afonso Paiva, por todos os conselhos, todas as críticas construtivas que me engrandeceram como pesquisador e por me incentivar a sempre melhorar como pesquisador.

Agradeço à minha família carioca, que me deu casa, comida e carinho durante o meu mestrado. Seu Alípio e Dona Eloísa, vocês são bem mais que sogro e sogra. Os considero como pai e mãe. Obrigado por tudo!

Agradeço à minha família alagoana, esses sim, de sangue. Vocês sempre me inspiram e me fazer buscar o aperfeiçoamento profissional. Mesmo que isso signifique me distanciar um pouco mais de Alagoas. Pai, mãe, Nani e Vi, levo vocês no coração em todos os lugares que ando, em tudo o que eu faço e em tudo o que penso. Amo vocês.

E por fim, um agradecimento mais que especial e merecido à minha companheira da vida, aquela que me mostrou a minha essência, o meu verdadeiro eu. Te amo muito, Érika. Com você do meu lado, eu sempre quero me superar como pessoa, pois só assim, um dia estarei à sua altura. Você é uma pessoa iluminada e me orgulho muito de te ter ao meu lado em todo amanhecer. Te amo de amor e de paixão!

MODELAGEM DA CIRCULAÇÃO EM EVENTOS SUBINERCIAIS NA BAÍA DE GUANABARA - RJ

Ivenis Italo Capistrano Pita

Dezembro/2019

Orientadores: Mauro Cirano
            Afonso de Moraes Paiva

Programa: Meteorologia

Vários estudos foram elaborados com foco em processos subinerciais na plataforma continental adjacente à Baia de Guanabara (BG), onde evidenciam a importância do vento local, vento remoto e Corrente do Brasil na circulação da plataforma continental adjacente à BG. Esta dissertação tem como objetivo identificar os mecanismos reguladores das variações subinerciais da BG. Para este estudo, foram realizados 3 experimentos 2D com o modelo DELFT3D, com várias configurações em relação à forçantes atmosférica e hidrodinâmica. Além disso, análises independentes de conjuntos de dados (nível do mar, correntes médias ao longo da coluna d'água, transporte de volume da Corrente do Brasil, vento local, vento remoto e ocorrência de frentes frias) foram realizadas para subsidiar a identificação dos principais mecanismos forçantes da banda subinercial da BG. A propagação de Ondas Confinadas Costeiras (OCC) na plataforma continental adjacente à BG causa uma variação média observada de 27,8 $\pm$ 11,2 cm nas estações dentro da BG, com um período médio de 6,8 $\pm$ 2,8 dias. Além disso, OCC foram responsáveis por variações de até 67,3 cm na estação da Ilha Fiscal (IFI) em eventos isolados. Em termos de transporte de volume da Corrente do Brasil, foi encontrada uma maior correlação com o nível subinercial da BG para períodos maiores que 60 dias (corr de 0,31) se comparada à banda subinercial (corr de 0,21). Além disso, as OCCs forçadas por vento remoto e a Corrente do Brasil são os principais mecanismos reguladores da variação do nível subinercial da BG. O vento local desempenha um papel secundário na condução de movimentos subinerciais na BG. O transporte de volume

na entrada da baia calculado atraves das 3 simulações realizadas representaram entre 6,1 e 10,8%, entre 6,1 e 10,8%, e entre 6,9 e 12,2%, respectivamente, o valor do transporte resultante ao longo de um ciclo de maré.

Abstract of Dissertation presented to IGEO/UFRJ as a partial fulfillment of the requirements for the degree of Master of Science (M.Sc.)

MODELING OF THE CIRCULATION IN SUBINERTIAL EVENTS AT
GUANABARA BAY - RJ

Ivenis Italo Capistrano Pita

December/2019

Advisors: Mauro Cirano
            Afonso de Moraes Paiva

Department: Meteorology

Various studies focused on subinertial processes in South Brazil Bight (SBB), showing the importance of local wind, remote wind, and Brazil Current (BC). This manuscript aims to identify the main forcing mechanisms of subinertial variability in Guanabara Bay (GB). Three depth-averaged experiments were performed using DELFT3D, with different atmospheric and hydrodynamic forcings. In addition, independent dataset (sea level, depth-averaged current, BC volume transport, local and remote wind, and cold front occurrence) analysis were performed to support the identification of the main forcing mechanisms of GB subinertial sea level and depth-averaged velocity. The propagation of Coastal Trapped Waves (CTW) along SBB caused sea level to vary by 27.8 $\pm$ 11.2 cm with periods of 6.8 $\pm$ 2.8 days inside GB. Furthermore, CTWs were responsible, in isolated events, for up to 67.3 cm level variation in Ilha Fiscal (IFI) station. The correlation between the BC volume transport and the subinertial level in GB was higher for periods greater than 60 days (0.31) if compared to the subinertial band (0.22). Hence, remote wind forced CTWs and the BC are the most important forcing mechanisms of subinertial sea-level variability in GB. Finally, local wind plays a secondary role in driving subinertial motions in GB. The volume transport at the bay entrance obtained in the three simulations were between 6.1 and 10.8%, 6.1 and 10.8%, and 6.9 and 12.2%, respectively, of the net volume transport over a tidal cycle.

Contents

List of Figures

List of Tables

Acronyms

ACS Adjacent Continental Shelf. 2, 9, 10, 18, 50

ADCP Acoustic Doppler Current Profiler. 14

BC Brazil Current. 1, 3, 5, 9, 23, 30–32, 60–62

CFSR Climate Forecast System Reanalysis. 14, 16, 19, 20, 40, 44, 50

CTW Coastal Trapped Wave. 1, 5–7, 9, 15, 21, 23, 24, 26, 31, 43, 44, 50, 55, 60–62

GB Guabanara Bay. 1–5, 7, 9–11, 13–16, 19–21, 23, 26–28, 31–33, 36, 41, 43–45, 50, 55, 60–62

GLOSS Global Sea Level Observing System. 13

HYCOM Hybrid Coordinate Ocean Model. 19

IBI Ilha do Boqueirão. 12, 13, 16, 32

IFI Ilha Fiscal. 12, 13, 15, 16, 20, 27, 32–34, 55, 60, 61

METAR Meteorological Aerodrome Reports. 14, 20

NCEP National Centers for Environmental Prediction. 14

PAR Ponta da Armação. 13, 16

REMO Portuguese acronym for Brazilian Oceanographic Modeling and Observation Network. 19, 20, 33, 43, 61, 62

RS Rio Grande do Sul. 14, 15, 23, 24, 26, 31, 44, 50, 55

SACW South Atlantic Central Water. 3, 7, 10, 14

SBB South Brazil Bight. 1, 2, 6–8, 41, 61, 62

SiMCosta Portuguese acronym Brazilian Coast Monitoring System. 14

SSH Sea Surface Height. 19, 20

WBC Western Boundary Current. 8, 23, 30, 60, 61

Chapter 1

Introduction

The South Brazil Bight (SBB) is an important geomorphological feature of the Brazilian continental shelf. It is located between two capes (Cabo Frio at 23°S and Cabo de Santa Marta at 28.6°S). The SBB has a moon shape and an alongshore extension of 1000 km. In the central part, the continental shelf widens up to 200 km, but close to the two capes it narrows down to 50-60 km (CASTRO and LEE, 1995; DOTTORI and CASTRO, 2018). Tides, local and remote winds, baroclinic pressure gradients, and the Brazil Current (BC) can be identified as the main factors influencing the circulation in the SBB (CASTRO *et al.*, 2006). The inner shelf is sometimes influenced by baroclinic pressure gradients due to buoyancy advection from coastal freshwater inputs. Cold waters from south can penetrate into SBB during cold front events (STEVENSON *et al.*, 1998). This intrusion is restricted to the southern portion of SBB. During winter, however, wind anomalies are sufficiently strong to force relatively cold waters to flow close to Guabanara Bay (GB) (PIOLA *et al.*, 2000; PIOLA *et al.*, 2005).

Wind forcing, relative to the variability of the South Atlantic Subtropical High and atmospheric frontal systems play a major role in the evolution of subinertial dynamics in SBB (VALENTIM *et al.*, 2013). DE FREITAS *et al.* (2019) claimed that the vertical shear induced by near inertial oscillations are comparable to that generated by hurricanes and large storms. Furthermore, analyses of direct current measurements have shown the wind stress to be the main forcing mechanism of subinertial variability in coastal regions and middle shelf of upper SBB (CASTRO, 1990; STECH and LORENZZETI, 1992; CASTRO and MIRANDA, 1998; DOTTORI and CASTRO, 2009). However, part of this variability is not explained by local wind activity. This suggests that remote wind and Coastal Trapped Wave (CTW) may play an important role in SBB subinertial variability.

Around the globe, several studies have focused on the influence of subinertial processes in coastal bays and estuaries, and their water exchange with coastal regions (e.g., VALLE-LEVINSON, 1995; CIRANO and LESSA, 2007; MUSCARELLA *et al.*, 2011; SANKARANARAyANAN and FRINGER, 2013; AGUIAR *et al.*, 2019). VALLE-LEVINSON (1995) conducted a research regarding the description of subinertial processes at Chesapeake Bay – USA. Wind was attributed as the main forcing

for low-frequency changes in sea level at the lower bay. However, bottom stress and barometric pressure played a slight influence on subinertial sea level variability during summer months. SANKARANARAYANAN and FRINGER (2013) found local wind induced subinertial oscillations more efficiently than remote wind in San Francisco Bay. MUSCARELLA et $al.$ (2011) found persistent low-frequency currents flowing across the southern Delaware Bay mouth (up to 25 m s^{-1}), however, not sufficiently energetic to influence surface transport processes. Finally, CIRANO and LESSA (2007), and AGUIAR et $al.$ (2019) reported the influence of subinertial process in a Brazilian coastal bay. Low-frequency oscillations in sea level up to 17 cm were observed in Todos os Santos Bay (CIRANO and LESSA, 2007). In addition, AGUIAR et $al.$ (2019) asserted that subinertial exchange pulses between Todos os Santos Bay and its Adjacent Continental Shelf (ACS) are wind driven rather than density driven.

The GB is a coastal bay located in the state of Rio de Janeiro, Brazil (centered at 22°55'S and 43°10'W) and has the SBB as its ACS. GB has a surface area of approximately 3.84 x 10^8 m^2 and its islands cover 5.6 x 10^7 m^2 of the bay. Therefore, the water surface accounts for 3.28 x 10^8 m^2 (KJERFVE et $al.$, 1997; SEMADS, 2001). The bay is 36 km long, with a mean depth of 7.6 m (CASTRO and LEE, 1995). The main channel mostly follows the 30 m isobath, reaching depths up to 58 m (KJERFVE et $al.$, 1997). Different water volume estimates are observed in scientific literature. KJERFVE et $al.$ (1997) calculated a water volume of 1.87 x 10^9 m^3 for GB, whereas AMADOR (1997) and SEMADS (2001) estimated 3 x 10^9 m^3. This manuscript considers that GB has a water volume of 2.4 x 10^9 m^3, which is the product between the surface area and mean depth proposed by KJERFVE et $al.$ (1997) and AMADOR (1997) respectively.

Semidiurnal oscillations in GB sea surface level and velocity field are forced mainly by the tidal cycle (VIANA, 2017). Tides in GB are mixed with semidiurnal predominance (tidal form number of 0.33). Tidal currents at the GB entrance are stronger during flood (1.6 m s^{-1}) than ebb (1.0 m s^{-1}) tides. Currents reach around 0.5 m s^{-1} further into the bay. Therefore, tidal asymmetry occurs in GB and approximately 50% of the salt transported from the ACS to GB is due to tidal dispersion (KJERFVE et $al.$, 1997; KJERFVE et $al.$, 2001; VIANA, 2017). Tide is the main driving mechanisms of the GB circulation, as approximately 4/5 of the sea level variance of GB is explained by harmonical tidal constituents (FILIPPO, 1997; VIANA, 2017). The main tidal harmonic components in GB are: i) M$_2$ (principal lunar semi-diurnal constituent); ii) K$_2$ (Lunisolar semidiurnal constituent); iii) S$_2$ (Principal solar semidiurnal constituent); iv) O$_1$ (Lunar diurnal constituent) and v) K1 (Lunar diurnal constituent) (FILIPPO, 1997). BÉRGAMO (2006) observed that the net volume transport at the GB entrance varied from -4.15±1.85x10^3 m^3

s^{-1} to -7.31±2.16x10^3 m^3 s^{-1} during the neap-spring tidal cycle.

However, wind and freshwater input are also important to GB hydrodynamic processes. Denser waters, with temperature of 20.5 °C and salinity of 35.8, are driven by flood currents toward the inner parts of the GB. Local winds exert a greater influence on local circulation in shallow areas than in deeper regions. Salinity can vary from approximately 8 near river mouths and mangrove areas to 35 at the GB mouth (KJERFVE *et al.*, 1997; EICHLER *et al.*, 2001; BÉRGAMO, 2006). KJERFVE *et al.* (1997) found that eventual South Atlantic Central Water (SACW) inflow into GB occurs due to the Cabo Frio upwelling system, which is located at 100 km to the east of the bay entrance. In addition, CERDA and CASTRO (2014) asserted that the SACW intrusion into Cabo Frio coastal areas is promoted by: *a)* outer shelf slope; *b)* upwelling-favorable winds, and *c)* BC mesoscale variability. Therefore, the intrusion of SACW into GB could be indirectly related to the BC system.

The GB drainage basin covers an area of 4081 km^2 (SEMADS, 2001). Although 45 rivers and stream channels flow into the GB, only 6 rivers correspond to 85% of the total mean annual river input (JICA, 1994). Most rivers and stream channels are not continuously monitored. KJERFVE *et al.* (1997) estimated a mean annual freshwater discharge of 100 m^3 s^{-1} based on monthly mean climatological air temperature, precipitation rate and potential evapotranspiration. However, this value is not precise because it did not account for anthropological influence. KJERFVE *et al.* (2001) calculated a mean discharge of approximately 350 m^3 s^{-1}. The climate is characterized by a dry and a wet season in winter and summer respectively. Total annual rainfall ranges from 1000 mm to 2000 mm, but extremely intense showers (up to 50 mm per hour) may occur during summer (JICA, 1994; JUNIOR *et al.*, 2006; CLIMATEMPO, 2018). E/NE winds predominate in good weather situations, however cold fronts can drive the meteorological cycles over the year, specially in winter (JICA, 1994; JUNIOR *et al.*, 2006; CLIMATEMPO, 2018). An overall of 13 cold fronts reach the state of Rio de Janeiro during winter, with a mean interval of 6 days between consecutive fronts (STECH and LORENZZETI, 1992). Strong winds are also present in GB, mainly in summer, due to tropical storm events (FILIPPO, 1997; BÉRGAMO, 2006).

GB bathymetry is controlled by its geomorphological formation, by the sediment intake from the GB drainage basin, and by transport and sedimentation relative to currents. GB sediment characterization is shown in Figure 1. These processes result in a smooth bathymetry (SEMA, 1998 apud BÉRGAMO, 2006; KAUFMANN, 2009). Over the past 30 years, GB has been impacted by human-made activity. The surrounding areas of GB had been modified by an intense reconfiguration process (e.g., Oil activity, construction and expansion of shipyards, infrastructure develop-

ment relative to the Olympic games in 2016) (SOARES-GOMES *et al.*, 2016). In addition, GB sedimentation rate has increased in an accelerated rate in the last years, doubling from 0.6 (2011) to 1.25 cm yr^{-1} (2016). NETO and DA FONSECA (2011) proved that a greater portion of the debris floating in GB or drifting nearby in local beaches have land-based or nearshore source. The debris in GB are constituted of plastic, paper, metal, wood, among others (FRANZ, 2011).
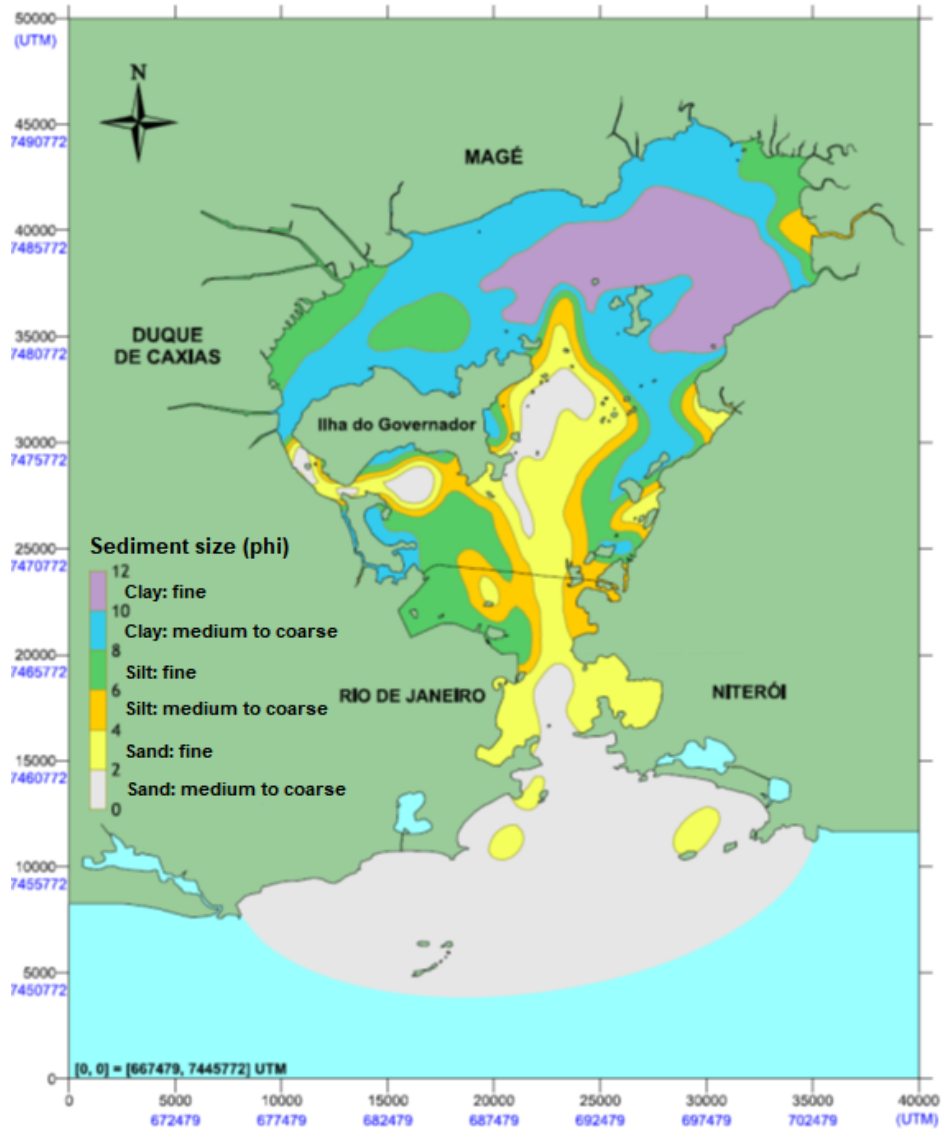
Figure 1: Sediment characterization of GB's bottom. Modified from KAUFMANN (2009).

GB hosts two ports, Port of Rio de Janeiro (the 2nd most important port in Brazil) and Port of Niterói, responsible for a transport of more than 7.5 x 10^6 tons of goods (e.g., oil, paper, salt, wheat and alcohol) in 2014. Only the Port of Rio de Janeiro generated a transit of more than 350.000 people annually. In addition, two oil refineries, representing a total of 17% of the national processed oil production, are located close by. Furthermore, two airports and two naval bases and a Navy's

shipyard are located in GB. Based on that, GB is considered a national security area and one of the most important bays in Brazil (KJERFVE *et al.*, 1997; BÉRGAMO, 2006; DRAP, 2018a; DRAP, 2018b; DRAP, 2018c).

Considering the subinertial band (> 3-day period), CTW induced by remote winds, local winds and BCvolume transport are some of the driving mechanisms of GB dynamics. The following paragraphs present the theoretical apparatus of these processes, focusing on their definition, examples of studies that relate a given mechanism to subinertial oscillations, and a general panorama of these processes in the study area.

Coastal Trapped Waves and Remote Winds

CTWs can be generated in all kinds of continental margins (BRINK, 1991). These waves are vorticity waves with period higher than the inertial period at mid-latitudes (D. M. HOLLAND, 1994; DOTTORI and CASTRO, 2018). A potential vorticity gradient with increasing depth across the continental shelf leads to CTW propagation along the continental shelf (D. M. HOLLAND, 1994). This propagation occurs with shallow water on the left in the Southern Hemisphere (BRINK, 1991; DOTTORI and CASTRO, 2018; S. ILLIG, 2018). These waves are an important way to spread the atmospheric energy along the continental shelf and influence the coastal circulation by enhancing mixing in a coastal region (BRINK, 1991; D. M. HOLLAND, 1994; HUTHNANCE, 1995). Coastal areas and other portions of continental shelf are influenced by remote winds partly because of CTW propagation (GILL e SCHUMANN, 1974).

The CTW formation starts with an alongshore wind stress, causing a cross-shore Ekman transport (Figure 2a). Therefore, a compensating flow in the opposite direction occurs below the surface Ekman layer. When this flow crosses lines of same depth, a local relative vorticity gradient is established (Figure 2b). This vorticity gradient results in an alongshore flow that, together with alongshore wind variability, generates an equatorward (in the Southern Hemisphere and for the western side of a given ocean basin) wave propagation (BRINK, 1991). A CTW also presents a second region of large amplitudes over the shelf edge (Figure 2c). In addition, the wave amplitude is continually incremented by local forcing as the wave propagates (EICHLER *et al.*, 2001). On the other hand, other forcing mechanisms can also be responsible for CTW generation. For example, diurnal tides can generate free CTWs at locations poleward of 30° (BRINK, 1991).

(a)

(b)

(c)
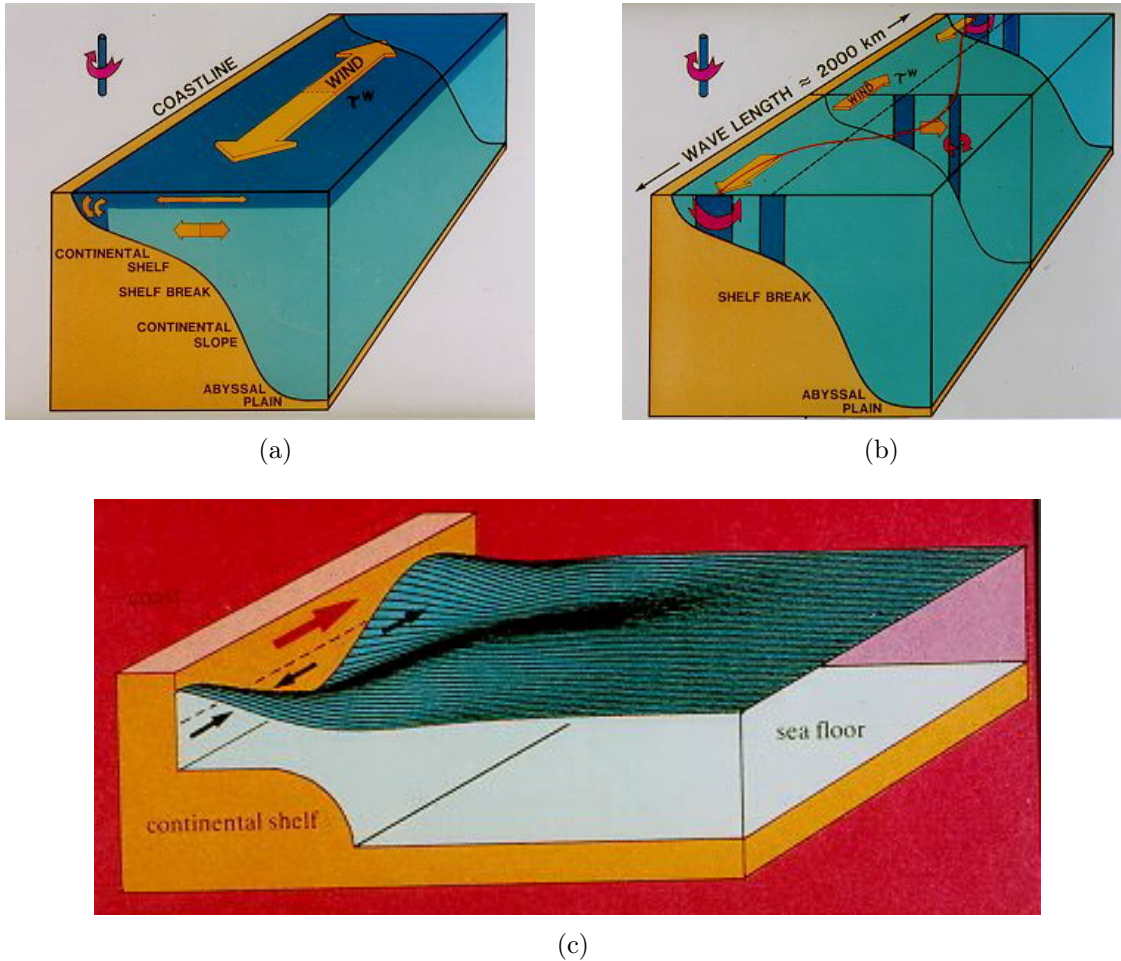
Figure 2: Scheme of CTW development. Initial setup involves: Earth's rotation, sloping continental shelf and variable external forcing, such as wind stress τ^w (a). The red line represents the new position of the parcel previously located along the dashed line (b). Only the water below the mixed layer is shown. The shape of a CTW is also presented (c). Modified from: TOMCZAK (2018).

The influence of CTWs on sea level have been analyzed along South American coast. CTWs forced by equatorial winds can be observed up to 30°S, reaching sea level variations of up to 15 cm on the Chilean coast (SHAFFER et al., 1997; LETH and MIDDLETON, 2004). In western South America, diverse studies are focused on the role of remote wind stress in subinertial sea level variability in the SBB (CASTRO and LEE, 1995; OLIVEIRA et al., 2006; CAMPOS et al., 2010; FILIPPO et al., 2012; DOTTORI and CASTRO, 2018).

DE FREITAS et al. (2019) observed near inertial oscillations with an average period of 7.3 days near the continental shelf break of Cabo Frio (northern portion of the SBB). In addition, equatorward CTWs with 6-7 day period were observed in the SBB and related to the displacement of a cold front along the area (CASTRO and LEE, 1995). The authors also observed that the 6-7 day period oscillation was better correlated with remote wind, located south of SBB, than with local wind.

FRANÇA (2013) stated that the CTWs that propagate along the Brazilian coast are generated on the Argentinian continental shelf between 40 and 45°S. Speeds of CTW propagation tend to vary along the SBB, reaching up to 11 m s^{-1} in the central part, where the shelf is about 200 km long, and up to 7 m s^{-1} in its northernmost part, where the shelf is narrow (50 km) (DOTTORI and CASTRO, 2018).

In terms of wind variability, the South Atlantic Subtropical High dominates the large-scale wind field with first quadrant (N-E) winds throughout the entire year (DOTTORI and CASTRO, 2018). On the other hand, S-SW winds are related to equatorward cold fronts along the SBB, which are frequent over the year (CERDA and CASTRO, 2014).

Local Winds

The atmosphere can influence directly the sea level variability in different ways. The most effective one is the inverse barometer effect (WOODWORTH *et al.*, 2019). An increase (decrease) of 1 mbar in the atmospheric pressure is sufficient for a decrease (increase) of approximately 1 cm in sea level (RODEN and ROSSBY, 1999). However, in coastal shallow areas, such as GB, the wind stress can be considered the most important atmospheric forcing directly responsible for sea level variability (WOODWORTH *et al.*, 2019). As the wind speed is proportional to the squared root of wind stress (PUGH and WOODWORTH, 2014), the more intense the wind is, more momentum is transferred to the ocean, causing coastal sea level oscillations specially when the wind-driven transport is blocked by the continent. Modeling analysis performed by SUURSAAR and KULLAS (2006) showed that an increase of 2 m s^{-1} in the wind component could lead to a 3 cm mean sea level variation in regions of Baltic Sea (Western coast of Estonia).

In the SBB, the South Atlantic Subtropical High drives most of the large-scale wind variability. Therefore, N-NE-E winds occur over the year (DA SILVA *et al.*, 1994). Local changes are related to cold front events, when S-SW winds prevail without seasonal distinction (CASTRO and MIRANDA, 1998). In addition, upwelling favorable winds may cause SACW intrusions into coastal areas CASTRO FILHO, 1997). Therefore, prevailing winds along SBB can be considered an important forcing mechanism of subinertial dynamics in GB.

In the city of Rio de Janeiro, the local wind pattern is modulated by the sea breeze system. JACINTO (2018) stated that a daily modulation in the meridional wind component occurs between RJ-3 station and Santos Dumont Airport at 10 m up to 150 m height, which is the band responsible for the sea breeze system. In addition, with increasing height, the wind pattern acquires a distinct zonal modulation with daily period. In the inner portion of GB, the wind direction fans out and nearly orthogonal winds approach the coast. A southeasterly/easterly wind pattern is

dominant in the middle-west portion of the bay (PIMENTEL *et al.*, 2014).

Boundary Currents

The link between the ocean and coastal areas is the boundary currents. Boundary current dynamics can cause important effects on coastal areas, such as coastal upwelling, sea level oscillations, enhance/decrease of primary productivity (TODD *et al.*, 2019). Boundary currents influence coastal sea level variability specially from monthly to interannual timescales PONTE *et al.*, 2019). TODD *et al.* (2019) stated that the spatial variability and strength of the Western Boundary Current (WBC) impact the mean sea level locally. In fact, EZER (2015) argued that the influence of boundary currents on coastal sea level is possibly one of the reasons for the difference between observed and modeled coastal sea level. Because of the geostrophic component, the intensity of WBCs can exert influence on coastal areas by: *i*) changing the cross-current subsurface density structure and/or *ii*) altering the slope of the sea surface level (DOMINGUES *et al.*, 2018).

In the North Atlantic Ocean, previous studies (e.g., EZER *et al.*, 2013; WOODWORTH *et al.*, 2014; GODDARD *et al.*, 2015; EZER, 2016) demonstrated that a decrease of 1 Sv in the Gulf Stream transport could result in a increase of 0.5-3 cm in sea level along the northeastern U.S. coast. In the southeastern coast of the U.S, Florida Current dynamics is the major source of sea level variability (DOMINGUES *et al.*, 2018). In addition, DOMINGUES *et al.* (2018) demonstrated that an increase of 1°C in Florida Current temperature can result in a sea level rise of 12.5 cm, considering only the effect of thermal expansion.

In the South Atlantic Ocean, there is enough space for progress in terms of knowledge of the influence of BC interannual variability at the SBB and its impact on coastal sea level (GOES *et al.*, 2019). For instance, GOES *et al.* (2019) suggested that a variation of up to 20 cm in near-shore sea level could result from coastal upwelling induced by the BC variability.

As previously mentioned, the main factors influencing the circulation in the ACS are local wind stress, remote winds (as driving mechanisms of CTWs), BC variability and tides (CASTRO *et al.*, 2006). In addition, previous studies pointed local wind stress (SUURSAAR and KULLAS, 2006), remote winds (VALLE-LEVINSON, 1995; MUSCARELLA *et al.*, 2011; SANKARANARAYANAN and FRINGER, 2013; AGUIAR *et al.*, 2014), and boundary current variability (EZER *et al.*, 2013; WOOD-WORTH *et al.*, 2014; GODDARD *et al.*, 2015; EZER, 2016; DOMINGUES *et al.*, 2018; GOES *et al.*, 2019) as forcing mechanisms of subinertial sea level variability in different coastal regions. Considering the above and excluding the effect of tides, this manuscript hypothesizes that BC variability, local and remote winds play a major role in GB subinertial dynamics. Therefore, the main objective of this thesis is to identify the dominant forcing mechanisms of subinertial variability in GB. To achieve this goal: *i*) an evaluation of DELFT3D model's performance in reproducing extreme subinertial events during a 4-year simulation; *ii*) quantification of the subinertial volume transport along key sections in the bay, and *iii*) analysis of the propagation of subinertial pulses towards shallow GB waters were performed.

It should be noted that the knowledge of water dynamics, at any temporal scale, in a given coastal marine environment has fundamental importance for a wide range of activities, such as management of urban structures, understanding of the dispersion of pollutants, renewal and water quality, operational activities of ships, ports and vessels in general. This knowledge is crucial for coastal planning, as well as to management and emergency measures to minimize environmental and socioeconomic impacts.

1.1 Historic of previous studies focusing at Guanabara Bay

Most scientific papers about GB were based on environmental or biological concerns. JUNIOR *et al.* (2006) analyzed the impact of Icaraí sewage outfall in the GB water quality. Environmental and sanitary conditions were discussed by FISTAROL *et al.* (2015) and SOARES-GOMES *et al.* (2016). The scientific community is also engaged in the discussion about the impact of rubbish in GB beaches (NETO and DA FONSECA, 2011; DE CARVALHO and NETO, 2016). In addition, issues related to how sediment metals vary along the bay (FONSECA *et al.*, 2013; ABREU *et al.*, 2016) and how pollution, in general, impacts some marine species (BITTENCOURT *et al.*, 2017; CAMARGO *et al.*, 2017) were also addressed.

In terms of marine organisms, most studies are about fishes and fish larvae. The purpose of these studies goes from the changes of how fishermen catch their

fishery along the decades to how different the patterns of fish distribution and fish larvae are in GB over the year (CASTRO *et al.*, 2005; CORRÊA and VIANA, 2016; LOTO *et al.*, 2018). Other marine animals are also reported in the literature, such as squids, dolphins and mollusks, focusing on their distribution along the bay and what controls their spatial patterns (e.g., NEVES *et al.*, 2013; AZEVEDO *et al.*, 2017; MORAES and LAVRADO, 2017).

Studies focusing on remote sensing applications in GB have been published in a lower scale compared to papers about environmental issues. BRAGA *et al.* (1993) performed a local water quality evaluation using imagery data, while an assessment of remotely sensed chlorophyll-a concentration along the bay was prepared by OLIVEIRA *et al.* (2016). It is important to mention that some authors used physical parameters as a secondary focus of their articles. EICHLER *et al.* (2001) used foraminifera as indicators of ocean water masses. Benthic foraminifera and ichthyofauna were also analyzed under different gradients of temperature and salinity forced by the seasonality of SACW intrusions (EICHLER *et al.*, 2003; DA SILVA JR *et al.*, 2016). Finally, studies on short-time scale variability of organisms due to inertial frequency events are also found in the literature (GUENTHER *et al.*, 2018).

The most important works in terms of GB dynamics are KJERFVE *et al.* (1997) and KJERFVE *et al.* (2001). The authors described the oceanographic characteristics of GB, focusing on: tidal variability; currents; salinity and temperature patterns, and the resulting vertical stratification; residual tidal and gravitational circulation. Tides in GB are mixed with semidiurnal predominance (tidal form number of 0.33). Tidal currents at the GB entrance are stronger during flood (1.6 m s^{-1}) than ebb (1.0 m s^{-1}) tides. Currents reach values around 0.5 m s^{-1} in the inner bay. GB has a strong tidal circulation. Approximately 50% of the salt transported from the ACS to GB is due to tidal dispersion (KJERFVE *et al.*, 1997; KJERFVE *et al.*, 2001).

In addition, other studies based on physical processes were performed in GB. Even though not published in scientific journals, some researchers are worth to mention regarding their findings. BÉRGAMO (2006) stated that when tidal motions are less intense (neap tide events), baroclinic effects also become responsible for the salt transport into the bay. To obtain a full understanding of transport processes in GB, the lateral velocity shear must be considered (BÉRGAMO, 2006). SAMPAIO (2003) used a model to analyze water mass exchange between GB and the ACS. Particles displaced along the ACS are promptly washed out of the modeled area. In simulations of good weather conditions, surface particles tend to flow inshore while particles close to the bottom tend to flow back to the ocean.

Hydrodynamic numerical modeling has also been implemented in GB to simulate different events. These studies are important for preventive actions and are

used as base for future decisions. ROSSO (1997) implemented a hydrodynamic model to study the oil transport inside GB. In addition, DOS SANTOS (2017) simulated different IPCC scenarios to evaluate their impacts under sea level rise due to climate change.

This manuscript is structured in 4 chapters. The methodology, data and model experiments are presented in the second chapter. Chapter 3 presents the results in the following sections: i) independent data analysis, ii) model performance, iii) experiments modeled, and specific scenarios. Finally, some closing considerations and recommendations are presented in the last chapter.

Chapter 2

Material and Methods

This chapter is divided in two sections, Independent Data and DELFT3D. The first section presents every dataset used in this thesis and a detailed step-by-step sequence of data processing and analysis. The second section covers the model DELFT3D, including (i) a brief description, (ii) the data used as forcings, (iii) validation against observed data, (iv) the sensitivity experiments and (v) the case studies.

2.1 Independent Data

2.1.1 Data Acquisition

A total of 6 independent databases were used to enable an in-depth discussion of the results. The period of acquisition of all databases and their locations are indicated in Figures 3 and 4, respectively.
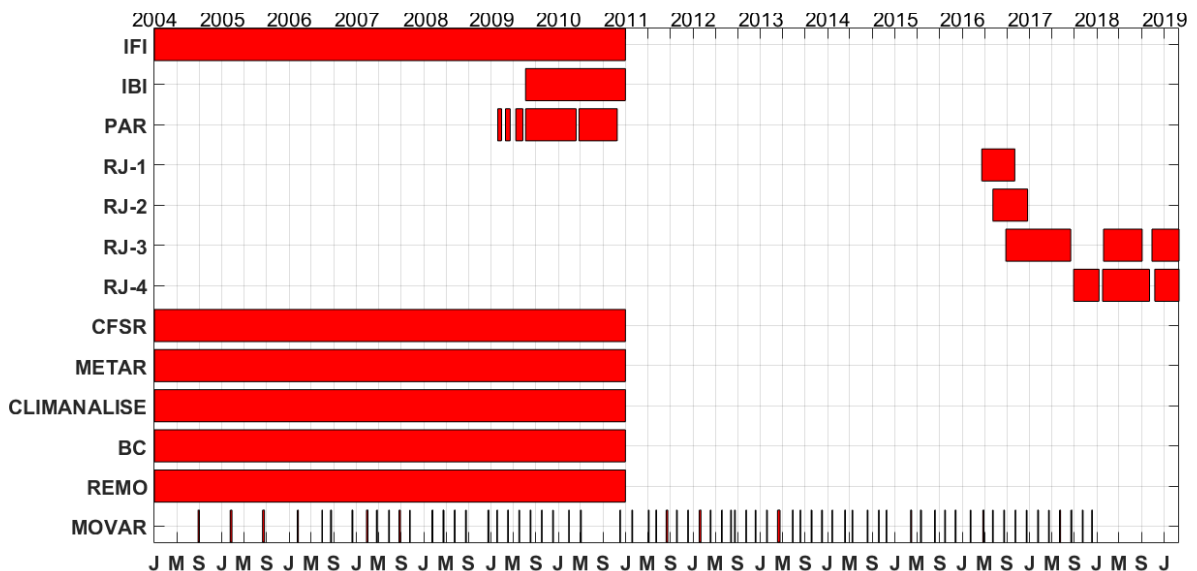
Figure 3: Time line of all data used in this study. Sea level stations (IFI, IBI and PAR), SiMCosta stations (RJ-1, RJ-2, RJ-3 and RJ-4), CFSR wind fields, METAR and CLIMANALISE reports, BC altimetry data, XBT data from MOVAR and REMO outputs are indicated.

Sea surface level data was acquired at 3 stations: Ilha Fiscal (IFI); Ilha

do Boqueirão (IBI) and Ponta da Armação (PAR). Data was kindly provided by the Brazilian Navy Hydrographic Center. In addition, IFI data was obtained under the scope of Global Sea Level Observing System (GLOSS). Hourly sea surface level was collected in the following periods: from 01/01/2007 to 31/12/2010 (all dates are shown in the format of dd/mm/yyyy of month/yyyy) at IFI station; from 07/07/2009 to 31/12/2010 at IBI station, and from 06/02/2009 to 16/11/2010 at PAR station. IFI, IBI, and PAR stations are located inside GB (Figure 4c).

(a)

(b)

(c)
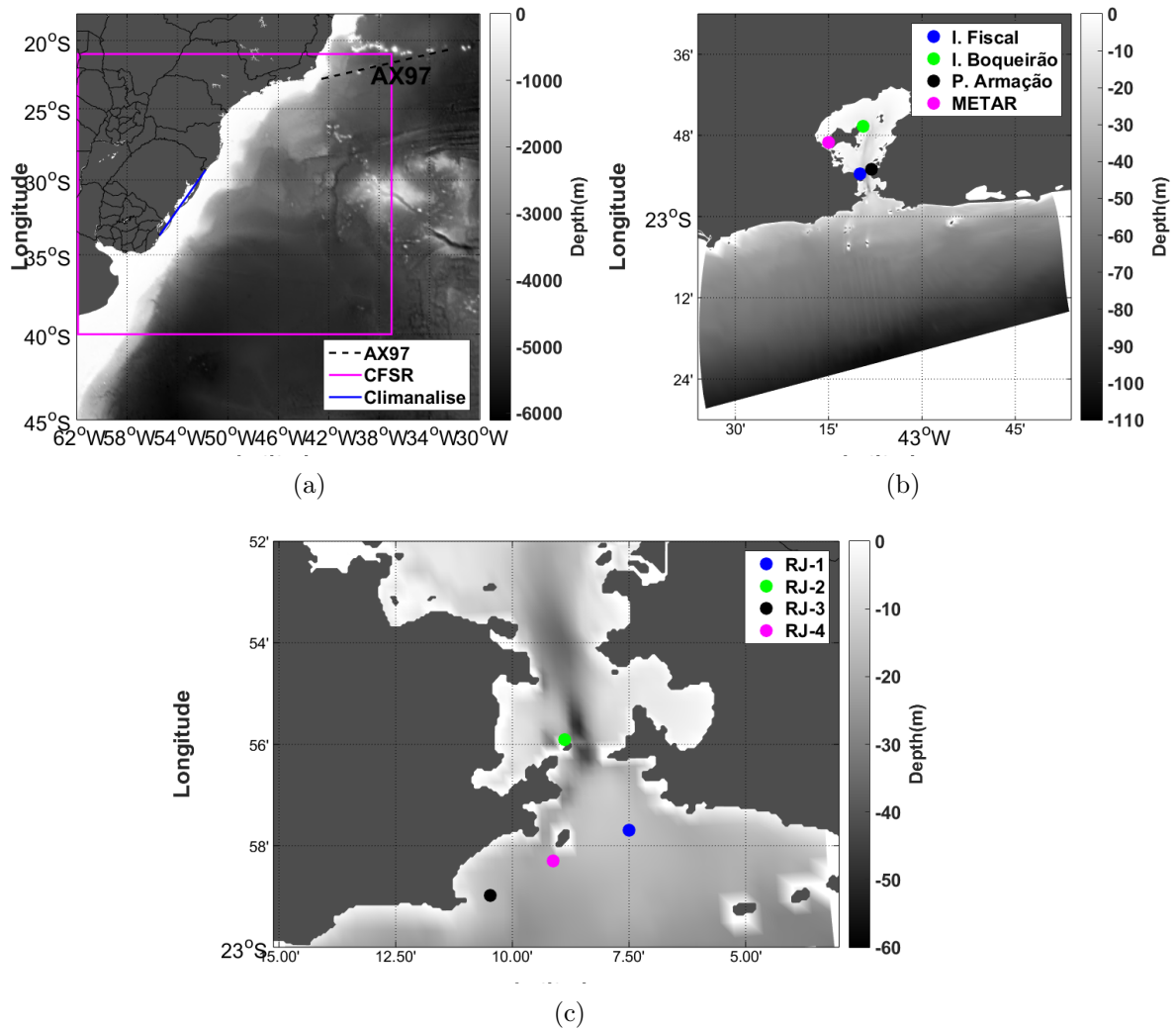
Figure 4: Bathymetry of the area surrounding SBB (a), GB (b), and the GB entrance (c). Location of the AX97 transect (black dashed line), wind field from CFSR (magenta line) and searching area for Climanalise data (blue line) are shown in top left panel. Locations of Ilha Fiscal, Ilha do Boqueirão, Ponta da Armação (blue circle, green circle, and black circle respectively) and METAR stations (magenta circle) can be observed in top right panel. SiMCosta stations are represented by blue, green, black, and magenta circles (RJ-1, RJ-2, RJ-3, and RJ-4 respectively) in the bottom panel.

Velocity data was obtained from the Brazilian Coast Monitoring System

(SiMCosta). A total of 4 Acoustic Doppler Current Profiler (ADCP) installed on 4 meteo-oceanographic buoys (RJ-1 to RJ-4) displaced close to the GB entrance (Figure 4b) acquired data from 2016 to 2019. RJ-1 and RJ-2 are no longer in service, but RJ-3 and RJ-4 remain collecting real-time meteo-oceanographic data (Figure 3). Each ADCP measures the velocity (intensity and direction) through the water column in 20 equally distant bins. Intensity and direction were converted into U and V components. In addition, few gaps in velocity data were interpolated.

Wind data were obtained from two databases. Hourly Meteorological Aerodrome Reports (METAR) from Tom Jobim Airport (Figure 4b) collected from 2004 to 2010 (Figure 3) were analyzed to obtain 10 m wind intensity and direction, and converted to U and V wind components. The data obtained from this station was used to characterize the wind pattern in GB and used as atmospheric forcing in one of the sensitivity experiments. In addition, Climate Forecast System Reanalysis (CFSR) product, provided by the National Centers for Environmental Prediction (NCEP), was obtained from 2004 to 2010 (Figure 3, SAHA *et al.*, 2010). CFSR has a temporal resolution of 1 hour and spaced every $0.312°$. 10 m U and V wind components were obtained in a rectangle ranging from 21 to 40°S and 37 to 62°W (Figure 4a). This subset comprises areas of possible remote winds influence. An area close to GB (from 22° to 24°30'S and 40° to 43°45'W) were selected to evaluate the influence of local winds on GB water level. This area was chosen because it covers zones where alongshore winds tend to blow. For this area, U and V components were rotated anticlockwise considering the orientation of the 200 m isobath (further information are given in Section 3.1.2). Climanalise reports were used to obtain the date of cold front events along the coast of Rio Grande do Sul (RS) (Figure 4a). A total of 48 reports elaborated from 2007 to 2010 (Figure 3) were analyzed and 340 days with cold fronts were observed.

BC volume transport from 2004 to 2010 (Figure 3) were calculated based on GOES *et al.* (2019)'s methodology. Altimetry Sea Surface Height (SSH) data (delayed-time, daily Ssalto/Duacs) produced by Archiving, Validation and Interpretation of Satellite Oceanographic data (AVISO) from 2004 to 2010 was used in this study (Figure 3). Altimetry data has a horizontal resolution of $0.25°$. SSH anomalies were calculated from a period of 10 years (1993-2012). To estimate the BC volume transport based on altimetry, the XBT based geostrophic velocity must be known first. To estimate geostrophic velocities along the AX97 transect (Figure 4a), the relative dynamic height was calculated using temperature profiles (AX97 XBT data) and updated salinity estimates, assuming the $\sigma_\theta = 26.8$ kg m^{-3} isopycnal surface as reference level, which is approximately the interface between the SACW and Antarctic Intermediate Water (DA SILVEIRA *et al.*, 2008; PEREIRA *et al.*, 2013; BILÓ *et al.*, 2004; LIMA *et al.*, 2016). The use of Argo-based monthly climatology

absolute dynamic topography's value at the isopycnal reference level returns the absolute dynamic height (e.g., YU *et al.*, 2006). The absolute velocity field from the XBT data was obtained from the absolute dynamic topography using the thermal wind relation. The BC volume transport is the minimum cumulative transport between 41 and 36°W obtained from the integration of cross-section velocities from the surface to the $\sigma_\theta = 26.8$ kg m^{-3} isopycnal level. Daily altimetry-based BC volume transport was obtained from a series of regressions. Firstly, the relative dynamic height is regressed from the absolute dynamic topography, then SSH is obtained from the relative dynamic height. Therefore, a link between altimetry and XBT data can be established. The final step was to obtain the velocity fields using the thermal wind relation and the respective volume transport using the same approach as for XBT-based BC volume transport.

2.1.2 Data Analysis

After gathering all independent timeseries (sea level, velocity components, 10 m wind components and BC volume transport), a 9th order low-pass Butterworth filter with a 3-day cutoff period was applied on each timeseries to obtain the subinertial band of each variable (Figure 5a). The 3-day cutoff period was selected to remove as much tidal signal as possible in the sea level data. Afterwards, IFI subinertial level was daily averaged to decrease Nyquist frequency, allowing a more sophisticated response for a 24-day cutoff period high-pass Butterworth ($11^{th}order$) filter (Figure 5b). Therefore, it was possible to separate CTW periods (3 to 24 days) from seasonal influence (> 24 days). After that, CTW peaks were identified in the 3 to 24-day filtered IFI data. Positive peaks with minimal prominence of 10 cm and separated from another peak for at least 3 days were considered. A CTW was classified as an extreme event if it presents a value greater than twice the level's standard deviation. The frequency of CTW crests at IFI up to 2 days after a cold front event on RS coast was calculated. A 2-day lag was chosen because is the time a CTW travels all the way along the continental shore from RS to GB , considering 11 m s^{-1} as the average velocity of CTW propagation (DOTTORI and CASTRO, 2018). The amplitude of each CTW observed was calculated by the difference of height from positive to negative peaks. A negative peak was identified considering the same approach used above (≥ 10 cm amplitude and 3 days far from consecutive negative peaks). The period of each CTW was twice the time difference between a positive and negative peak.
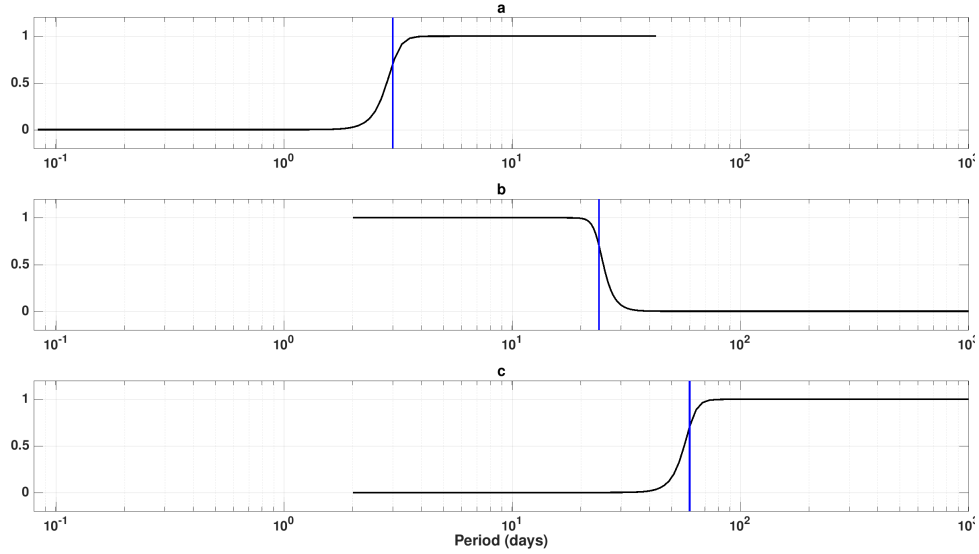
Figure 5: Response function of filters used (low-pass filter a and c, and high-pass filter b). Blue vertical lines represent the cutoff period of each filter (3 days (a), 24 days (b) and 60 days (c)).

Maximum correlation of zonal and meridional CFSR wind components with subinertial IFI level and respective lag were calculated to analyze the response of GB level to remote wind fluctuations. In addition, the same calculation was made for local wind alongshore and cross-shore components.

IFI level and BC volume transport were filtered using a 60-day cutoff period Butterworth ($11^{th} order$) filter (Figure 5c) to analyze the influence of BC transport seasonality on GB level. The maximum correlation of BC volume transport with IFI level and respective lag were calculated for both subinertial and $\geq$ 60 days bands. Finally, an analysis of low-frequency ($\geq$ 60 days) GB level was performed. Daily means for every Julian day (1 to 365) of IBI and IFI timeseries were performed. Elevated gaps in PAR timeseries precluded this analysis. The same approach was used for BC volume transport. The entire time series of each dataset (Figure 3, BC volume transport and sea level data at IFI and IBI stations) were used in this analysis.

2.2 DELFT3D

DELFT3D is an aquatic environment model, which integrates flow and transport models aspects, developed by Deltares. The flow module of this system (DELFT3D-FLOW) provides the hydrodynamic basis for other modules, such as waves, morphology, ecology, and water quality. DELFT3D a finite difference model based on an Arakawa C grid (Figure 6), where motion variables (u, v and w) are located at the faces of the grid, while scalar variables (such as water level and density) are calculated at the center of the cell.
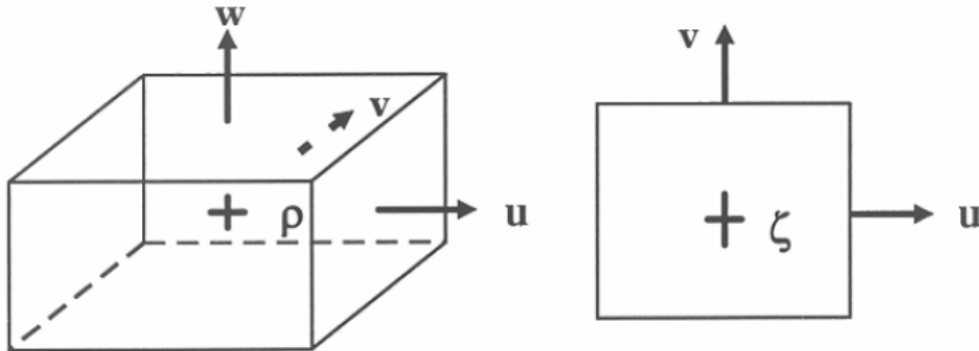
Figure 6: Grid staggering. 3D view (left panel) and top (right panel) of the grid cell. ζ and ρ are scalar variables and their values are displaced at the center of the grid cell ($+$). u, v and w represent vector variables and their values are located at the faces of the grid cell. Modified from Deltares (2013).

Simulations of two-dimensional (2DH, depth-averaged) or three-dimensional (3D) flow and resulting transport from tidal and/or meteorological forcing are performed by the flow module. In addition, the motion generated by gradients of temperature and salinity (density-driven flow) are also modeled by this module. DELFT3D-FLOW can be used in simulations of coastal areas, shallow seas, estuaries, rivers, lakes, and lagoons. The 2DH approach is mainly applied to study storm surges, tsunamis, and tidal waves in vertically well-mixed environments. On the other hand, 3D simulations are performed to understand flows with significant vertical gradients, such as those in upwelling/downwelling events, river input in bays, and thermal stratification.

DELFT3D-FLOW solves the Navier-Stokes equation for an incompressible fluid, considering shallow water and the Boussinesq assumptions. For further details on DELFT3D-FLOW model equations, see DELFT-FLOW (2014).

For a fully developed model, a well-constructed grid, precise bathymetry dataset, bottom sediment description of the area, initial and boundary condition datasets are required. The grid used in the experiments is shown on Figure 7. The

horizontal resolution of the grid varies from approximately 150 m in narrow areas (bay entrance) to 3 km in the ACS. The area of an individual grid cell could reach values up to 12 km^2 on the lower left corner of the continental shelf (Figure 8). The grid has a finer spatial resolution at the bay entrance where grid cells have surface areas of about 0.075 km^2.
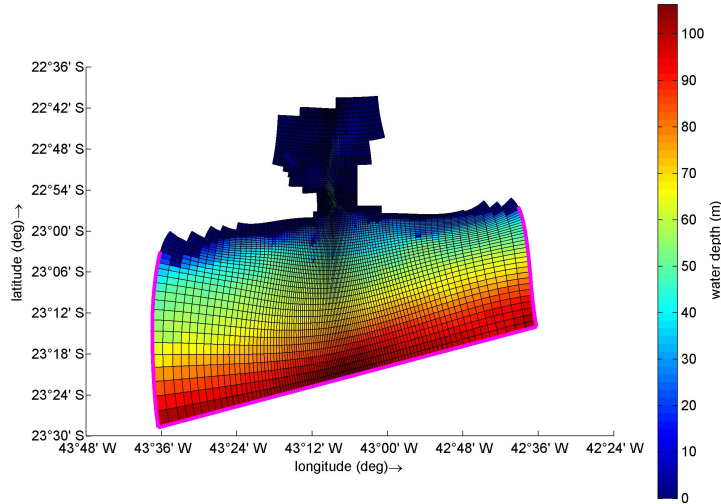
Figure 7: Model grid and bathymetry. Magenta line indicates the location of open boundaries and colorbar indicates the local bathymetry.
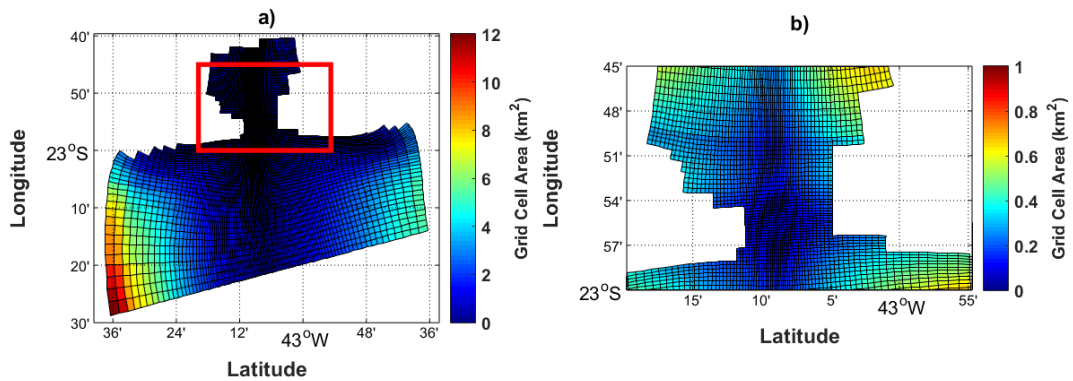
Figure 8: Spatial resolution of grid elements. Area of each grid cell for the entire domain (a) and the entrance (b). Red rectangle indicates the location of the area shown in the left panel.

Bathymetry data was obtained from nautical charts (DNH 1501, DNH 1506,

DNH 1511, DNH 1512, DNH 1513, DNH 1515 and DNH 1531) and high-resolution data provided by the Brazilian Navy Hydrographic Center. In addition, as different sediment grain-size characterization occurs on bay's bottom (Figure 1), different values of Manning coefficient must be applied along GB (Figure 9). This method is the same as described by DE SOUZA (2013).
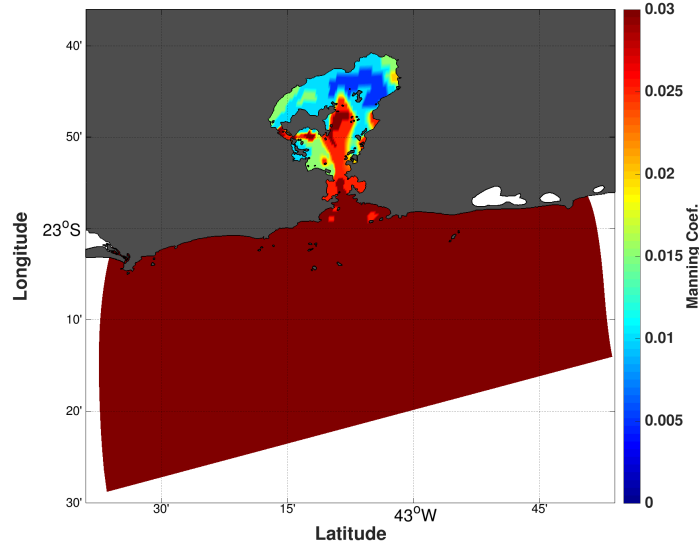
Figure 9: Manning coefficients used in grid experiments. Colorbar indicates the manning coefficient values.

All modeling experiments were hydrodynamically forced with hourly SSH, and both U and V depth-averaged velocity components. The hydrodynamic variables came from an experiment conducted under the scope of the Brazilian Oceanographic Modeling and Observation Network (REMO). The Physical Oceanographic Laboratory - (LOF/COPPE/UFRJ) kindly provided their outputs to be used in this thesis. A detailed description of the experiments performed under the scope or REMO was performed by LIMA *et al.* (2013) and GABIOUX *et al.* (2013). REMO used the Hybrid Coordinate Ocean Model (HYCOM)) to obtain hourly depth-averaged velocity field and SSH (REMO, 2016). HYCOM uses a hybrid coordinate system, where the vertical coordinate is isopycnal in open, stratified ocean, followed by z coordinate in the weakly-stratified upper-ocean mixed layer. In shallow water areas, HYCOM uses sigma coordinates, which follows the bathymetry (HALLIWELL, 2004). REMO's atmospheric forcing is from a CFSR product ($1/4°$ spatial resolution). It consists of 10 m wind components, temperature, rainfall, short, and long-wave radiation among other variables. In this experiment, the South Atlantic Ocean is simulated from 2004 to 2010 without the effect of tides providing hourly outputs on a $1/24°$grid.

As the only variables monitored were sea level and horizontal velocity, Sea

Surface Height (SSH) and depth averaged velocities were set to zero as initial conditions. However, the hydrodynamic forcing was used at the open boundaries (Figure 7a). The open boundaries were the Riemann type and forced with SSH and depth-averaged velocity time series.

A total of 3 experiments from January 2007 to December 2010 were conducted in this study (Table 1). This period was chosen after a statistical comparison between the subinertial sea level observed at IFI station and the REMO subinertial sea level modeled for the grid cell closest to IFI station. The first experiment (EXP 1) consisted of the DELFT3D model hydrodynamically forced by REMO's special product. The second experiment (EXP 2) was performed with the same setting as EXP 1, but with an atmospheric forcing from hourly subinertial METAR wind data. Finally, the last experiment (EXP 3) was similar to EXP 2, but values from wind components were provided by CFSR. The wind rose of METAR and CFSR data for all period modeled are presented in Figure 10. As an in situ data, the METAR dataset is the reference wind data in GB. On the other hand, the CFSR dataset describes the mean wind pattern on the continental shelf.

Table 1: Description of the experiments performed in terms of hydrodynamic and atmospheric forcing.

	EXP 1	EXP 2	EXP 3
Hydrodynamic Forcing **(Level and depth averaged velocity)**	REMO	REMO	REMO
Atmospheric Forcing **(Wind intensity and direction)**	Without	METAR	CFSR
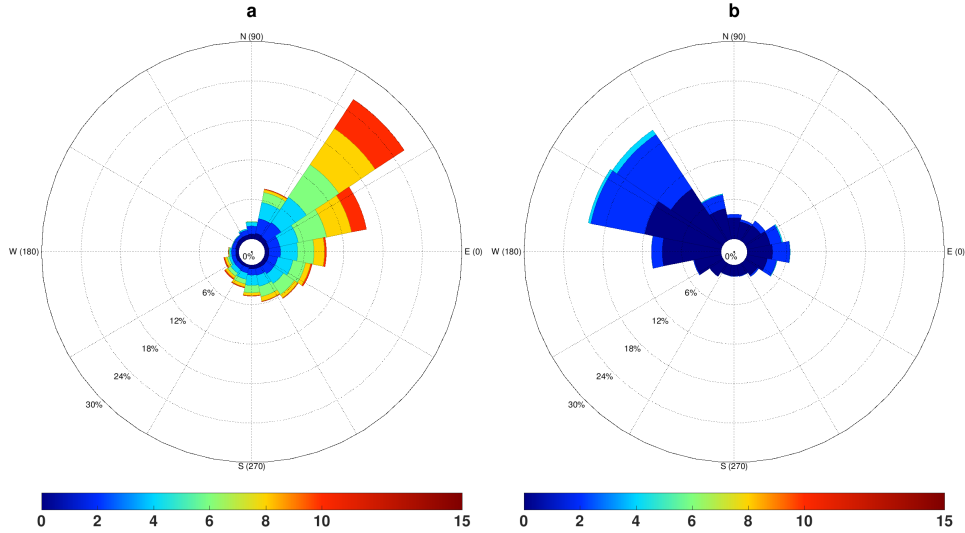
Figure 10: Wind rose for CFSR (a) and METAR (b) data from 2007 to 2010. Colorbar represents wind intensity (m s^{-1}).

Three periods were chosen to evaluate in detail the influence of the forcing mechanisms mentioned in this study. The first case observed was a period between 12/08/2010 and 20/08/2010. This period was characterized by a CTW event with SW/S offshore winds. The following case was observed from 27/05/2007 to 05/06/2007 and was similar to the first case, but with offshore winds varying from SW to NE direction. The last case studied occurred from 15/11/2008 to 04/12/2008. This period started with the passage of a CTW then, intense and persistent NE winds took place and finally, another CTW traveled towards lower latitudes.

Finally, the cross-section component of the depth-averaged velocity was compared along three cross sections along GB to assess how subinertial pulses step into GB. The sections are located between the entrance of the bay and the middle portion of GB (Figure 11). From Figure 12, it is possible to compare the model bathymetry to the gridded bathymetry for the section (interpolated from high-resolution in situ data).
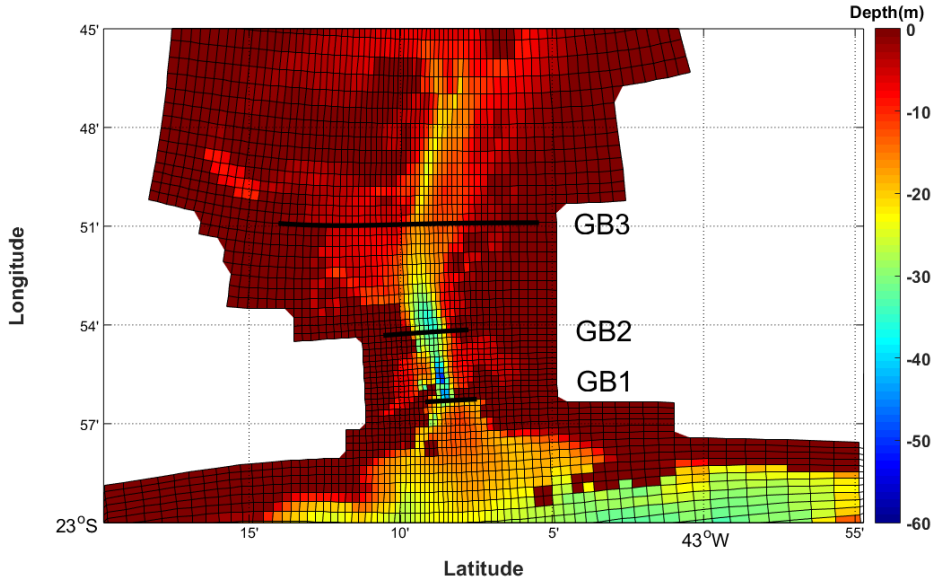
Figure 11: Grid bathymetry at the GB entrance. Location of GB1, GB2, and GB3 sections are indicated by black lines.
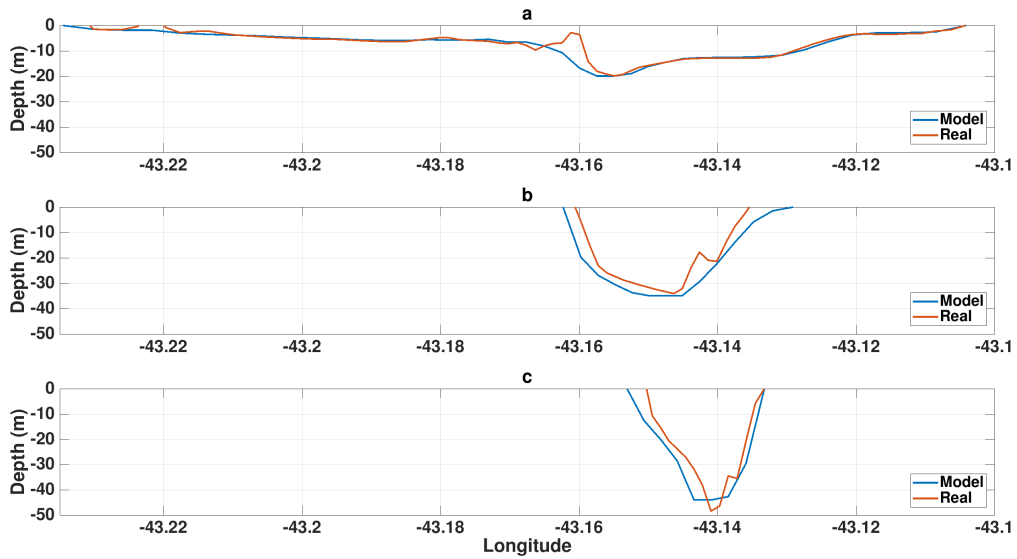
Figure 12: Depth of sections GB3 (*a*), GB2 (*b*) and GB1 (*c*) based on observed data (red line) are compared against DELFT3D bathymetry (blue line).

22

Chapter 3

Results and discussion

3.1   Independent Data

This section presents all results obtained from independent datasets analyzed (level data provided by Brazilian Navy Hydrographic Center, velocity data from SiMCosta, wind data from CFSR and METAR, period of cold front events from CLIMANALISE, and BC Volume transport from altimetry and XBT data). These data were analyzed to study the influence of CTW, remote and local winds, and WBC in sea level in GB. In addition, the effect of low-frequency ($\geq$ 60-day period) level oscillations is considered.

3.1.1   Influence of Coastal Trapped Waves and Remote Wind

As mentioned before in Chapter 1, remote wind has the potential to impact coastal areas located great distances away mainly because of CTW propagation. Therefore, cold front events in the CTW generation area can be considered a good proxy for the influence of CTW on GB's subinertial sea level. Among the cold front events on the coast of RS, and IFI sea level filtered between 3 and 24 days from 2007 to 2010 (Figure 13), a total of 172 CTWs with sea level variation greater than 10 cm were identified between 2007 and 2010. Overall, 48 CTWs were observed in 2007, 42 in 2008, 43 in 2009, and 39 in 2010. Furthermore, cold front events occurred during a total of 340 days between 2007 and 2010. The year with more cold front days was 2007 (102 days), followed by 2008 (85 days), 2009 (79 days), and 2010 (74 days). The year with more cold front days on the coast of RS was also the one with more CTWs observed in GB. The lower occurrence of CTW events in 2010 can be explained by the decreased number of days with cold fronts on the coast of RS in that year. On the other hand, 2010 was the year when more CTW reached positive extreme values (11 in 2010, 6 in 2007, 5 in 2008 and 4 in 2009) and presented the greater correlation between CTW crest and occurrence of cold fronts on RS coast (Table 2). Therefore, the greater the number of cold fronts days on RS coast, the greater the amount of CTW events that reached GB. But the magnitude of the CTW was not related to the amount of cold fronts observed. It is probably related to the intensity of the cold front. It is important to mention that from 2007

to 2009, a LaNiña event took place, and from 2009 to 2010 a strong ElNiño event happened (BOM, 2020). Those dates coincide with the minimum and maximum number of extreme cold fronts of the RS coast, respectively. Overall, the CTW events presented a mean observed variation of 27.8 ± 11.2 cm, with a mean period of 6.82 ± 2.85 days (Figure 14). The maximum sea level variation caused by a CTW was 67.3 cm.
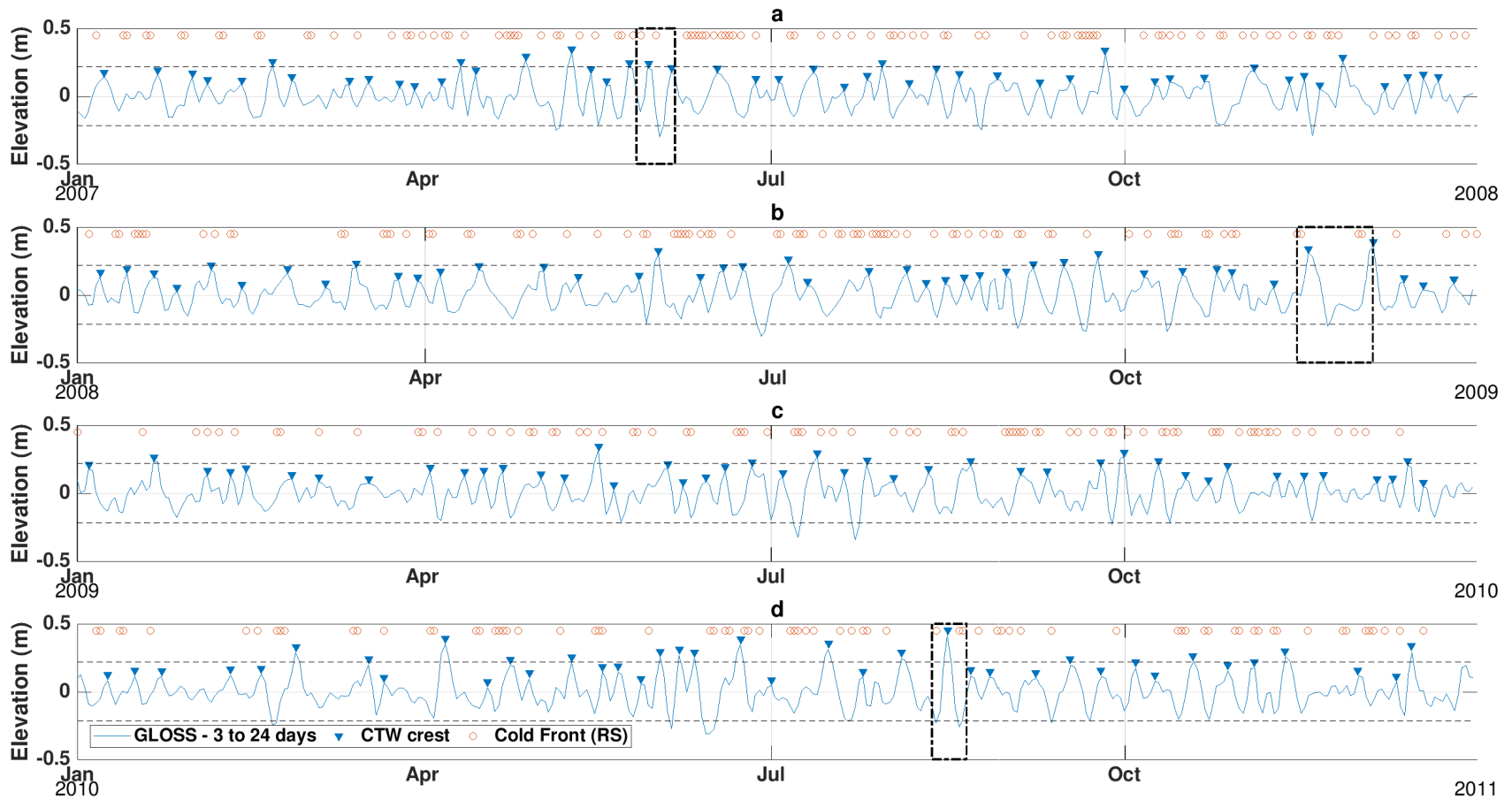
Figure 13: Relation between subinertial level in IFI (blue line) and occurrence of cold fronts on RS coast (red circles) for 2007 (*a*), 2008 (*b*), 2009 (*c*), and 2010 (*d*). Location of CTW crests is also shown (blue triangles). The dashed boxes represent selected periods used as case studies.

Table 2: Frequency of CTW crests at IFI up to 2 days after a cold front event on RS coast from 2007 to 2010 and for each year.

2007	2008	2009	2010	Total
0.56	0.66	0.66	0.73	0.64
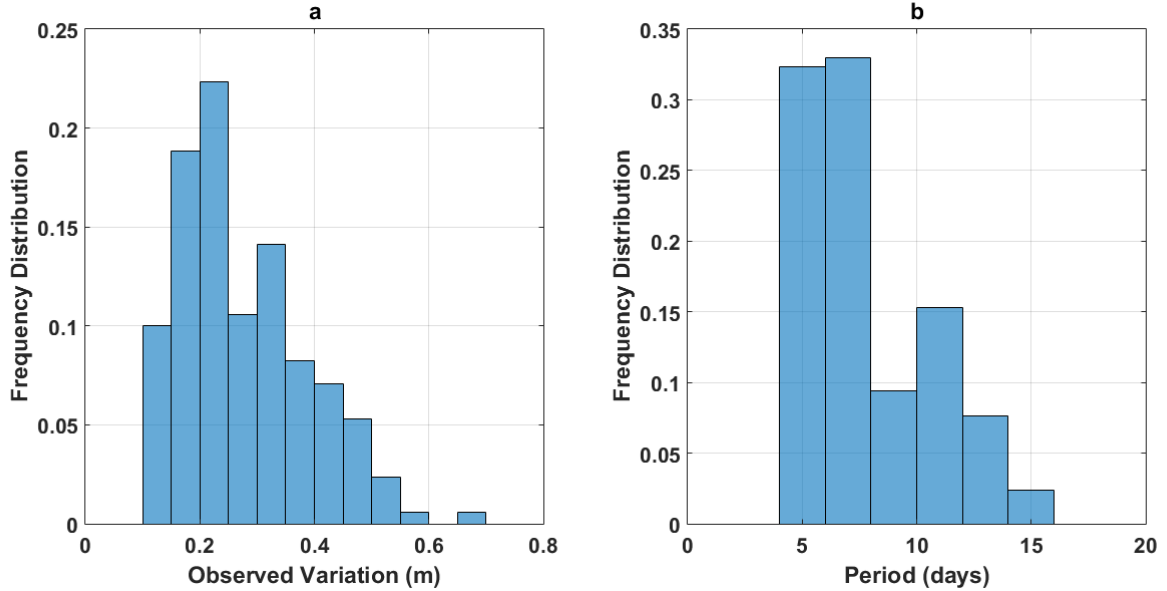
Figure 14: Histogram of observed sea level variation (a) and period (b) for all CTWs identified in Figure 13.

The comparison between IFI 3-24 days filtered sea level and cold front events was a first estimate of how remote areas could impact the subinertial in GB, but lacks confidence because timeseries data was compared against isolated events. Therefore, a comparison of subinertial CFSR wind with subinertial IFI level was made (Figure 15). For both U and V wind components, the RS coast exhibited the highest correlation with IFI sea level (0.65 and 0.66, respectively). This result corroborates with the hypothesis of this study since it shows that CTW and remote winds play an important influence in GB subinertial sea level variability. In addition, the lag (1.5 day) for both components agrees with the mean CTW propagation velocity observed by DOTTORI and CASTRO (2018). A CTW with speed of approximately 10 m s^{-1} would take between 1.5 and 2 days to travel from RS coast to GB.
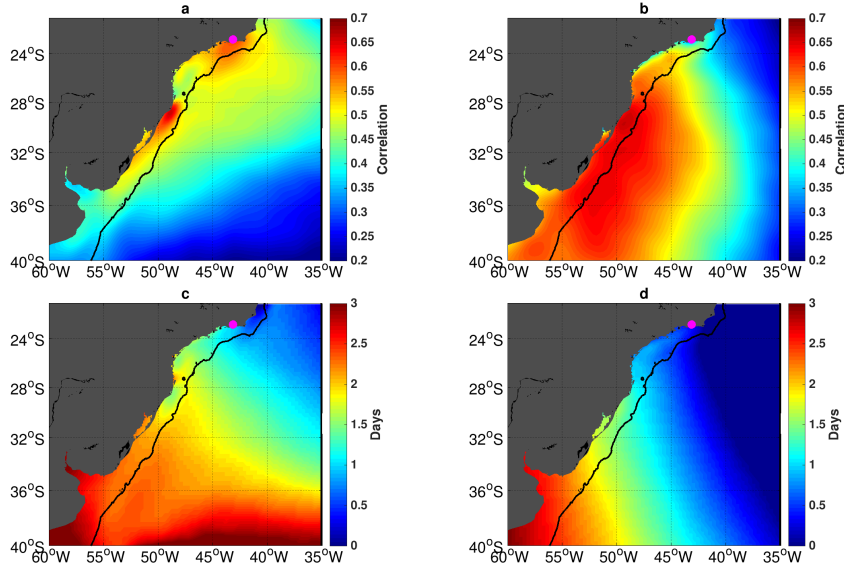
Figure 15: Maximum correlation between remote wind velocity and subinertial IFI's sea level for U and V components (a and b respectively) and respective lags of maximum correlation (c and d respectively). IFI location is indicated by a magenta circle.

3.1.2 Influence of Local Wind

In terms of the influence exerted by the wind in the vicinity of GB, a correlation analysis with IFI subinertial sea level can identify which aspect is more important in driving GB subinertial sea level variability. The use of alongshore and cross-shore components (along and cross 200 m isobath) allows a direct inference with Ekman transport and wind setup, respectively. Figure 16 shows that the highest correlation values were found on the continental shelf adjacent to GB (0.58 for the alongshore and 0.59 for the cross-shore components). The correlation between wind intensity considering alongshore and cross-shore wind components with IFI sea level exhibited comparable intensities, which suggests that Ekman transport and local wind setup have similar impacts on IFI subinertial sea level. Cross-shore wind component caused a more rapid response on subinertial sea level (a lag of approximately 20 hours), while alongshore wind component exhibited a slower response (a lag of approximately 30 hours). In addition, the approach of different rotation angles was crucial for a better understanding of the wind influence on IFI subinertial sea level due to the abrupt change of continental shelf orientation.
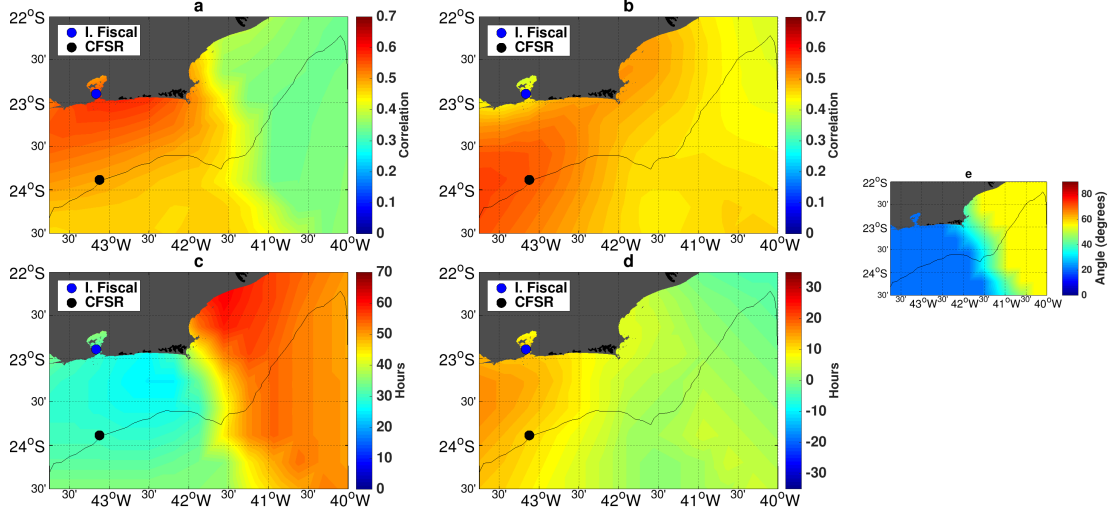
Figure 16: Maximum correlation between local wind velocity and IFI subinertial sea level for alongshore and cross-shore components (*a* and *b*, respectively), and respective lags of maximum correlation (*c* and *d* respectively). IFI location is indicated by a blue circle. The black circle represents the CFSR grid point used for comparison with IFI data. The angles of rotation used to obtain the alongshore and cross-shore wind components are presented in (*e*).

An important effect of local wind is to decrease the GB subinertial sea level. Intense and persistent E/NE winds have the alongshore component much greater than the cross-shore. This leads to an offshore Ekman transport, decreasing the GB subinertial sea level. This was observed in Figure 17, where strong and persistent E/NE winds led to decreasing sea level in GB. This process can be observed during some events (e.g., September 2007, October 2008, and November 2008). However, strong and persistent E/NE winds would not be enough to decrease the sea level in GB (e.g., October 2007, October 2009, and December 2010). This fact reinforces our hypothesis that different forcing mechanisms drive the subinertial sea level in GB. Finally, persistent but weak E/NE winds can not be associated to lower sea level in GB (e.g., March 2007, February 2009, and January and February 2010).
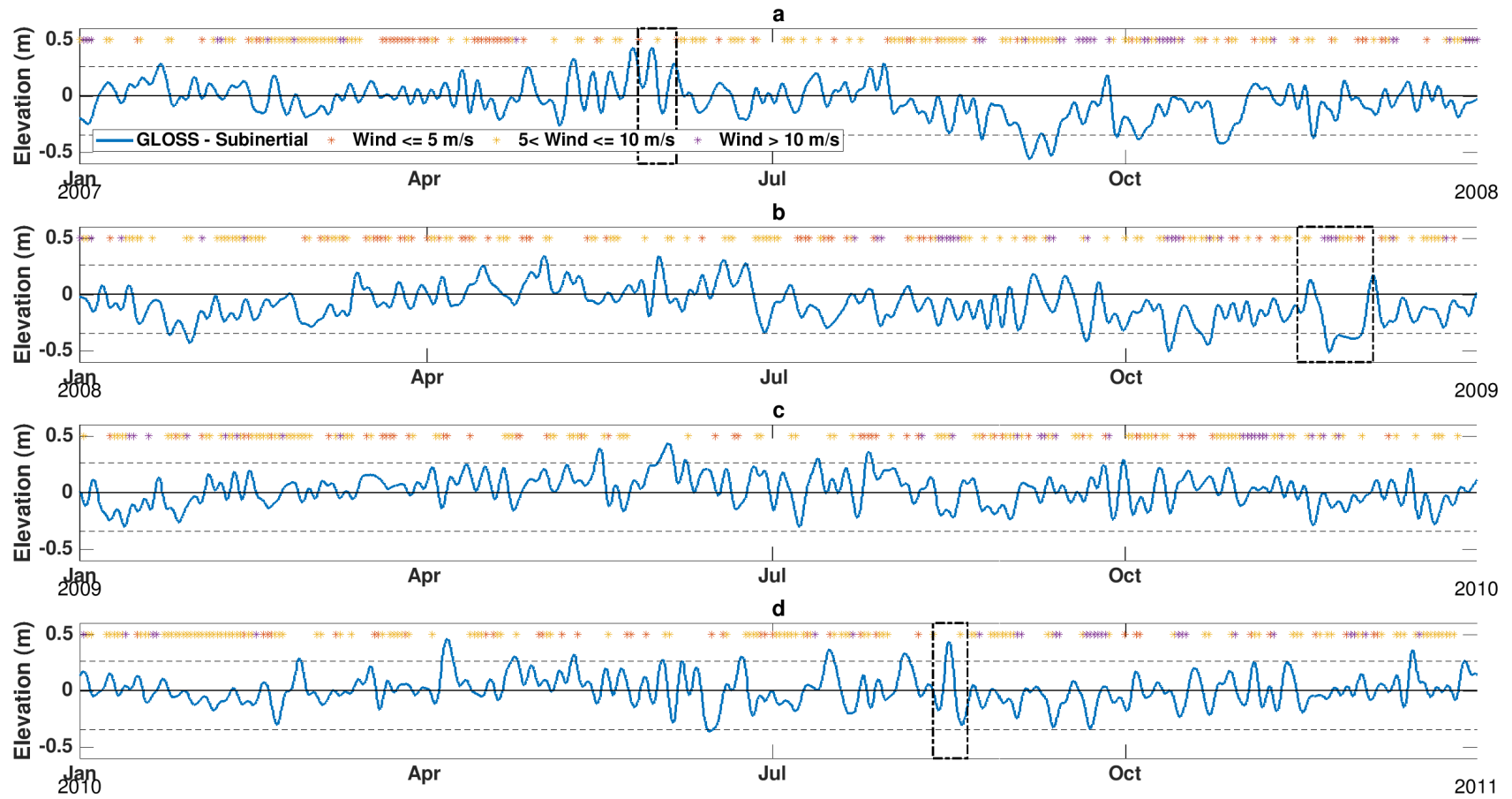
Figure 17: Time series of IFI subinertial sea level data from 2007 to 2010 (a to d). Intensity of easterly and northeasterly winds are indicated by coloured asterisks (orange for ≤ 5 m s^{-1}, yellow for > 5 and ≤ 10 m s^{-1} and purple for > 10 m s^{-1}). The location where wind components were extracted is indicated in Figure 16.

3.1.3 Influence of the Brazil Current

Another important forcing mechanism to be considered is the WBC. Even though, less intense than other WBCs (e.g., Gulf Stream, Kuroshio Current), the influence of BC variability on coastal areas worths to be analyzed. Power spectra of BC transport (Figure 18) shows more energetic processes among the ones with periods higher than 60 days. One energetic band was found centered around 65 days and a broad energetic band presents a period of hundreds days. Several less intense peaks were observed between 3 and 60 days. This finding shows that an important part of the BC volume transport is driven by low-frequency mechanisms and therefore an analysis of a $\geq$ 60-day period band is more suitable. Indeed, previous studies demonstrated the BC interannual variability, even relating its volume transport variability to Multivariate El Niño Index (DE AZEREDO, 2017; JUNIOR, 2005).
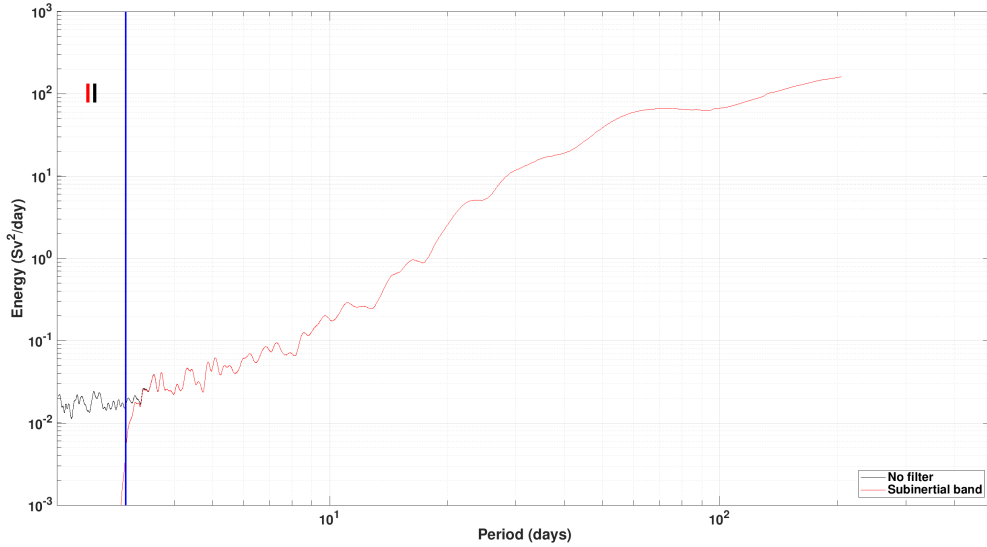
Figure 18: Power spectra for BC transport time series from 2007 to 2010. Power spectra for unfiltered data (black line), subinertial band (blue line) and $\geq$ 60 days band (red line) were calculated. Vertical thick lines represent the error bar for each time series. Vertical blue line represents the 3-day cutoff period.

Figure 19 shows the influence of long-period events on BC volume transport variability. While BC presents a subinertial volume transport of about -3.25 $\pm$ 1.83 Sv, its mean volume transport considering $\geq$ 60-day events is almost the same (-3.24 $\pm$ 1.60 Sv). In addition, subinertial BC volume transport reached extreme values (> 2*std) in 4 events (November/2009, February/2010, March/2010, and December/2010). In 3 out of 4 times, the low-frequency BC volume transport reached extreme values (November/2009, February/2010, and December/2010).
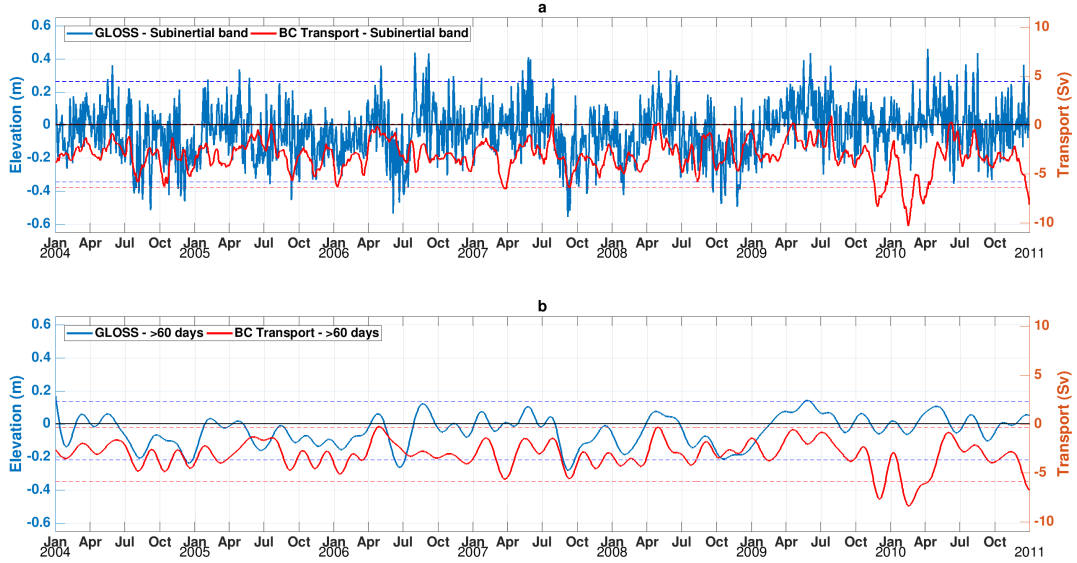
Figure 19: Time series of subinertial (a) and ≥ 60 days bands (b) for IFI sea level (blue line) and BC transport (red line) data. The dashed lines represent the extreme events indicated by two standard deviations from the associated mean.

Figure 19 and Table 3 show a greater similarity between GB level and BC volume transport in the low-frequency band (≥ 60 days) compared to the subinertial band. BC volume transport presented a correlation of 0.21 with GB level between 2004 and 2010 in the subinertial band and 0.31 in the low-frequency band. Almost every maximum correlation lag was less than a month. Furthermore, annual correlations higher than 0.50 were found for all remaining years apart from 2006 and 2010. An increased BC volume transport after November/2009 is evident, reaching up to -10 Sv (as this is not the scope of the present study, no further analysis will be made regard this topic). However, even with increased BC volume transport, a correlation of 0.14 (0.37) in the subinertial band (≥ 60 days band) between BC volume transport and GB level was found on 2010. That was the year when more intense CTWs reached GB (Figure 13) and a greater correlation with cold front occurrence at RS shoreline was found (Table 2), suggesting that extreme CTWs ($\geq 2 \times$STD) tend to overcome BC variability influence on GB sea level (no cold front occurrence before 2007 was analysed by this study).

Table 3: Correlation between subinertial IFI sea level data and BC volume transport from 2004 to 2010 and for each year. Correlations were calculated for two different windows (Subinertial band and ≥ 60 days band). Maximum correlation lags (in days) are presented in parentheses.

	2004	2005	2006	2007	2008	2009	2010	Total
Sub.	0.44 (-2)	0.29 (-85)	0.15 (0)	0.41 (-2)	0.33 (0)	0.36 (0)	0.14 (-22)	0.21 (-1)
≥ 60	0.73 (0)	0.58 (-77)	0.28 (-7)	0.66 (-6)	0.50 (0)	0.62 (-10)	0.37 (-28)	0.31 (-8)

3.1.4 The seasonal sea level pattern

GB low-frequency sea level tends to be positive during fall and winter, and negative during spring and summer (Figure 20). During summer, low-frequency sea level at IBI tend to be higher than at IFI. This difference can be related to the different period of data acquisition (Figure 3). Rapid changes in IBI mean sea level are explained by the lack of data, which adds uncertainties to the analysis. On a climatological perspective, the comparison of coastal sea level and BC transport shows a good agreement in seasonal scales. A possible mechanism for that is related to the cross-shore pressure gradient that supports the BC, as an intense BC volume transport is related to an intense pressure gradient, lowering the sea level in GB. On the other hand, a weakening of the BC volume transport would relax this pressure gradient and, as a result, the sea level in GB increases.
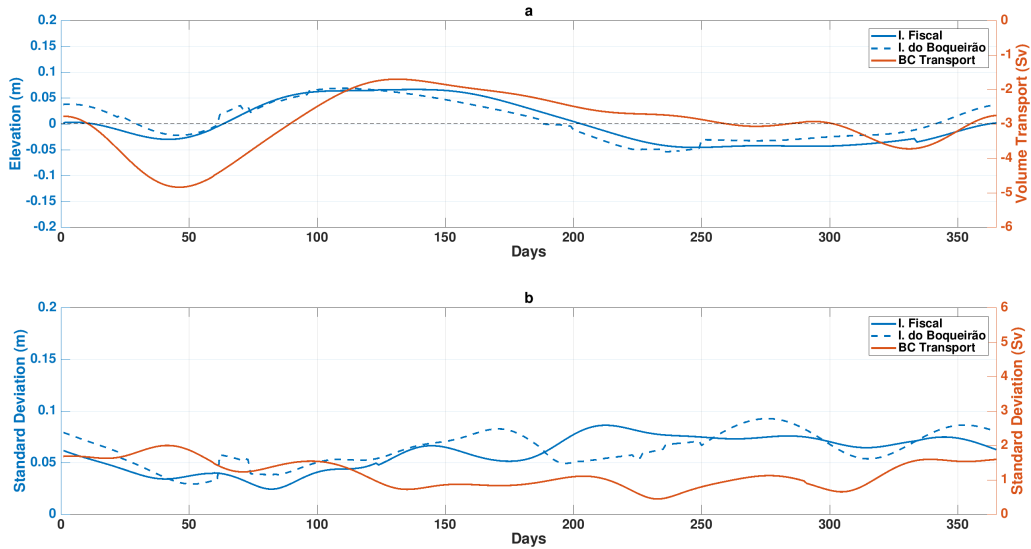
Figure 20: Climatology of the daily mean (a) sea level at IFI (blue lines), IBI (red lines) stations and the BC volume transport. The respective standard deviation is presented in (b).

3.2 DELFT3D performance

This section presents the performance of DELFT3D in modeling subinertial processes in GB. It is divided into 3 subsections: *i*) Modeled period, *ii*) Sea level, and *iii*) depth-averaged velocity.

3.2.1 Modeled period

Firstly, as REMO output ranges from 2004 to 2010, an analysis of REMO performance in modeling subinertial level in GB must be done to choose the modeling period that REMO (DELFT3D boundary condition) provides the most adequate results compared to the observed data (Figure 21 and Table 4).
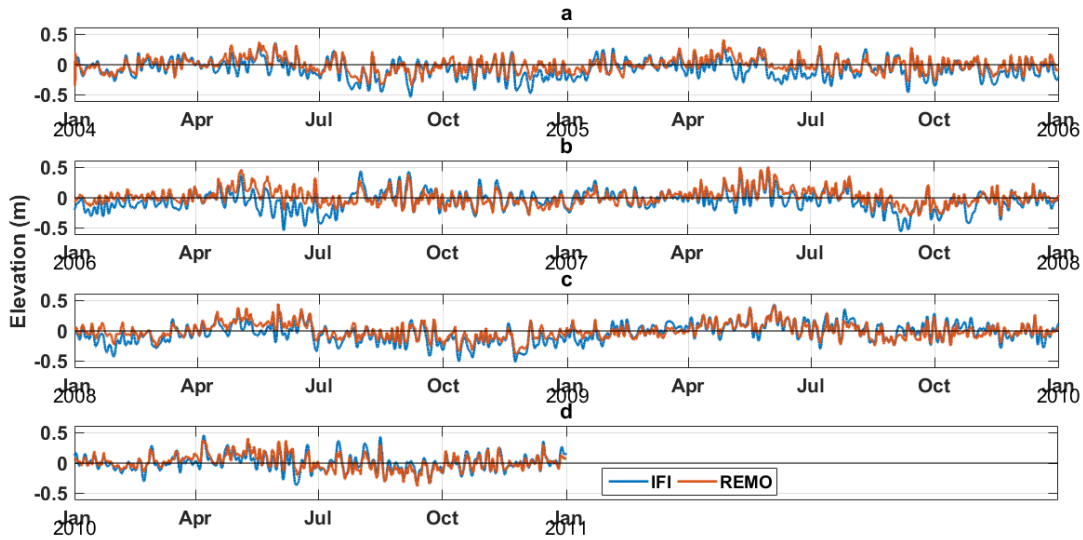
Figure 21: Subinertial sea level at the GB entrance for REMO's product (red line) and IFI station (blue line) from 2004 to 2005 (*a*), 2006 to 2007 (*b*), 2008 to 2009 (*c*), and 2010 (*d*).

Figure 21 shows that REMO product has an satisfactory overall performance in modeling subinertial processes at IFI station. Table 4 shows a correlation of 0.78 for the whole period (2004 to 2010), however 2006 presented a considerably lower correlation compared to the following years (0.61). In addition, no significant differences were found for the standard deviations of REMO and IFI. Therefore, the period from 2007 to 2010 was chosen for modeling purposes. As this analysis focused on choosing the best period for modeling subinertial processes in GB, no further analysis were performed regarding REMO performance.

Table 4: Statistical comparison between subinertial sea level (in m) from REMO outputs and IFI for each year between 2004 and 2010. Mean, standard deviation, root mean squared error (RMSE), correlation coefficient and coefficient of determination are shown.

		2004	2005	2006	2007	2008	2009	2010	Total
IFI	Mean	-0.0741	-0.0652	-0.0510	-0.0399	-0.0913	0.0248	0.0082	-0.0412
	STD	0.1555	0.1368	0.1550	0.1557	0.1527	0.1320	0.1341	0.1516
REMO	Mean	-0.0212	0.0019	0.0023	0.0174	-0.0186	0.0076	0.0105	0.0000
	STD	0.1265	0.1106	0.1235	0.1323	0.1355	0.1106	0.1275	0.1249
	RMSE	0.0860	0.0849	0.1255	0.0892	0.0658	0.0742	0.0754	0.0933
	Corr.	0.7394	0.7843	0.6146	0.8194	0.9022	0.8268	0.8349	0.7888
	R^2	0.6950	0.6150	0.3780	0.6720	0.8140	0.6840	0.6790	0.6220

3.2.2 Sea level response

After choosing the modeled period, an analysis of DELFT3D performance can be made. Figure 22 shows the modeled subinertial sea level at IFI station for every experiment performed compared against observed data. It was shown that the modeled subinertial sea level presents a good agreement when compared to the observed subinertial sea level at IFI. Sea level reached values up to 46.6 cm and 38 cm during events of increasing sea level and events of decreasing sea level, respectively. In addition, almost every extreme event was observed in all three experiments, but less intense compared to the observed data. Extreme events tend to occur throughout the year with no seasonal distinction, but the more likely period for extreme events is from April to October for both observed and modeled data.

Figure 22: Subinertial sea level at Ilha Fiscal station from 2007 to 2010 (*a* to *d* respectively). IFI (blue line), EXP 1 (red line), EXP 2 (black line), and EXP 3 (magenta line) are shown. Respective coloured dashed lines represent the two standard deviation interval. Table 1 shows the details of the 3 experiments mentioned above.

All three experiments presented a good correlation with IFI, IBI and PAR observed data (≥ 0.83, ≥ 0.74, ≥ 0.79, respectively) (Tables 5, 6 and 7). The correlation calculated between DELFT3D experiments and IFI sea level data was also similar to the correlation obtained between REMO output and IFI data from 2007 to 2010 (0.8358, not shown). It is important to mention that this fact does not invalidate the higher resolution model, once it propagates from the continental shelf subinertial dynamics towards inner GB, where scarce spatial coverage data were possible before these simulations.

Table 5: Correlation between IFI subinertial sea level and modeled experiments (EXP 1, EXP 2, and EXP 3) for the same period as in Figure 3 for IFI. The standard deviation, root mean squared error (RMSE) and coefficient of determination are also presented.

	IFI	EXP 1	EXP 2	EXP 3
Corr.	–	0.837	0.837	0.838
STD	0.151	0.120	0.120	0.123
R^2	–	0.700	0.700	0.701
Mean	0.025	-0.011	-0.011	-0.013
RMSE	–	0.066	0.066	0.067

Table 6: Correlation between IBI subinertial sea level and modeled experiments (EXP 1, EXP 2, and EXP 3) for the same period as in Figure 3 for IBI. The standard deviation, root mean squared error (RMSE) and coefficient of determination are also presented.

	IBI	EXP 1	EXP 2	EXP 3
Corr.	–	0.742	0.742	0.739
STD	0.146	0.120	0.120	0.125
R^2	–	0.550	0.550	0.547
Mean	0.025	0.017	0.017	0.013
RMSE	–	0.072	0.072	0.077

Table 7: Correlation between PAR subinertial sea level and modeled experiments (EXP 1, EXP 2, and EXP 3) for the same period as in Figure 3 for PAR. The standard deviation, root mean squared error (RMSE) and coefficient of determination are also presented.

	PAR	EXP 1	EXP 2	EXP 3
Corr.	–	0.795	0.795	0.794
STD	0.126	0.120	0.120	0.123
R^2	–	0.632	0.632	0.630
Mean	0.030	-0.027	-0.027	-0.031
RMSE	–	0.053	0.053	0.054

3.2.3 Depth-averaged velocity

As no observed velocity data was available between 2007 and 2010, current roses for the depth-averaged velocity from modeled outputs and observed data (for different periods) were compared (Figures 23, 24, 25, and 26). Observed data was collected between 2015 and 2019 (see Figure 4c for the location of the buoys). As different periods were compared, seasonal events (> 24 days) were disregarded. Events from 3 to 24 days period were considered instead.
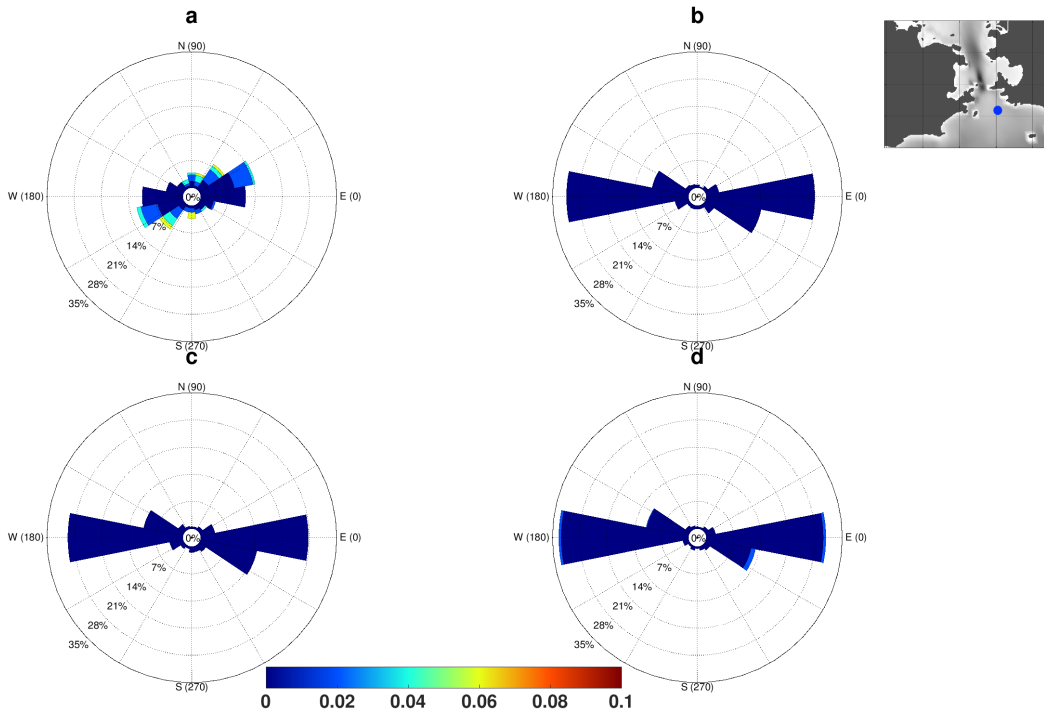
Figure 23: Current rose for 3 to 24-day period band depth-averaged velocity at RJ-1 station for SiMCosta data (a), EXP 1 (b), EXP 2 (c), and EXP 3 (d). Units in m s^{-1}. Location of the RJ-4 station is indicated by a blue circle on the upper right panel.
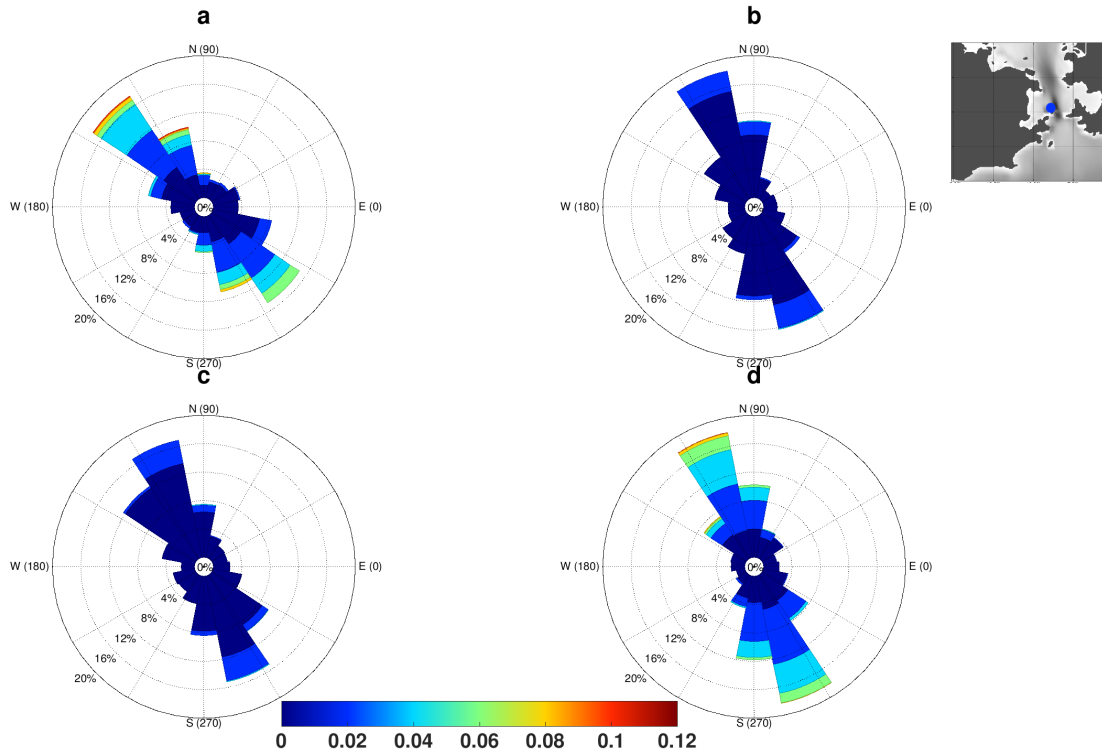
Figure 24: Current rose for 3 to 24-day period band depth-averaged velocity at RJ-2 station for SiMCosta data (*a*), EXP 1 (*b*), EXP 2 (*c*), and EXP 3 (*d*). Units in m s^{-1}. Location of the RJ-4 station is indicated by a blue circle on the upper right panel.

At RJ-1 and RJ-2 stations (Figures 23 and 24), DELFT3D experiments presented flow directions similar to the observed data (E/W and SE/NW oriented flow, respectively). EXP 3 showed depth-averaged velocities with magnitude comparable to observed data.
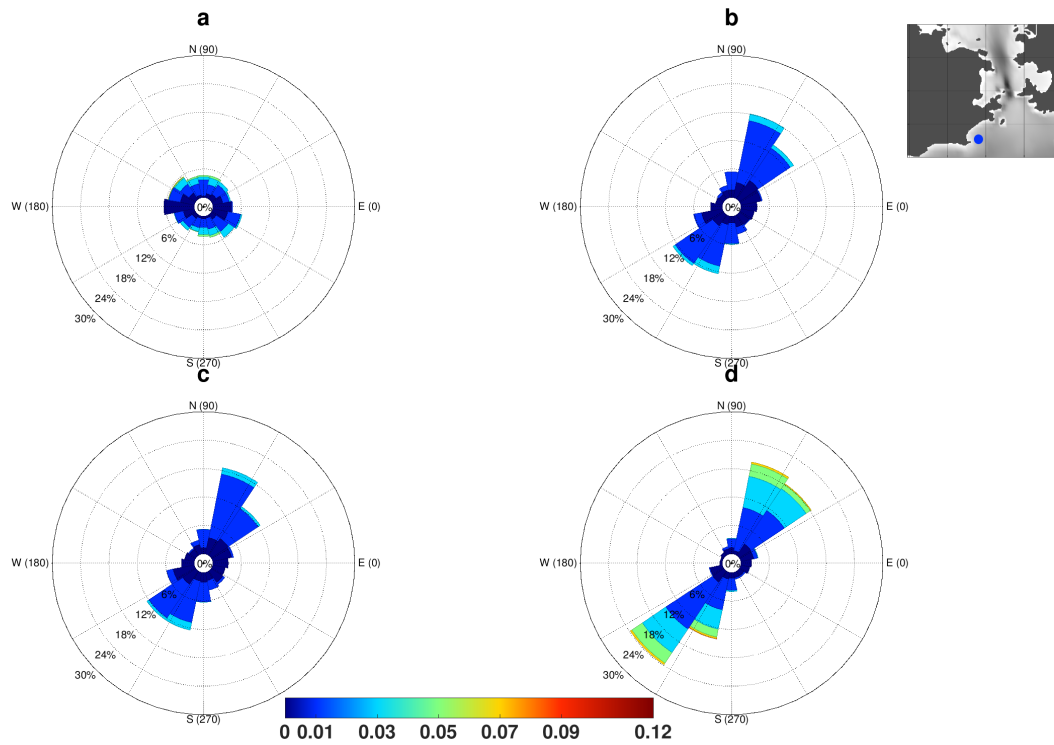
Figure 25: Current rose for 3 to 24-day period band depth-averaged velocity at RJ-3 station for SiMCosta data (*a*), EXP 1 (*b*), EXP 2 (*c*), and EXP 3 (*d*). Units in m s^{-1}. Location of the RJ-4 station is indicated by a blue circle on the upper right panel.
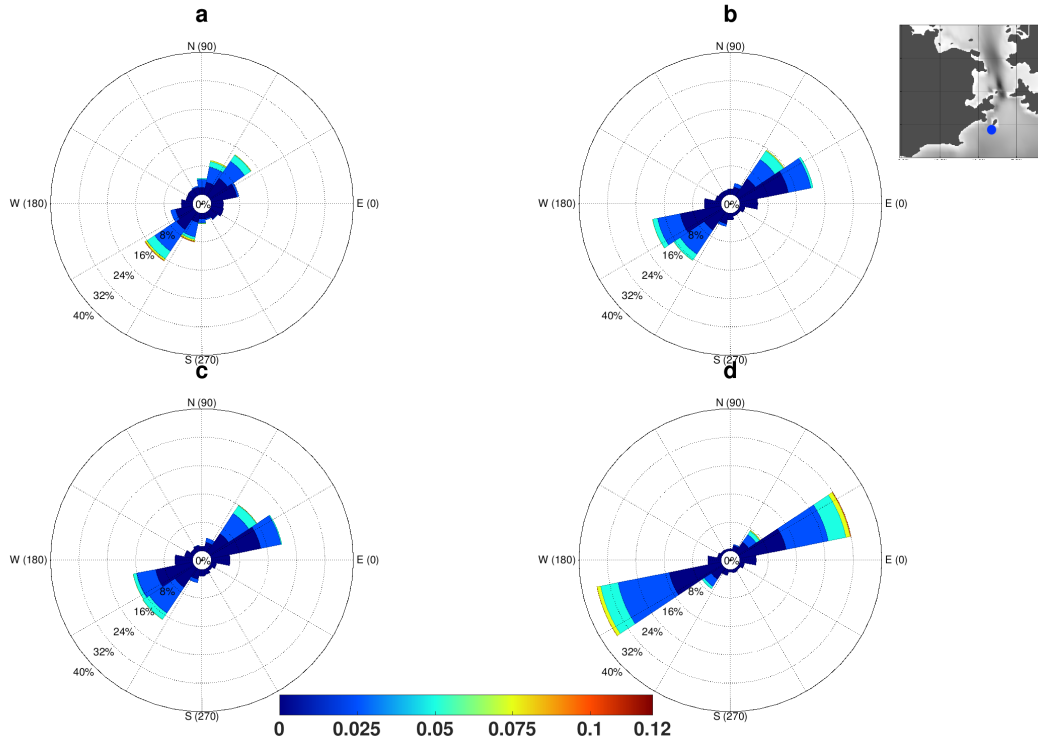
Figure 26: Current rose for 3 to 24-day period band depth-averaged velocity at RJ-4 station for SiMCosta data (*a*), EXP 1 (*b*), EXP 2 (*c*), and EXP 3 (*d*). Units in m s^{-1}. Location of the RJ-4 station is indicated by a blue circle on the upper right panel.

At RJ-3 station (Figure 25), while DELFT3D experiments presented a NE/SW oriented flow, observed data presented a flow with no prevailing direction. Those differences between modeled and observed depth-averaged velocity are, possibly, explained by processes with spatial scale less than 1 km, which is the horizontal grid resolution at RJ-3 station. Finally, RJ-4 station presented a good agreement with observational data (Figure 26). A SW/NE oriented flow with similar intensities was observed in every modeling experiment and observed data. EXP 3 (CFSR as atmospheric forcing) presented more intense depth-averaged velocities compared to other experiments.

3.3 DELFT3D experiments

After a 4-year simulation of GB subinertial dynamics, similar values of transport were observed for all experiments, but EXP 3 tends to present a slightly more intense transport compared to EXP 1 and 2 in all 3 sections (Figures 27, 28, and 29). Inflow events in GB1 (Figure 27) reached values up to 1663 m^3 s^{-1} (EXP 1), 1642 m^3 s^{-1} (EXP 2), and 2035 m^3 s^{-1} (EXP 3). Outflow events in GB1, on the other hand, reached values down to -1737 m^3 s^{-1} (EXP 1), -1749 m^3 s^{-1} (EXP2), and -1892 m^3 s^{-1} (EXP 3) (Figure 27).

The values shown above indicate the importance of subinertial processes in GB dynamics. This importance becomes evident when compared to subinertial volume transport values in Todos os Santos Bay, which presents a volume of approximately 11.4 × 10^9 m^3 (4.8 times greater than in GB) (AGUIAR *et al.*, 2019). In Todos os Santos Bay, the subinertial volume transport reached values up (down) to approximately +4000 (-4000) m^3 s^{-1} (around 2 times the volume transport modeled in GB outermost section). It is important to mention that this fact could also be related to topographic constrains in areas north of SBB (DOTTORI and CASTRO, 2018; DE FREITAS *et al.*, 2019).
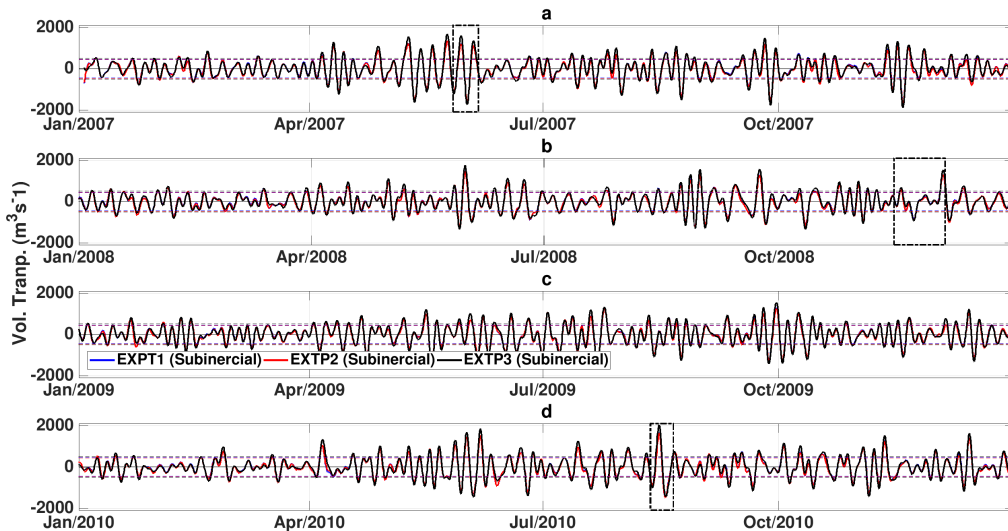
Figure 27: Modeled volume transport along GB1 from 2007 to 2010 (*a* to *d*, respectively). EXP 1 (blue line), EXP 2 (red line), and EXP 3 (black line) are shown. Respective coloured dashed lines represent the two standard deviation interval. Figure 11 indicates the geographical location of GB1 and Table 1 shows the details of the 3 experiments mentioned above. The dashed boxes represent selected periods used as case studies.

In GB2 (Figure 28), volume transport reached maximum inflow values close

to 1416 m^3 s^{-1} (EXP 1), 1432 m^3 s^{-1} (EXP 2), and 2069 m^3 s^{-1} (EXP 3), while offshore volume transport events reached values down to -1470 m^3 s^{-1} (EXP 1), -1612 m^3 s^{-1} (EXP 2), -1661 m^3 s^{-1} (EXP 1).

In GB3 (Figure 29), the extreme modeled volume transport were less intense than that modeled in the previous sections. Inflow events in GB3 reached values up to 1144 m^3 s^{-1} (EXP 1), 1118 m^3 s^{-1} (EXP 2), and 1630 m^3 s^{-1} (EXP 3), while the outflow values were -1143 m^3 s^{-1} (EXP 1), -1155 m^3 s^{-1} (EXP 2) and, -1234 m^3 s^{-1} (EXP 3).
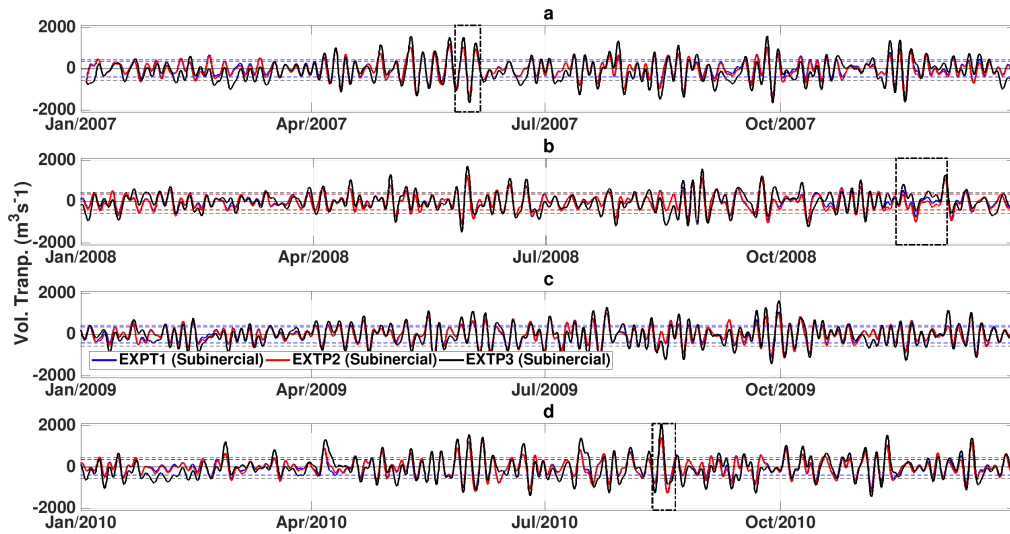
Figure 28: As in Figure 27, but for section GB2.
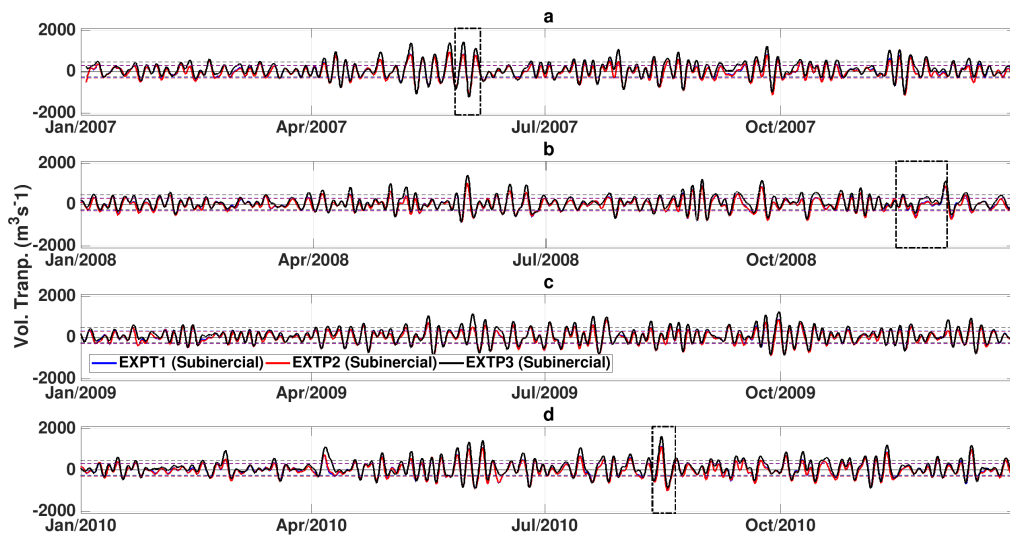
Figure 29: As in Figure 27, but for section GB3.

42

The variability of the volume transport decreases from GB1 to GB3 in all experiments (Table 8). Lower transport in GB3 could be related to the distance from the bay entrance, geometry of the section, and differences between modeled and "real" bathymetry (Figure 12). However, in inner GB areas, the influence of CFSR wind increase, resulting in a greater volume transport and variability compared to EXP 1 and 2. In addition, based on a comparison to the net volume transport in a spring tidal cycle, the subinertial volume transport across GB1, in both EXP 1 and EXP 2, is between 6.1 and 10.8% the value of the tide influence in GB. This value varies between 6.9 and 12.2% in the EXP 3. The value adopted for the net volume transport in a tidal cycle was obtained for a section closed to GB1 by BÉRGAMO (2006).

Table 8: Standard deviation of volume transport (m^3 s^{-1}) for each section (GB1, GB2, and GB3) for each experiment (EXP 1, EXP 2, and EXP 3).

	EXP 1	EXP 2	EXP 3
GB1	449	449	505
GB2	379	392	504
GB3	301	305	359

In terms of subinertial sea level, a decrease in correlation was observed in inner GB stations (Tables 5, 6 and 7). In general, the standard deviation of the observed subinertial sea level was greater than the modeled values. To some extent, this difference was expected, as the REMO's output, used as boundary condition for the model, exhibited a lower variability compared to observed IFI data (Table 4). EXP 3 presented slightly greater standard deviation compared to EXP 1 and EXP 2. This could be explained by the use of an offshore wind as local forcing.

3.3.1 Case studies

To analyze the influence of different forcing mechanisms, 3 periods were chosen as case studies. The influence of a CTW event on the GB subinertial dynamics was analyzed in two scenarios, where different offshore wind patterns (SW/S winds and SW/NE winds) were chosen. In addition, a period with E/NE persistent offshore winds established among two consecutive CTWs was chosen in order to understand the effect of an intense and persistent E/NE wind on GB subinertial dynamics. In each case study, 3 stages were chosen aiming a better visualization of the whole period. T_1 represents the stage of maximum inflow across GB1 in case studies 1 and 2, and the stage of maximum outflow across GB1 in case study 3. T_2 represents a stage of significantly low volume transport across GB1. T_3 represents the stage of maximum outflow across GB1 in case studies 1 and 2, and the stage of maximum

inflow across GB1 in case study 3. In addition, all case studies exhibited at least one extreme volume transport event during inflow and outflow for all three sections (Figures 27, 28 and 29).

Case study 1: A CTW event with varying offshore SW/S winds

From 12/08/2010 to 21/08/2010, a CTW, generated from a cold front system along RS coast, propagated along the GB's adjacent shelf (Figure 13d). It is important to mention that 2010 was the year with more extreme CTWs among the modeled period. Another important aspect is that, between 12/08/2010 and 21/08/2010, no NE/SE offshore wind were identified in CFSR data (Figure 17d). Under this scenario (more specifically in EXP 3) the adjacent shelf was under the effect of intense SW/S winds which decreased in magnitude during case study 1 (Figures 30c, 31c, and 32c). EXP 2 had easterly winds (less than 4 m s^{-1}) as atmospheric forcing, with occasional northerly winds (2.5 m s^{-1}).

Based in Figures 30, 31, and 32, it can be observed that the CTW was responsible for a sea level variation of approximately 53 cm in all three experiments. The entire bay responded as a whole to the increase and decrease in water level. In addition, depth-averaged velocities ranged between -3 and 5 cm s^{-1} (EXP 1), -3.5 and 6 cm s^{-1} (EXP 2), and -4.5 and 8 cm s^{-1} (EXP 3), at GB main channel. Without the influence of wind (EXP 1), the CTW entered GB as a well-behaved flow. Deeper areas exhibited greater velocities and shallower areas exhibited near zero velocities. It can be observed that the wind acted in transferring energy to the currents, resulting in recirculation cells inside the bay. EXP 2 exhibited less intense recirculation cells when compared to EXP 3.

In EXP 2, more recirculation cells were observed during inflow (Figure 30b). A 4 m s^{-1} easterly wind was responsible for the establishment of recirculation cells in shallow areas ($\leq$ 10 m) between GB1 and GB2, and on the inner GB. When wind intensity decreased (Figures 31b and 32b), the flow pattern became more similar to that in EXP 1 (Figures 31a and 32a) but recirculation cells were still present in shallow areas.

Considering the EXP 3, intense SW winds (Figure 30c) transferred too much energy to the ocean, creating intense recirculation cells in shallow areas. This intense wind (11 m s^{-1}) generated an intense flow in the eastern portion of the main channel. Afterward, the wind weakened (7 m s^{-1}) and changed direction (N and E) (Figures 31c and 32c). This change in wind pattern decreased the intense flow formed by intense SW winds. In addition, easterly winds were not sufficiently strong to intensify the flow in the western portion of the main channel as intense SW winds were in the eastern portion of the main channel.

The volume transport in each experiment is shown in Figure 33. Volume

transport ranged approximately from +1640 to -1490 m^3 s^{-1} (EXP 1 and EXP 2) and from +2030 to -1440 m^3 s^{-1} in EXP 3. The wind did not alter significantly the sea level and transport in EXP 2 compared to EXP 1. The pattern of accumulative volume transport were similar for EXP 1 and EXP 2, however, it changed slightly in the shallower section (GB3) (Figure 33a-c), where the wind could modify more effectively the depth-averaged velocity.

Considering the EXP 3, intense SW/S winds were observed during T_1 and T_2, resulting in a different volume transport pattern along the sections (Figure 33). During the inflow, the maximum volume transport in EXP 3 was almost 24% greater than in EXP 2 and EXP 3. This result shows that the intense SW winds had a strong potential to impact the subinertial dynamic in GB. On the other hand, easterly wind (T_3) did not impact strongly the volume transport along GB (Figure 33c, f and i), once the pattern was similar to those in previous experiments.
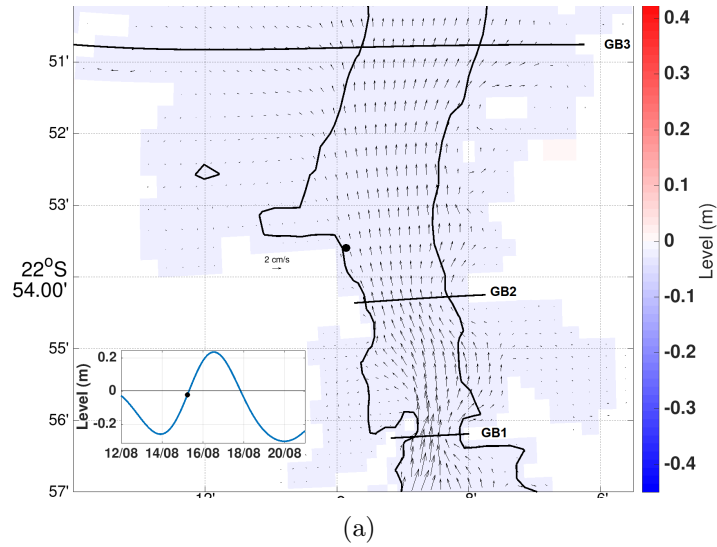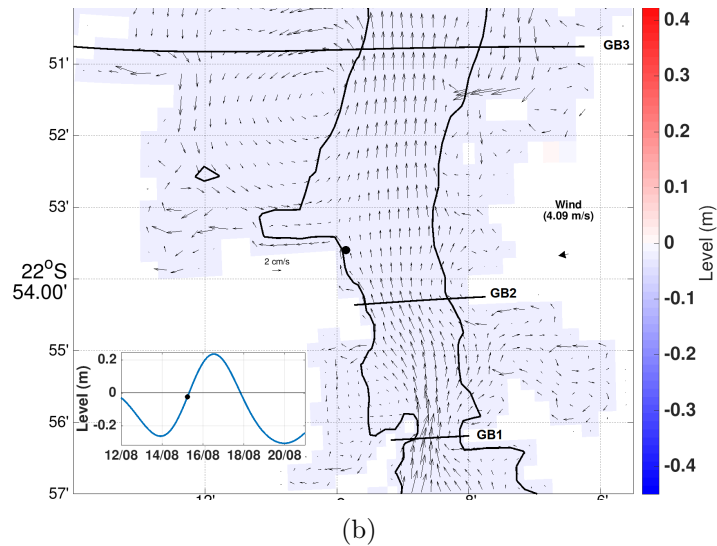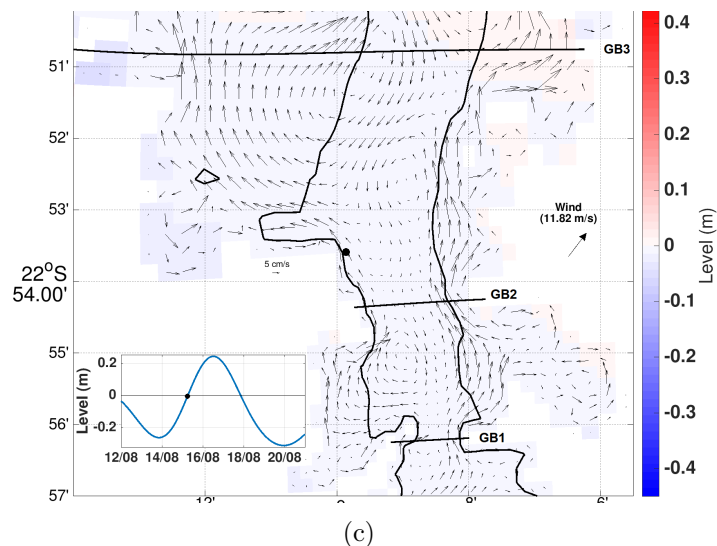
Figure 30: GB depth-averaged velocity and sea level representation for EXP 1 (a), EXP 2 (b), and EXP 3 (c) for T_1 (inflow situation) of case study 1 (black circle in sea level time series). Colorbar represents the sea level and black arrows indicate depth-averaged velocities. Location of sections GB1, GB2 and GB3, and IFI (black circle) are indicated. Bold line represents the 10 m isobath. Instant wind magnitude and direction are also indicated.

46

Figure 31: GB depth-averaged velocity and sea level representation for EXP 1 (*a*), EXP 2 (*b*), and EXP 3 (*c*) for T_2 (highest sea level situation) of case study 1 (black circle in sea level time series). Colorbar represents the sea level and black arrows indicate depth-averaged velocities. Location of sections GB1, GB2 and GB3, and IFI (black circle) are indicated. Bold line represents the 10 m isobath. Instant wind magnitude and direction are also indicated.

Figure 32: GB depth-averaged velocity and sea level representation for EXP 1 (a), EXP 2 (b), and EXP 3 (c) for T_3 (outflow situation) of case study 1 (black circle in sea level time series). Colorbar represents the sea level and black arrows indicate depth-averaged velocities. Location of sections GB1, GB2 and GB3, and IFI (black circle) are indicated. Bold line represents the 10 m isobath. Instant wind magnitude and direction are also indicated.

48
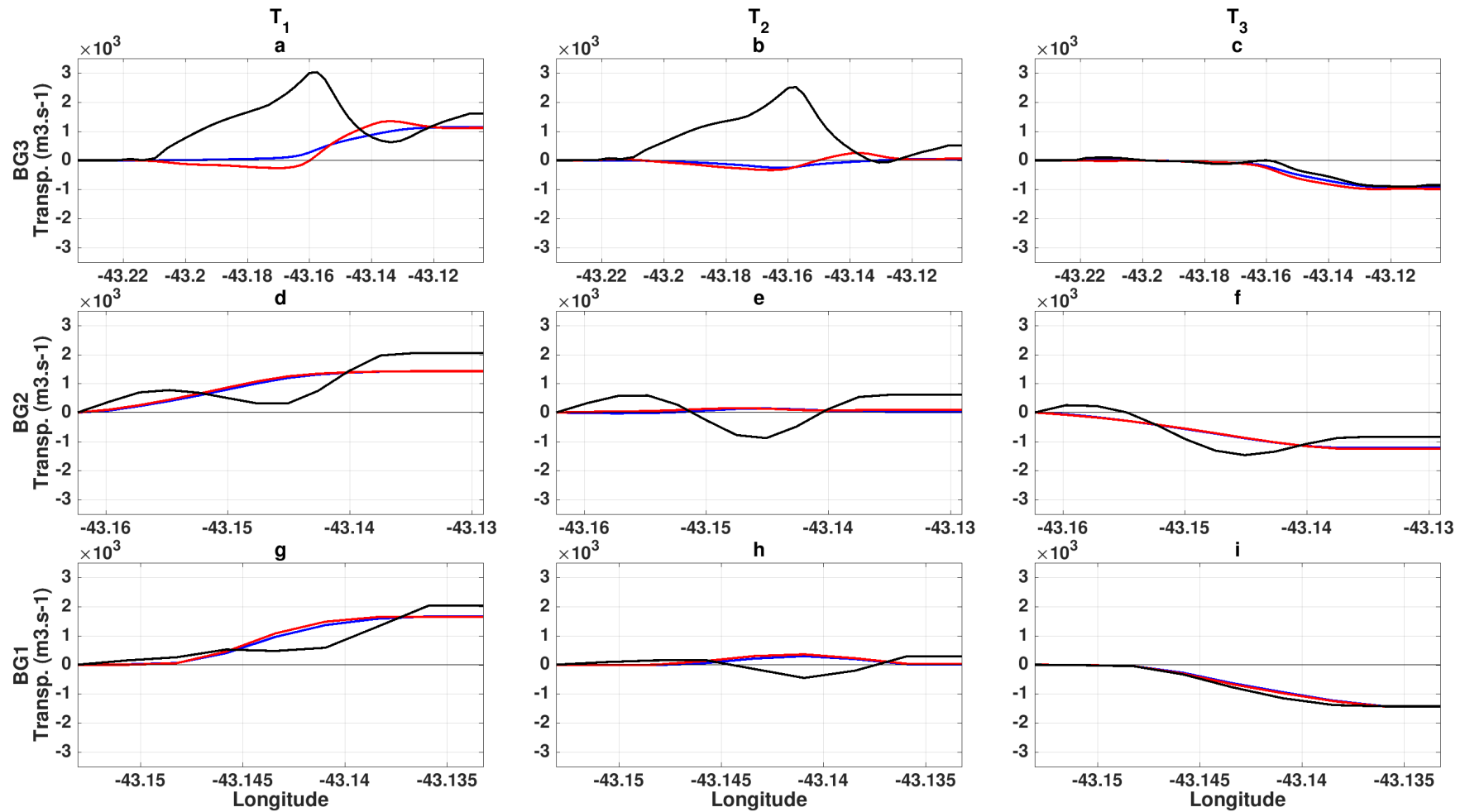
Figure 33: Cumulative volume transport along sections GB3 (a to c), GB2 (d to f), and GB1 (g to i) for case study 1. Left panels represent T_1, central panels represent T_2, and right panels represent T_3. EXP 1, EXP 2, and EXP 3 are represented by blue, red and black lines respectively.

Case study 2: A CTW event with varying offshore SW/NE winds

The second case study has some similarities with the previous one. Between 27/05/2007 and 05/06/2007, a CTW, generated from a cold front system along RS coast, propagated along the GB's ACS (Figure 13a). Just like case study 1, no NE/SE offshore wind was observed in CFSR data (Figure 17a). The only difference here is that the offshore wind reversed completely its direction (from SW to NE) from the beginning to the end of the case study 2 (Figures 34c, 35c, and 36c). EXP 2 exhibited easterly winds (less than 4 m s^{-1}) in the beginning of the period but decreased to 0.5 m s^{-1}.

With the arrival of the CTW at the GB entrance, GB subinertial sea level increased 35 cm in all experiments. At the main channel, velocities reached 3.5, 4 and 9 cm s^{-1} for EXP 1, EXP 2, and EXP 3, respectively. The greatest velocity found in EXP 3 occurred because of the intense SW wind (up to 11.6 m s^{-1}). The intense flow in the eastern portion of GB, observed in case study 1 was also observed in case study (Figure 35c). In addition, the passage of the CTW caused a sea level variation of 43 cm in all experiments. Velocities reached -3.5 cm s^{-1} (EXP 1), -3.5 cm s^{-1} (EXP 2), and -5 cm s^{-1} (EXP 3) at the main channel.

Considering the EXP 3 during the outflow, the wind was blowing in the opposite direction, but weaker (NE 8.5 m s^{-1}), therefore the wind influence was not sufficiently strong to overcome the pre-established pattern, resulting in weaker outflow currents (-5 cm s^{-1}).

The volume transport reached up to 1200 m^3 s^{-1} (EXP 1 and EXP 2), and 1600 m^3 s^{-1} (EXP 3) during the inflow (Figure 37). During the outflow, the volume transport reached down to -1600 m^3 s^{-1} (EXP 1 and EXP 2), and -1730 m^3 s^{-1} (EXP 3). The outflow volume transport was greater compared to the inflow, because the level variation caused by the CTW was 8 cm higher than the sea level increase caused by the arrival of the CTW at the GB entrance.
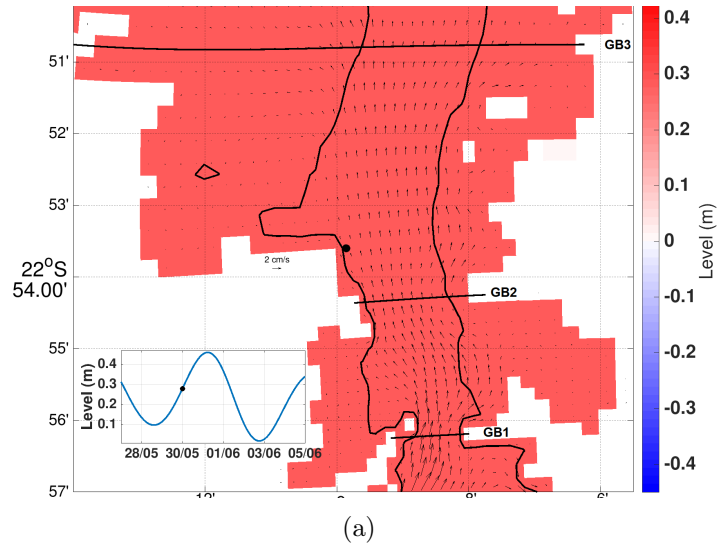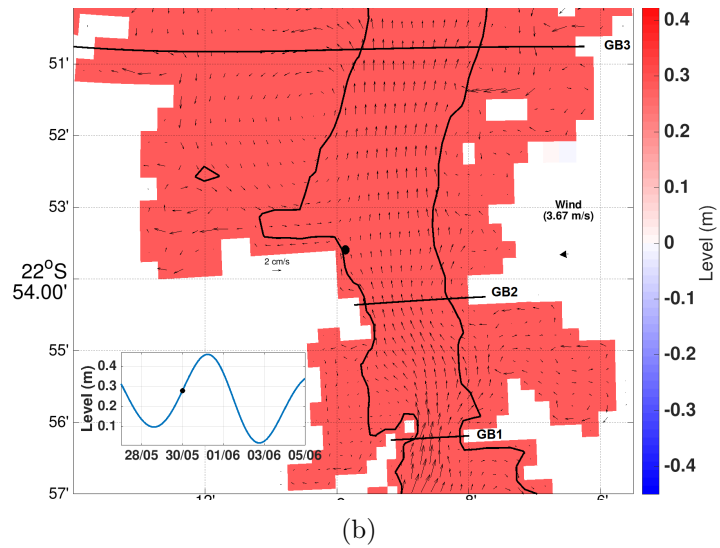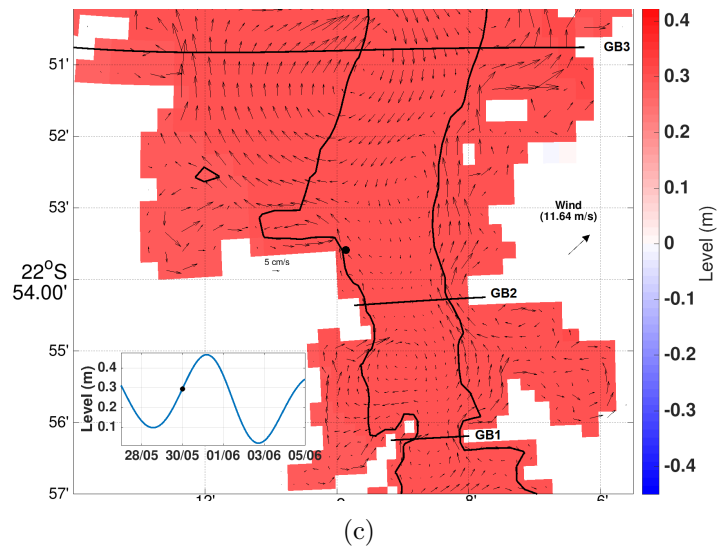
Figure 34: GB depth-averaged velocity and sea level representation for EXP 1 (a), EXP 2 (b), and EXP 3 (c) for T_1 (inflow situation) of case study 2 (black circle in sea level time series). Colorbar represents the sea level and black arrows indicate depth-averaged velocities. Location of sections GB1, GB2 and GB3, and IFI (black circle) are indicated. Bold line represents the 10 m isobath. Instant wind magnitude and direction are also indicated.
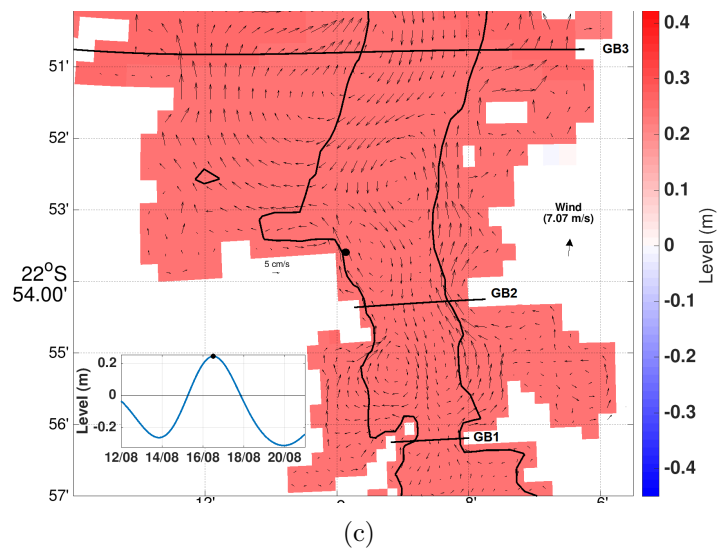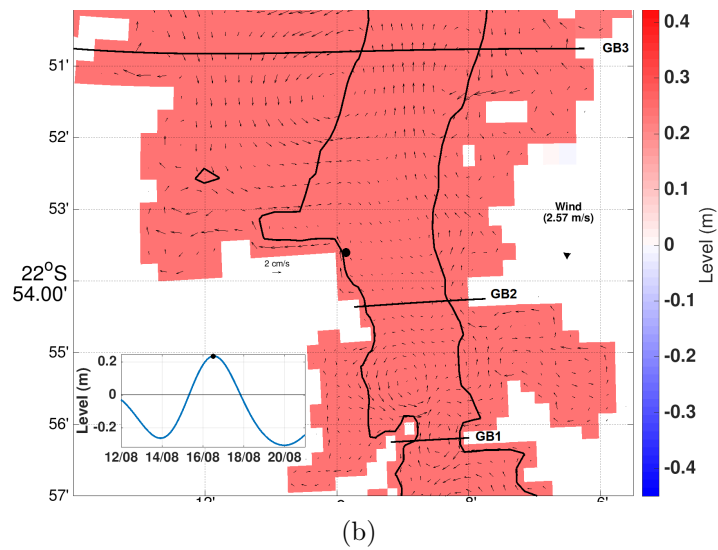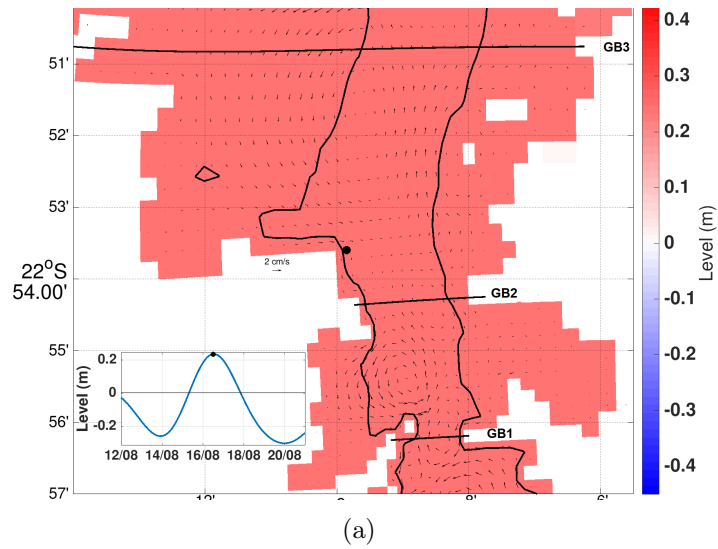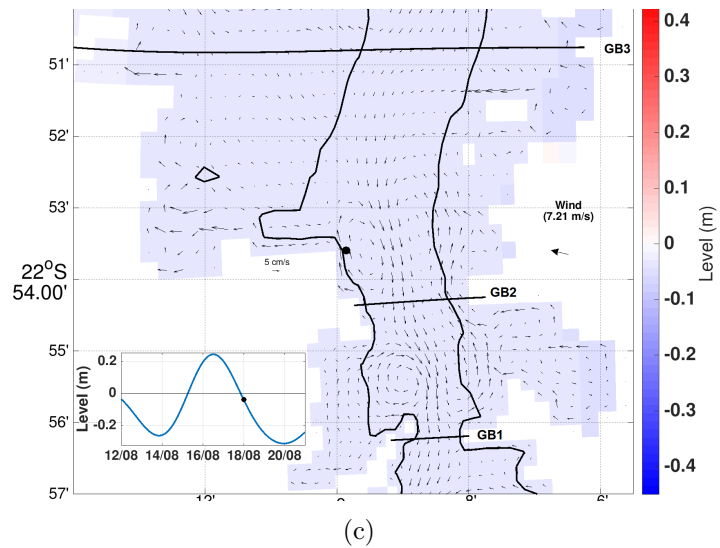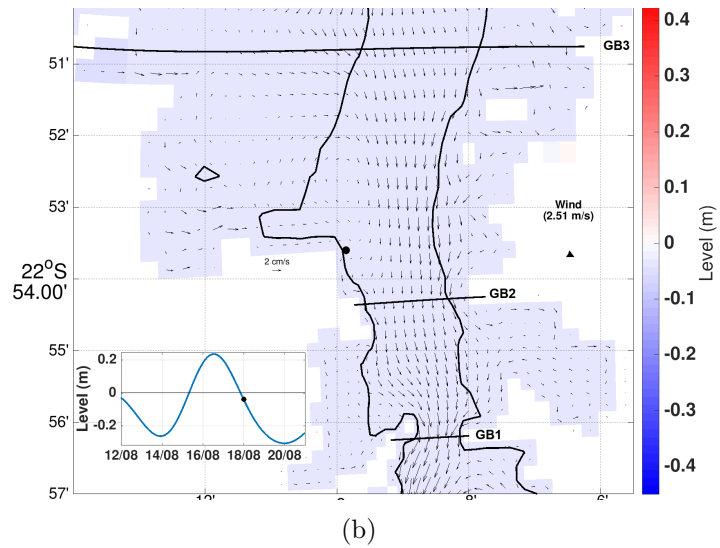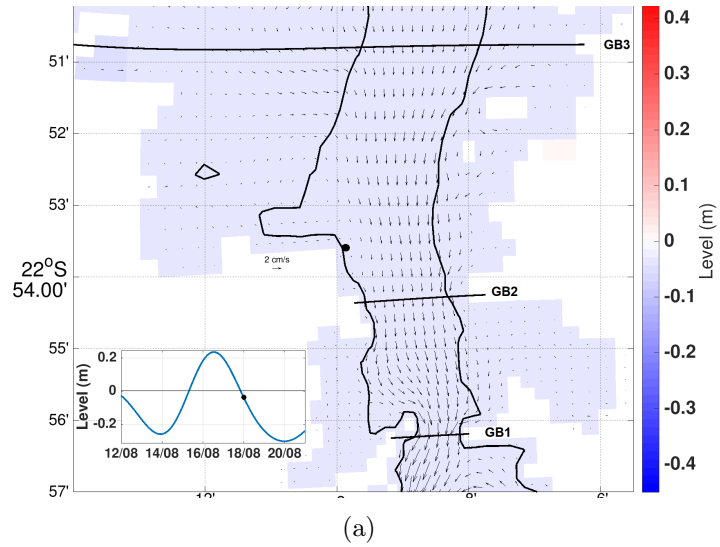
Figure 35: GB depth-averaged velocity and sea level representation for EXP 1 (a), EXP 2 (b), and EXP 3 (c) for T_2 (highest situation) of case study 2 (black circle on sea level time series). Colorbar represents the sea level and black arrows indicate depth-averaged velocities. Location of sections GB1, GB2 and GB3, and IFI (black circle) are indicated. Bold line represents the 10 m isobath. Instant wind magnitude and direction are also indicated.

Figure 36: GB depth-averaged velocity and sea level representation for EXP 1 (a), EXP 2 (b), and EXP 3 (c) for T_3 (outflow situation) of case study 2 (black circle in sea level time series). Colorbar represents the sea level and black arrows indicate depth-averaged velocities. Location of sections GB1, GB2 and GB3, and IFI (black circle) are indicated. Bold line represents the 10 m isobath. Instant wind magnitude and direction are also indicated.

Figure 37: Same as Figure 33, but for case study 2.

Case study 3: The influence of E/NE winds

Finally, the case study 3 occurred from 15/11/2008 to 06/12/2008. Intense E/NE winds prevailed between 2 CTWs that propagated equatorward from the RS coast. The first CTW was responsible for an increase of 15.2 cm in IFI sea level (Figures 38, 39, and 40). During the outflow, intense and persistent E/NE winds took place (Figure 17b), associated with the CTW passage, leading to a 40.8 cm decrease in the subinertial sea level in GB (Figure 38).

Persistent offshore NE winds maintained the sea level close to -27 cm in GB for all experiments (Figure 39). During this period, depth-averaged velocities were wind driven once EXP 1 presented near-zero flow. For EXP 2 and EXP 3, a major recirculation cell was observed between GB2 and GB3 (Figure 39b and c).

Afterwards, NE offshore winds weakened and another CTW took place due to a southern cold front passage. Because of that, the GB subinertial level raised 44 cm in all experiments (Figure 40). At the main channel, velocities ranged from -2 to 4 cm s^{-1} (EXP 1), from -3.5 to 4.5 cm s^{-1} (EXP 2), and from -4 to 6 cm s^{-1} (EXP 3) during the outflow and inflow, respectively.

Figure 41 compares the cumulative volume transport for each experiment along GB1, GB2, and GB3. Along GB1, the volume transport reached values down to 879 m^3 s^{-1} (EXP 1), 900 m^3 s^{-1} (EXP 2), and 919 m^3 s^{-1} during the outflow.

After the first CTW event, intense E/NE winds (onshore and offshore) were responsible for a decrease in the volume transport inflow/outflow by one order of magnitude. The volume transport varied from –100 to +280 m^3 s^{-1} (EXP 1), from –140 to +340 m^3 s^{-1} (EXP 2), and from –140 to +220 m^3 s^{-1} (EXP 3). Finally, E/NE winds weakened and another CTW event occurred. This event was related to a volume transport of approximately +1290 m^3 s^{-1} in both EXP 1 and EXP 2, and +1520 m^3 s^{-1} in EXP 3. The volume transport observed in T_3 was 18% higher compared to EXP 1 and EXP 2 because of an intense SW wind. In other words, an intense SW wind (8.99 m s^{-1}) was responsible for an increase of approximately 230 m^3 s^{-1} in the net volume transport at GB entrance. Moderate E winds, as observed in EXP 2 (Figure 40b), did not cause any change in volume transport, just in local circulation. The direction of the wind tends to be as important as the intensity in order to effectively impact the volume transport in GB.
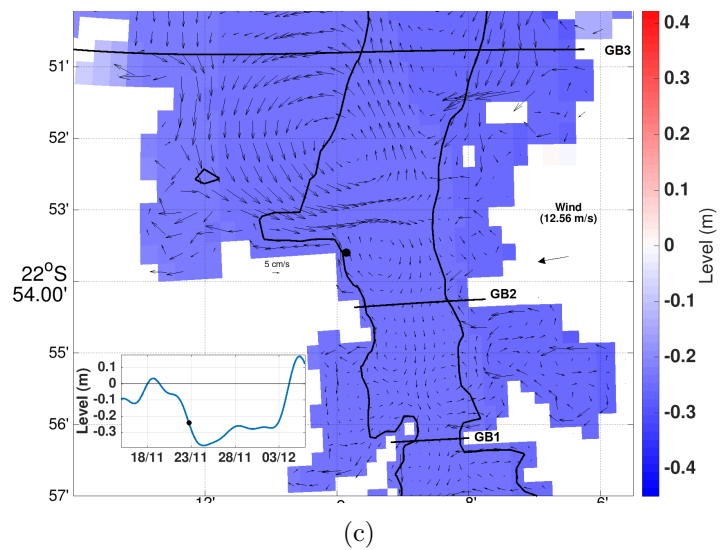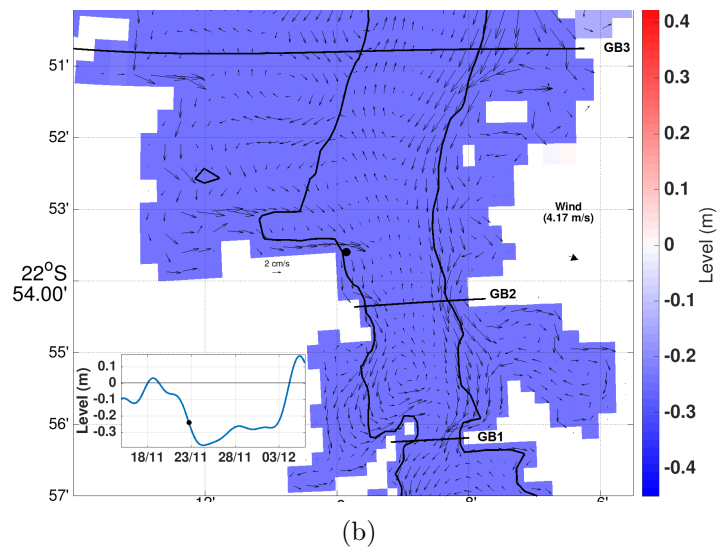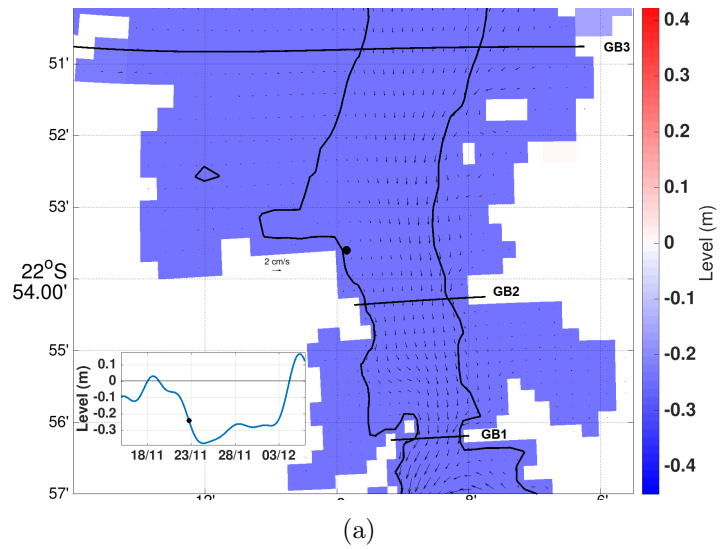
Figure 38: GB depth-averaged velocity and sea level representation for EXP 1 (a), EXP 2 (b), and EXP 3 (c) for T_1 (outflow situation) of case study 3 (black circle on sea level time series). Colorbar represents the sea level and black arrows indicate depth-averaged velocities. Location of sections GB1, GB2 and GB3, and IFI (black circle) are indicated. Bold line represents the 10 m isobath. Instant wind magnitude and direction are also indicated.
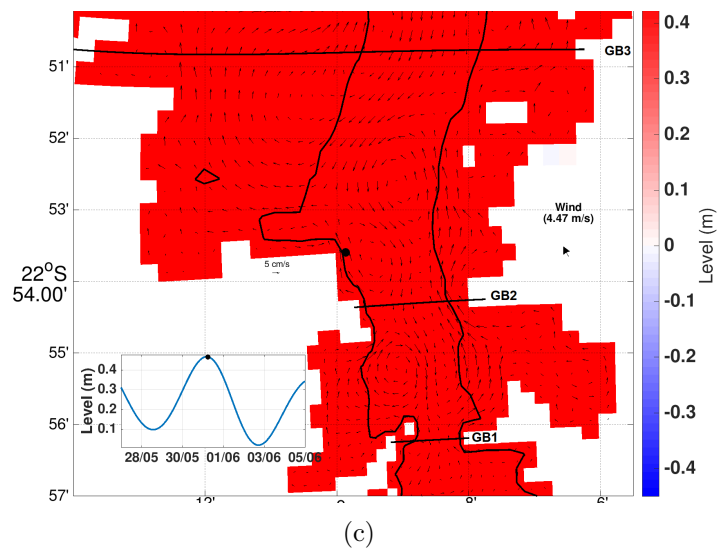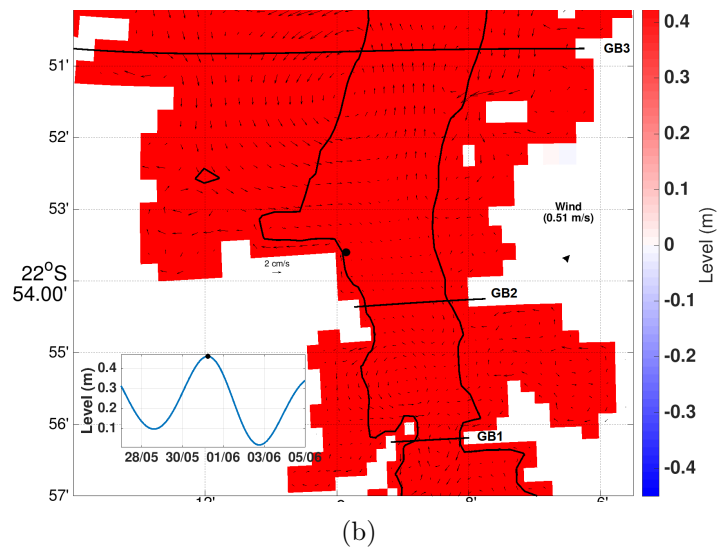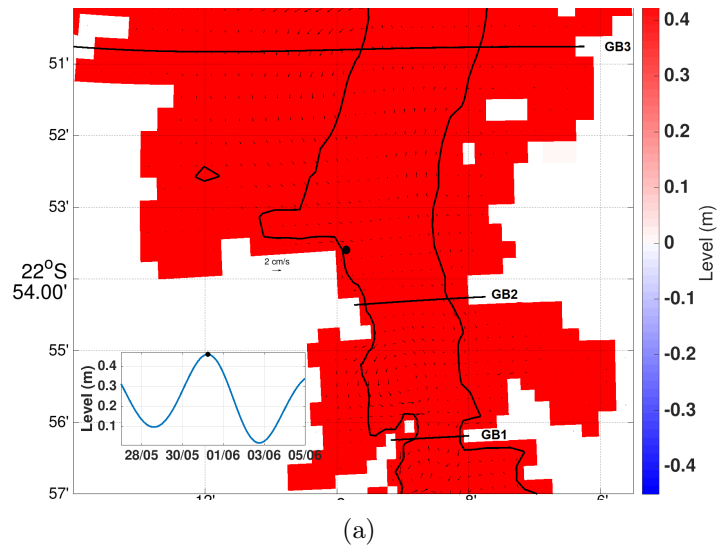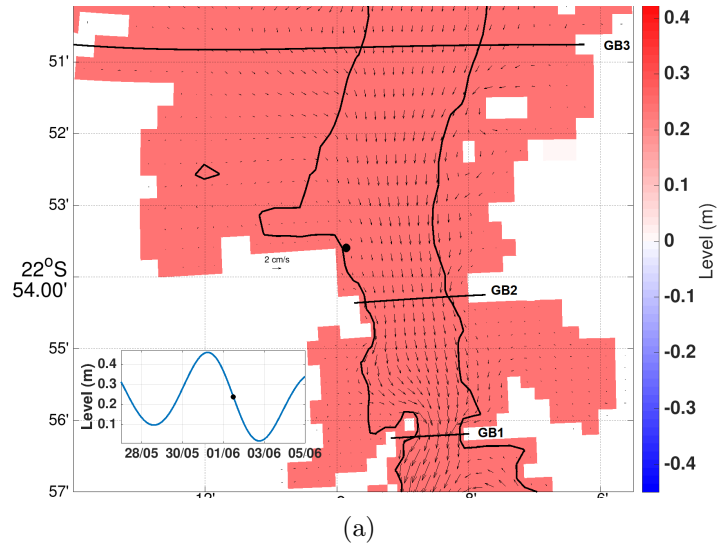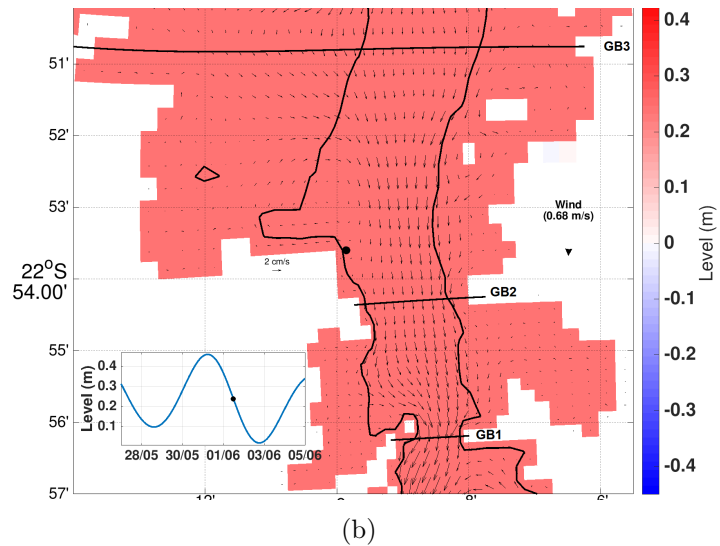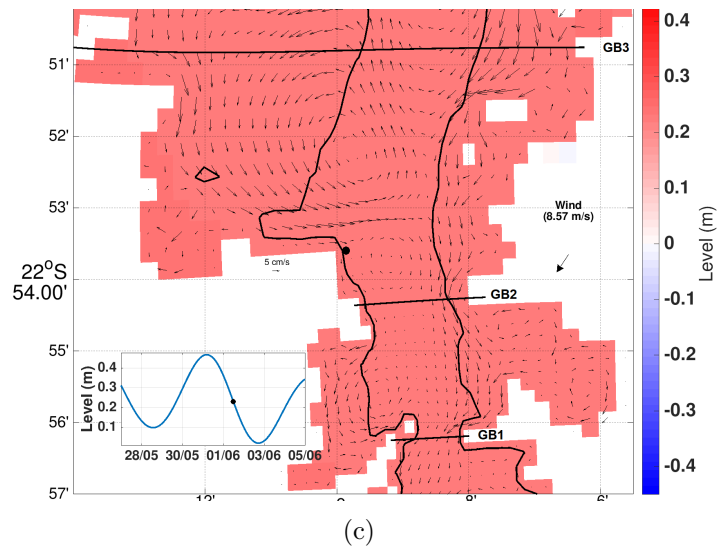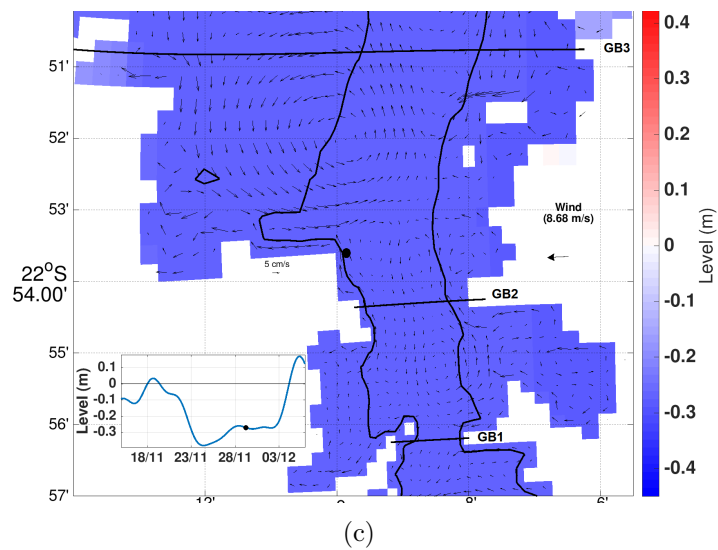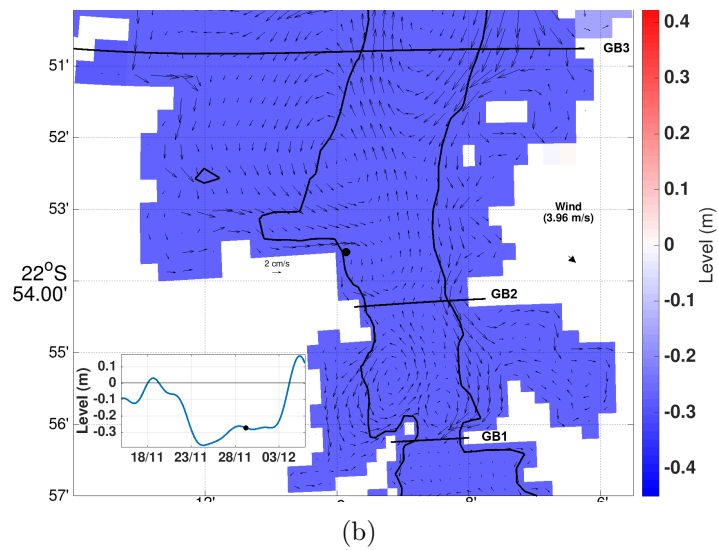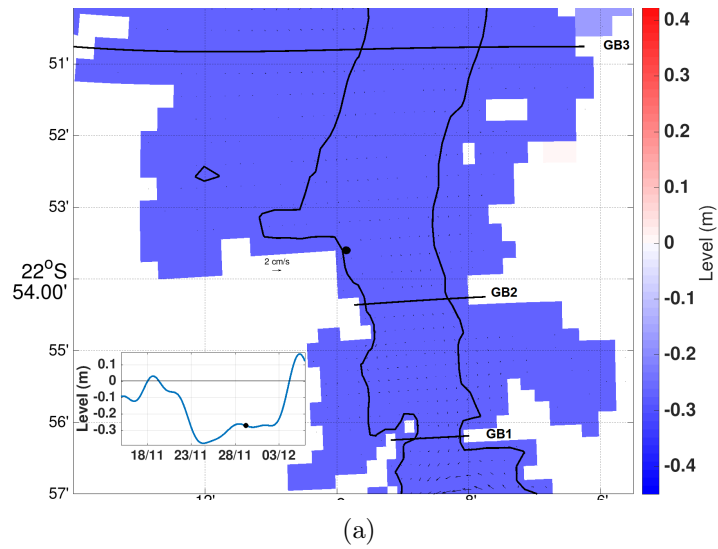
Figure 39: GB depth-averaged velocity and sea level representation for EXP 1 (a), EXP 2 (b), and EXP 3 (c) for T_2 (low sea level situation) of case study 3 (black circle on sea level time series). Colorbar represents the sea level and black arrows indicate depth-averaged velocities. Location of sections GB1, GB2 and GB3, and IFI (black circle) are indicated. Bold line represents the 10 m isobath. Instant wind magnitude and direction are also indicated.
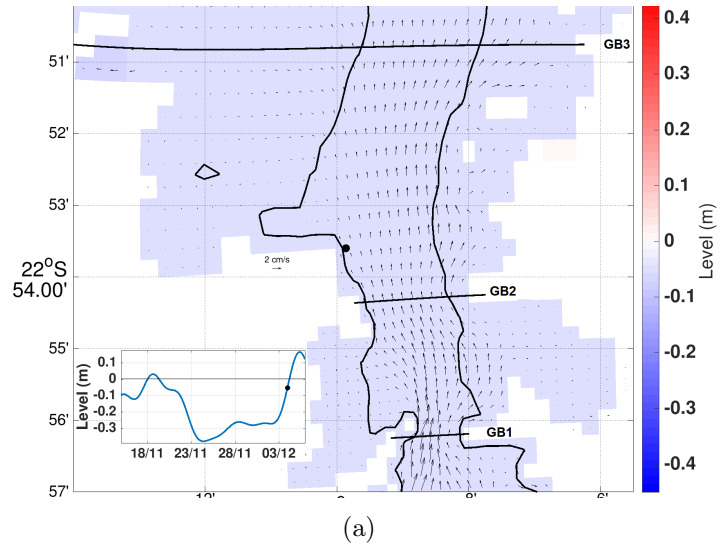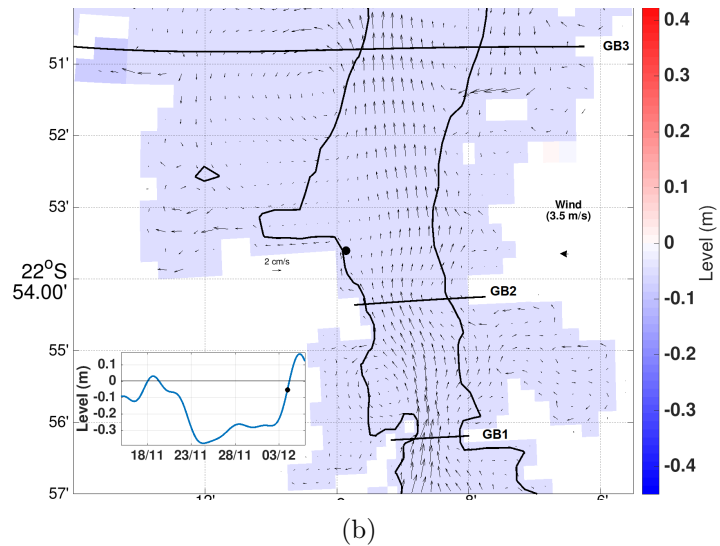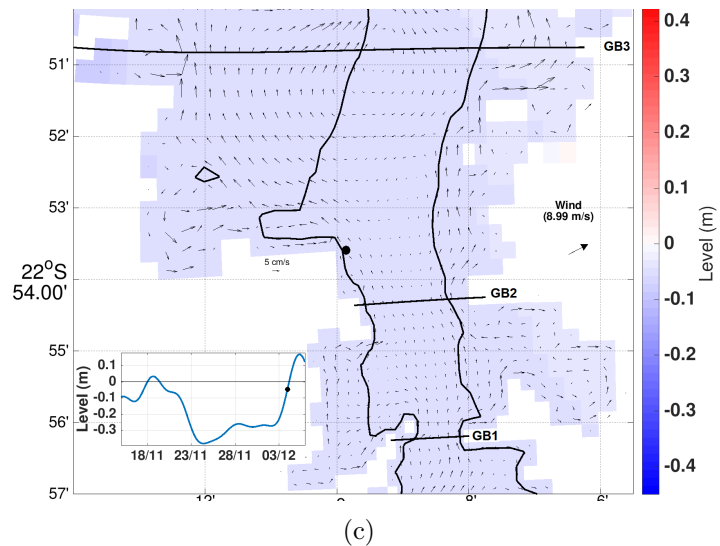
Figure 40: GB depth-averaged velocity and sea level representation for EXP 1 (a), EXP 2 (b), and EXP 3 (c) for T_3 (inflow situation) of case study 3 (black circle on sea level time series). Colorbar represents the sea level and black arrows indicate depth-averaged velocities. Location of sections GB1, GB2 and GB3, and IFI (black circle) are indicated. Bold line represents the 10 m isobath. Instant wind magnitude and direction are also indicated.
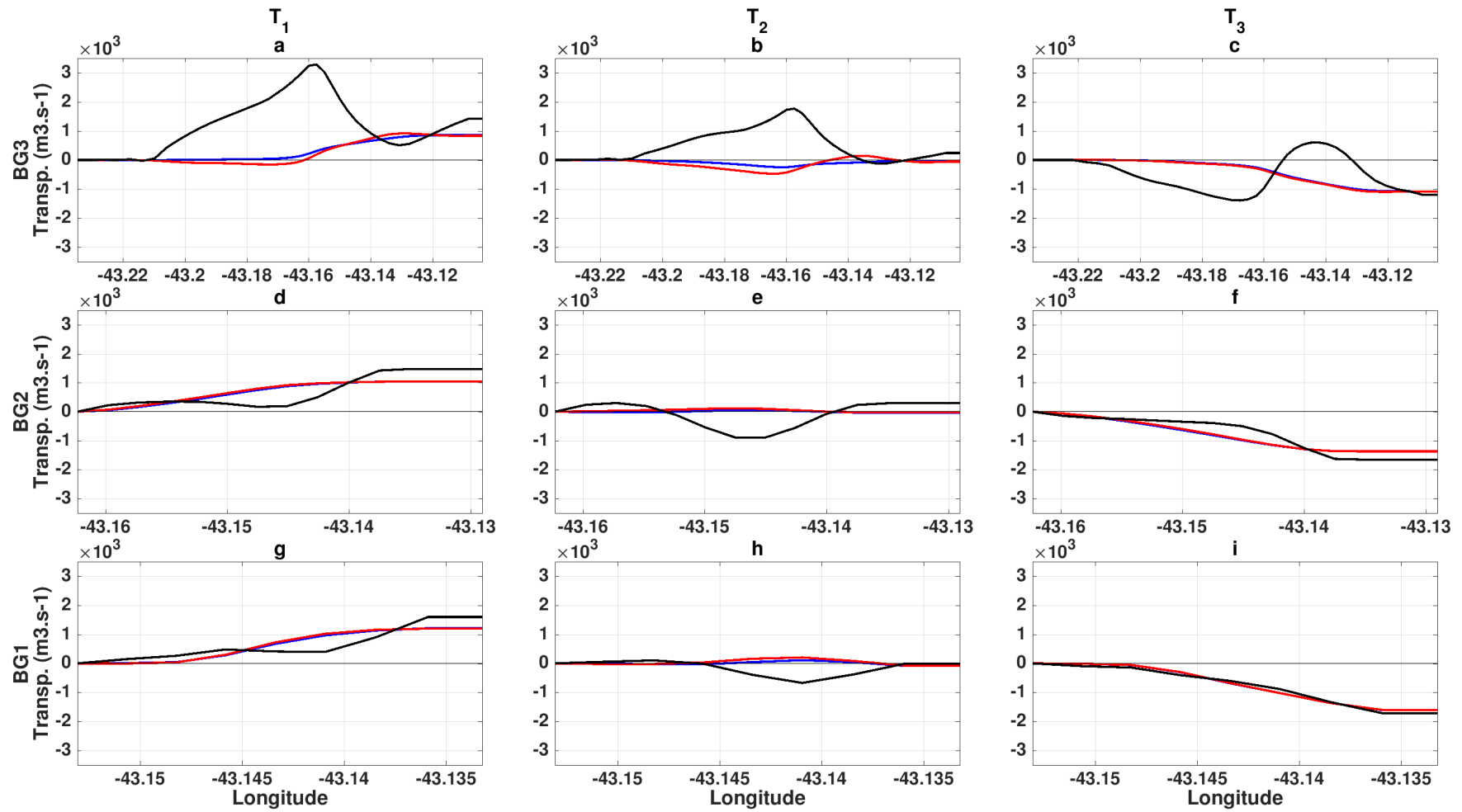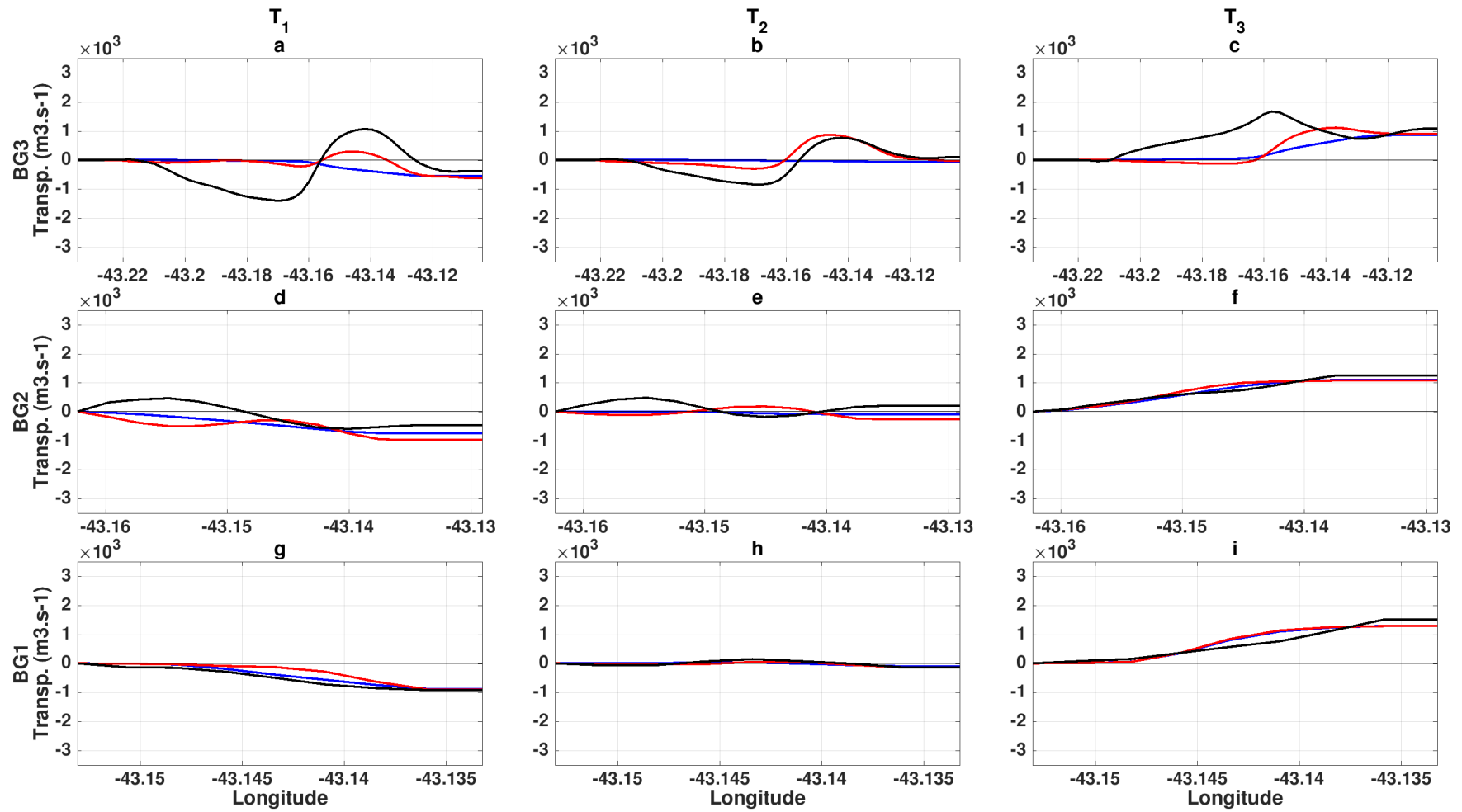
Figure 41: Same as Figure 33, but for case study 3.

Chapter 4

Conclusions

The present study accomplished its main goal of defining the main driving mechanisms of subinertial dynamics in GB. All proposed mechanisms were proved to be important processes in driving the local subinertial dynamics. CTWs have an important impact on GB subinertial dynamics in terms of sea level variability. The CTW events exhibited a mean observed variation of 27.8 ± 11.2 cm, with a mean period of 6.82 ± 2.85 days. Isolated CTW events were responsible for up to 67.2 cm sea level variation at Ilha Fiscal station. A link between CTW and remote winds were confirmed and the higher correlation between alongshore wind and GB sea level in the subinertial band was found on the coast of RS. The year of 2007 was the year with more cold front days on the coast of RS and also the one with more CTWs observed in GB. In addition, 2010 was the year where more extreme CTW events occurred in GB.

The use of altimetry data combined with *in situ* measurements allowed a better understanding of BC influence on GB subinertial dynamics. Most of the energy of BC volume transport was concentrated on low-frequency events ($\geq$ 60-day period). Overall, a greater correlation between BC volume transport with IFI subinertial sea level was found in the $\geq$ 60-day period band (0.31) compared to subinertial band (0.21). A lower correlation was found in 2010 compared to other years. On the other hand, 2010 was the year with most extreme CTW events. Therefore, it reinforces the fact that GB has different forcing mechanisms influencing its subinertial sea level. In this particularly year, remote winds (extreme CTW events) were the main forcing mechanism influencing GB subinertial dynamics, rather than the WBC variability.

Remote winds forced CTWs and BC are the most important forcing mechanisms driving the subinertial sea level variability in GB. Local winds also play an important role, where the correlation with subinertial sea level is comparable to remote wind components. The correlation of local winds intensity for both alongshore and cross-shore wind components with IFI sea level exhibited similar values, suggesting that Ekman transport and local wind setup have similar impacts on IFI subinertial sea level. The cross-shore wind component caused a more rapid response in subinertial sea level, while the alongshore wind component caused an impact in

IFI subinertial sea level in a slower response time.

DELFT3D model successfully reproduced the subinertial variability in GB in terms of subinertial sea level. However, a special attention needs to be made for the velocity field in terms of improving its observational data and boundary conditions. A continuously *in situ* velocity timeseries, acquired in the same period of the sea level data, allows a model velocities validation. Thus, a more robust validation of model results could be accomplished.

Even thought, velocity data was not extensively used to evaluate DELFT3D performance, it is possible to state that the volume transport along the bay exhibited a considerable intensity compared to that in Todos os Santos Bay, which is almost 5 times larger than GB, but approximately 2 times greater in terms of subinertial volume transport. The SBB shape in the northern portion also acts on diminish CTW propagation towards Todos os Santos Bay. Also, the volume transport in EXP 1, EXP 2, and EXP 3 were between 6.1 and 10.8%, 6.1 and 10.8%, and 6.9 and 12.2%, respectively, the value of the tide influence in GB, at spring tide conditions, which highlights the importance of subinertial processes in GB dynamics.

In all the three experiments, subinertial events propagated almost instantly in the entire bay in terms of sea level. In other words, subinertial water sea level along GB oscillates in a similar phase throughout the entire bay.

Among all the three experiments, the one without the effect of local winds showed a more well-behaved velocity pattern, where greater intensity flows occurred along the main channel. In shallower areas, the flow decreased significantly. Recirculation cells were observed only when the flow reversed.

Experiments 2 and 3 highlighted the importance of local wind for the subinertial velocity field. The flow exhibited more recirculation cells in shallower areas. EXP 3 demonstrates the importance of offshore winds in driving volume transport. Even thought, the velocity field inside the bay intensified, with excessively recirculation cells, offshore winds greatly contributed to volume transport close to the GB entrance. In addition, local SW winds established intense velocities along the eastern margin of the bay, while SE winds did not intensify currents in the western margin of GB.

The present study contributed to build up the knowledge about GB subinertial dynamics, however more initiatives have to be made to achieve a better understanding of GB low-frequency events. Furthermore, both Ekman transport and wind setup influence on GB subinertial dynamics deserve to be topic of a more engaged discussion. This thesis also contributed to the understanding of how BC influences GB dynamics. However, more studies should address the influence of WBC on coastal subinertial dynamics. A first proposition would be to analyze BC volume transport variability in the light of boundary condition data (REMO product, in

this case). In other words, an understanding of how REMO products represent the BC would enhance the discussion on this topic, because it would be possible to compare the modeled BC transport variability to the modeled GB subinertial sea level. Finally, further analysis should be made regarding the relation between ENSO events and extreme cold fronts in the southern Brazil, and consequently, the number and intensity of CTW that propagates towards the SBB.

Reference List

[1] ABREU, I. M., CORDEIRO, R. C., SOARES-GOMES, A., et al., 2016, "Ecological risk evaluation of sediment metals in a tropical Euthrophic Bay, Guanabara Bay, Southeast Atlantic", *Marine pollution bulletin*, v. 109, n. 1, pp. 435–445.

[2] AGUIAR, A., VALLE-LEVINSON, A., CIRANO, M., et al., 2019, "Ocean-estuary exchange variability in a large tropical estuary", *Continental Shelf Research*, v. 172, pp. 33–49.

[3] AMADOR, E. D. S., 1997, "Baía de Guanabara e ecossistemas periféricos: homem e natureza", *Edição do Autor, Rio de Janeiro*, p. 539.

[4] AZEVEDO, A., CARVALHO, R., KAJIN, M., et al., 2017, "The first confirmed decline of a delphinid population from Brazilian waters: 2000–2015 abundance of Sotalia guianensis in Guanabara Bay, south-eastern Brazil", *Ecological indicators*, v. 79, pp. 1–10.

[5] BÉRGAMO, A. L., 2006, *Características hidrográficas, da circulação e dos transportes de volume e sal na Baía de Guanabara (RJ): variações sazonais e moduladas pela maré.* Tese de Doutorado, Universidade de São Paulo.

[6] BILÓ, T. C., DA SILVEIRA, I. C. A., BELO, W. C., et al., 2014, "Methods for estimating the velocities of the Brazil Current in the pre-salt reservoir area off southeast Brazil (23°S–26°S)", *Ocean Dynamics*, v. 64, n. 10, pp. 1431–1446.

[7] BITTENCOURT, L., LIMA, I. M., ANDRADE, L. G., et al., 2017, "Underwater noise in an impacted environment can affect Guiana dolphin communication", *Marine pollution bulletin*, v. 114, n. 2, pp. 1130–1134.

[8] BOM, B. O. M., 2020. "Australian climate influences timeline: El Niño and La Niña events". `http://www.bom.gov.au/climate/influences/timeline/`. [Online; accessed 15-January-2020].

[9] BRAGA, C. Z. F., SETZER, A. W., DE LACERDA, L. D., 1993, "Water quality assessment with simultaneous Landsat-5 TM data at Guanabara Bay, Rio de Janeiro, Brazil", *Remote Sensing of Environment*, v. 45, n. 1, pp. 95–106.

[10] BRINK, K., 1991, "Coastal-trapped waves and wind-driven currents over the continental shelf", *Annual Review of Fluid Mechanics*, v. 23, n. 1, pp. 389–412.

[11] CAMARGO, M. Z., SANDRINI-NETO, L., CARREIRA, R. S., et al., 2017, "Effects of hydrocarbon pollution in the structure of macrobenthic assemblages from two large estuaries in Brazil", *Marine pollution bulletin*, v. 125, n. 1-2, pp. 66–76.

[12] CAMPOS, R. M., DE CAMARGO, R., HARARI, J., 2010, "Caracterização de eventos extremos do nível do mar em Santos e sua correspondência com as re-análises do modelo do NCEP no Sudoeste do Atlântico Sul", *Revista Brasileira de Meteorologia*, v. 25, n. 2.

[13] CASTRO, B. M., LEE, T. N., 1995, "Wind-forced sea level variability on the southeast Brazilian shelf", *Journal of Geophysical Research*, v. 100, n. C8 (aug), pp. 16045–16056.

[14] CASTRO, B. M., 1990, "Wind driven currents in the Channel of São Sebastião:winter, 1979", *Boletim do Instituto Oceanografico, USP*, v. 38, n. 2, pp. 111–132.

[15] CASTRO, B. D., MIRANDA, L. D., 1998, "Physical oceanography of the western Atlantic continental shelf located between 4°N and 34°S", *The sea*, v. 11, n. 1, pp. 209–251.

[16] CASTRO, B. D., LORENZZETTI, J., SILVEIRA, I. D., et al., 2006, "Estrutura termohalina e circulação na região entre o Cabo de São Tomé (RJ) e o Chuí (RS)". In: *O ambiente oceanográfico da plataforma continental e do talude na região sudeste-sul do Brasil*, Edusp São Paulo, pp. 11–120.

[17] CASTRO, M. S., BONECKER, A. C. T., VALENTIN, J. L., 2005, "Seasonal variation in Fish Larvae at entrance of Guanabara Bay, Brazil", *Brazilian Archives of Biology and Technology*, v. 48, pp. 121–128.

[18] CASTRO FILHO, B. M. D., 1997, *Correntes e massas de água da plataforma continental norte de São Paulo*. Tese de Doutorado, Universidade de São Paulo.

[19] CERDA, C., CASTRO, B. M., 2014, "Hydrographic climatology of South Brazil Bight shelf waters between São Sebastião (24°S) and Cabo São Tomé (22°S)", *Continental Shelf Research*, v. 89, pp. 5–14.

[20] CIRANO, M., LESSA, G. C., 2007, "Oceanographic characteristics of Baía de Todos os Santos, Brazil", *Revista Brasileira de Geofísica*, v. 25, n. 4, pp. 363–387.

[21] CLIMATEMPO, 2018. "Chuva forte se espalha pelo RJ". `https://www.climatempo.com.br/noticia/2018/02/21/chuva-forte-se-espalha-sobre-o-rj-7167`. [Online; accessed 27-October-2019].

[22] CORRÊA, B., VIANNA, M., 2016, "Spatial and temporal distribution patterns of the silver mojarra Eucinostomus argenteus (Perciformes: Gerreidae) in a tropical semi-enclosed bay", *Journal of fish biology*, v. 89, n. 1, pp. 641–660.

[23] D. M. HOLLAND, T. W., 1994, "The effects of stratification and alongshore currents on the propagation of coastal-trapped waves", *Continental Shelf Research*, v. 14, n. 1, pp. 57–77.

[24] DA SILVA, A. M., YOUNG, C. C., LEVITUS, S., 1994, "Atlas of surface marine data 1994, vol. 3, Anomalies of heat and momentum fluxes", *NOAA Atlas NESDIS*, v. 8, pp. 413.

[25] DA SILVA JR, D., PARANHOS, R., VIANNA, M., 2016, "Spatial patterns of distribution and the influence of seasonal and abiotic factors on demersal ichthyofauna in an estuarine tropical bay", *Journal of fish biology*, v. 89, n. 1, pp. 821–846.

[26] DA SILVEIRA, I., LIMA, J., SCHMIDT, A., et al., 2008, "Is the meander growth in the Brazil Current system off Southeast Brazil due to baroclinic instability?" *Dynamics of Atmospheres and Oceans*, v. 45, n. 3-4, pp. 187–207.

[27] DE AZEREDO, V. M., 2017, *IMPACTOS DO EL NIÑO 1997/1998 SOBRE A DINÂMICA DA CORRENTE DO BRASIL*. Tese de Mestrado, Universidade Federal do Rio de Janeiro.

[28] DE CARVALHO, D. G., NETO, J. A. B., 2016, "Microplastic pollution of the beaches of Guanabara Bay, Southeast Brazil", *Ocean & coastal management*, v. 128, pp. 10–17.

[29] DE FREITAS, P. P., AMORIM, F. D. L. L., MILL, G. N., et al., 2019, "Observations of near-inertial oscillations along the Brazilian continental shelf break", *Ocean Dynamics*, v. 69, n. 10, pp. 1203–1215.

[30] DE SOUZA, V. F., 2013, *Modelagem numérica da hidrodinâmica e do transporte de sedimentos no Porto do Rio de Janeiro*. Tese de Doutorado, Instituto Militar de Engenharia.

[31] DELFT-FLOW, 2014. "Delft3D-FLOW User Manual v3.15.34158". .

[32] DOMINGUES, R., GONI, G., BARINGER, M., et al., 2018, "What caused the accelerated sea level changes along the US East Coast during 2010–2015?" *Geophysical Research Letters*, v. 45, n. 24, pp. 13–367.

[33] DOS SANTOS, R. T. F., 2017, *Efeitos da subida do nível do mar na inundação costeira na costa leste do Brasil devido às mudanças climáticas*. Tese de Doutorado, Universidade Federal do Rio de Janeiro.

[34] DOTTORI, M., CASTRO, B. M., 2009, "The response of the Sao Paulo Continental Shelf, Brazil, to synoptic winds", *Ocean Dynamics*, v. 59, pp. 603–614.

[35] DOTTORI, M., CASTRO, B. M., 2018, "The role of remote wind forcing in the subinertial current variability in the central and northern parts of the South Brazil Bight", *Ocean Dynamics*, v. 68, n. 6, pp. 677–688.

[36] DRAP, 2018. "Histórico de cargas anual 2008-2014. Porto do Rio". http://www.portosrio.gov.br/downloads/files/estatistica/histórico_de_cargas_anual_2008_a_2014_-_porto_do_rio.pdf, . [Online; accessed 05-March-2018].

[37] DRAP, 2018. "Histórico de Cargas anual 2008-2014. Porto de Niterói". http://www.portosrio.gov.br/downloads/files/estatistica/histórico_de_cargas_anual_2008_a_2014_-_porto_de_niterói.pdf, . [Online; accessed 05-March-2018].

[38] DRAP, 2018. "Histórico de passageiros anual 2008-2014. Porto do Rio". http://www.portosrio.gov.br/downloads/files/estatistica/histórico_passageiros_anual_2008_a_2014_-_porto_do_rio.pdf, . [Online; accessed 05-March-2018].

[39] EICHLER, B. B., EICHLER, P. B., DE MIRANDA, L. B., et al., 2001, "Utilização de foraminíferos como indicadores da influência marinha na Baía de Guanabara, RJ, Brasil", *Pesquisas em Geociências*, v. 28, n. 2, pp. 251–262.

[40] EICHLER, P. P., EICHLER, B. B., DE MIRANDA, L. B., et al., 2003, "Benthic foraminiferal response to variations in temperature, salinity, dissolved

oxygen and organic carbon, in the Guanabara Bay, Rio de Janeiro, Brazil", *Anuário do Instituto de Geociências*, v. 26, pp. 36–51.

[41] EZER, T., 2015, "Detecting changes in the transport of the Gulf Stream and the Atlantic overturning circulation from coastal sea level data: The extreme decline in 2009–2010 and estimated variations for 1935–2012", *Global and Planetary Change*, v. 129, pp. 23–36.

[42] EZER, T., 2016, "Can the Gulf Stream induce coherent short-term fluctuations in sea level along the US East Coast? A modeling study", *Ocean Dynamics*, v. 66, n. 2, pp. 207–220.

[43] EZER, T., ATKINSON, L. P., CORLETT, W. B., et al., 2013, "Gulf Stream's induced sea level rise and variability along the US mid-Atlantic coast", *Journal of Geophysical Research: Oceans*, v. 118, n. 2, pp. 685–697.

[44] FILIPPO, A., KJERFVE, B., JÚNIOR, A. R. T., et al., 2012, "Low-frequency variability of sea level along the Mid-Atlantic Coast of South America, in 1983", *Brazilian Journal of Geophysics*, v. 30, n. 1.

[45] FILIPPO, A., 1997, *Passagem de frentes frias na Baía de Guanabara: impacto no nível do mar.* Tese de Mestrado, Departamento de Geoquimica, Universidade Federal Fluminense.

[46] FISTAROL, G. O., COUTINHO, F. H., MOREIRA, A. P. B., et al., 2015, "Environmental and sanitary conditions of Guanabara Bay, Rio de Janeiro", *Frontiers in microbiology*, v. 6, pp. 1232.

[47] FONSECA, E., NETO, J. B., SILVA, C., et al., 2013, "Stormwater impact in Guanabara Bay (Rio de Janeiro): evidences of seasonal variability in the dynamic of the sediment heavy metals", *Estuarine, Coastal and Shelf Science*, v. 130, pp. 161–168.

[48] FRANZ, B., 2011, "O lixo flutuante em regiões metropolitanas costeiras no âmbito de políticas públicas: o caso da cidade do Rio de Janeiro", *Rio de Janeiro*.

[49] FRANÇA, B. R. L., 2013, *ONDAS CONFINADAS COSTEIRAS NA PLATAFORMA CONTINENTAL SUL-SUDESTE DO BRASIL.* Tese de Mestrado, Ocean Engineering (COPPE), Universidade Federal do Rio de Janeiro.

[50] GABIOUX, M. G., DA COSTA, V. S., DE SOUZA, J. M. A. C., et al., 2013, "Modeling the South Atlantic Ocean from medium to high-resolution", *Brazilian Journal of Geophysics*, v. 31, n. 2, pp. 229–242.

[51] GILL, A., SCHUMANN, E., 1974, "The generation of long shelf waves by the wind", *Journal of Physical Oceanography*, v. 4, n. 1, pp. 83–90.

[52] GODDARD, P. B., YIN, J., GRIFFIES, S. M., et al., 2015, "An extreme event of sea-level rise along the Northeast coast of North America in 2009–2010", *Nature Communications*, v. 6, pp. 6346.

[53] GOES, M., CIRANO, M., MATA, M., et al., 2019, "Long-Term Monitoring of the Brazil Current Transport at 22°S From XBT and Altimetry Data: Seasonal, Interannual, and Extreme Variability", *Journal of Geophysical Research: Oceans*.

[54] GUENTHER, M., PARANHOS, R., REZENDE, C. E., et al., 2008, "Dynamics of bacterial carbon metabolism at the entrance of a tropical eutrophic bay influenced by tidal oscillation", *Aquatic Microbial Ecology*, v. 50, n. 2, pp. 123–133.

[55] HALLIWELL, G. R., 2004, "Evaluation of vertical coordinate and vertical mixing algorithms in the HYbrid-Coordinate Ocean Model (HYCOM)", *Ocean Modelling*, v. 7, n. 3-4, pp. 285–322.

[56] HUTHNANCE, J. M., 1995, "Circulation, exchange and water masses at the ocean margin: the role of physical processes at the shelf edge", *Progress in Oceanography*, v. 35, n. 4, pp. 353–431.

[57] JACINTO, L. D. F. R., 2018, *Descrição observacional de variáveis meteorológicas no município do Rio de Janeiro durante a passagem de sistemas frontais.* Tese de Mestrado, Instituto de Geociencias, Universidade Federal do Rio de Janeiro.

[58] JICA, 1994, *The study on recuperation of the Guanabara Bay ecosystem.* Japan International Cooperation Agency : Kokusai Kogyo Co., Ltd.

[59] JUNIOR, A. N. M., CRAPEZ, M. A. C., BARBOZA, C. D. N., 2006, "Impact of the Icaraí Sewage Outfall in Guanabara Bay, Brazil", *Brazilian Archives of Biology and Technology*, v. 49, pp. 643–660.

[60] JUNIOR, A. R. T., 2005, *Estudo numérico sobre tele-conexão atmosférica entre fenômenos oceânicos do Pacífico Equatorial e do Atlântico Sul.* Tese de Doutorado, PENO, UFRJ.

[61] KAUFMANN, C., 2009, *Estudo hidrodinâmico e de qualidade de água após revitalização do canal do fundão, Baía de Guanabara–RJ*. Tese de Doutorado, Tese de M. Sc.(Abril), COPPE/UFRJ, Rio de Janeiro, RJ, Brasil.

[62] KJERFVE, B., DE LACERDA, L. D., DIAS, G., 2001, "Baía de Guanabara, Rio de Janeiro, Brazil". In: *Coastal marine ecosystems of Latin America*, Springer, pp. 107–117.

[63] KJERFVE, B., RIBEIRO, C. H., DIAS, G. T., et al., 1997, "Oceanographic characteristics of an impacted coastal bay: Baía de Guanabara, Rio de Janeiro, Brazil", *Continental shelf research*, v. 17, n. 13, pp. 1609–1643.

[64] LETH, O., MIDDLETON, J. F., 2004, "A mechanism for enhanced upwelling off central Chile: Eddy advection", *Journal of Geophysical Research: Oceans*, v. 109, n. C12.

[65] LIMA, J. A. M., MARTINS, R. P., TANAJURA, C. A. S., et al., 2013, "Design and implementation of the Oceanographic Modeling and Observation Network (REMO) for operational oceanography and ocean forecasting", *Brazilian Journal of Geophysics*, v. 31, n. 2, pp. 210–228.

[66] LIMA, M. O., CIRANO, M., MATA, M. M., et al., 2016, "An assessment of the Brazil Current baroclinic structure and variability near 22°S in Distinct Ocean Forecasting and Analysis Systems", *Ocean Dynamics*, v. 66, n. 6-7, pp. 893–916.

[67] LOTO, L., MONTEIRO-NETO, C., MARTINS, R. R. M., et al., 2018, "Temporal changes of a coastal small-scale fishery system within a tropical metropolitan city", *Ocean & Coastal Management*, v. 153, pp. 203–214.

[68] MORAES, M. C. M., LAVRADO, H. P., 2017, "Distribution of loliginid squids in a eutrophicated tropical coastal bay", *Marine Biology Research*, v. 13, n. 3, pp. 330–341.

[69] MUSCARELLA, P., BARTON, N., LIPPHARDT JR, B., et al., 2011, "Surface currents and winds at the Delaware Bay mouth", *Continental Shelf Research*, v. 31, n. 12, pp. 1282–1293.

[70] NETO, J. A. B., DA FONSECA, E. M., 2011, "Variação sazonal, espacial e composicional de lixo ao longo das praias da margem oriental da Baía de Guanabara (Rio de Janeiro) no período de 1999-2008", *Revista de Gestão Costeira Integrada-Journal of Integrated Coastal Zone Management*, v. 11, n. 1, pp. 31–39.

[71] NEVES, R., ECHEVERRIA, C., PESSOA, L., et al., 2013, "Factors influencing spatial patterns of molluscs in a eutrophic tropical bay", *Journal of the Marine Biological Association of the United Kingdom*, v. 93, n. 3, pp. 577–589.

[72] OLIVEIRA, E. N., FERNANDES, A. M., KAMPEL, M., et al., 2016, "Assessment of remotely sensed chlorophyll-a concentration in Guanabara Bay, Brazil", *Journal of Applied Remote Sensing*, v. 10, n. 2, pp. 026003.

[73] OLIVEIRA, M., EBECKEN, F., NEVES, C. F., et al., 2006, "Coastal sea level response associated with frontal systems using conventional and NCEP/NCAR reanalysis data, a case study: Paranaguá Bay, Brazil". In: *Proceedings of*, v. 8, pp. 1883–1895.

[74] PEREIRA, J., CIRANO, M., ALMEIDA, M. M., et al., 2013, "A REGIONAL STUDY OF THE BRAZILIAN SHELF/SLOPE CIRCULATION (13°–31°S) USING CLIMATOLOGICAL OPEN BOUNDARIES", *Brazilian Journal of Geophysics*, v. 31, n. 2, pp. 289–306.

[75] PIMENTEL, L. C. G., MARTON, E., SOARES, M., et al., 2014, "Caracterização do regime de vento em superfície na Região Metropolitana do Rio de Janeiro", *Engenharia Sanitaria e Ambiental*, v. 19, n. 2.

[76] PIOLA, A. R., CAMPOS, E. J., MÖLLER JR, O. O., et al., 2000, "Subtropical shelf front off eastern South America", *Journal of Geophysical Research: Oceans*, v. 105, n. C3, pp. 6565–6578.

[77] PIOLA, A. R., MATANO, R. P., PALMA, E. D., et al., 2005, "The influence of the Plata River discharge on the western South Atlantic shelf", *Geophysical Research Letters*, v. 32, n. 1.

[78] PONTE, R. M., CARSON, M., CIRANO, M., et al., 2019, "Towards comprehensive observing and modeling systems for monitoring and predicting regional to coastal sea level", *Frontiers in Marine Science*, v. 6, n. 437.

[79] PUGH, D., WOODWORTH, P., 2014, *Sea-level science: understanding tides, surges, tsunamis and mean sea-level changes.* Cambridge University Press.

[80] REMO, 2016. "Base Hidrodinâmica para a METAREA V - B_H_MV.1: Rede de Modelagem e Observação Oceanográfica (REMO)". .

[81] RODEN, G. I., ROSSBY, H. T., 1999, "Early Swedish contribution to oceanography: Nils Gissler (1715–71) and the inverted barometer effect", *Bulletin of the American Meteorological Society*, v. 80, n. 4, pp. 675–682.

[82] ROSSO, T., 1997, *Modelo hidrodinâmico para o transporte de manchas de óleo em regiões costeiras.* Tese de Doutorado, COPPE/UFRJ, Rio de Janeiro, RJ, Brasil.

[83] S. ILLIG, E. CADIER, M. L. B. M. K., 2018, "Subseasonal Coastal-Trapped Wave Propagations in the Southeastern Pacific and Atlantic Oceans: 1. A New Approach to Estimate Wave Amplitude", *Journal of Geophysycal Research: Oceans*, v. 123, pp. 3915–3941.

[84] SAHA, S., MOORTHI, S., PAN, H.-L., et al., 2010. "NCEP Climate Forecast System Reanalysis (CFSR) Selected Hourly Time-Series Products, January 1979 to December 2010". Disponível em: <https://doi.org/10.5065/D6513W89>.

[85] SAMPAIO, M., 2003, "Estudo de Circulação Hidrodinâmica 3D e Trocas de Massas d'Água da Baía de Guanabara–RJ", *UFRJ. Rio de Janeiro.*

[86] SANKARANARAYANAN, S., FRINGER, O. B., 2013, "Dynamics of barotropic low-frequency fluctuations in San Francisco Bay during upwelling", *Continental Shelf Research*, v. 65, pp. 81–96.

[87] SEMADS, 2001, *Bacias Hidrográficas e Rios Fluminenses: Síntese informativa por macrorregião ambiental.* Secretaria de Estado de Meio Ambiente e Desenvolvimento Sustentável do Estado do Rio de Janeiro.

[88] SHAFFER, G., PIZARRO, O., DJURFELDT, L., et al., 1997, "Circulation and low-frequency variability near the Chilean coast: Remotely forced fluctuations during the 1991–92 El Nino", *Journal of Physical Oceanography*, v. 27, n. 2, pp. 217–235.

[89] SOARES-GOMES, A., DA GAMA, B. A. P., NETO, J. B., et al., 2016, "An environmental overview of Guanabara Bay, Rio de Janeiro", *Regional Studies in Marine Science*, v. 8, pp. 319–330.

[90] STECH, J. L., LORENZZETTI, J. A., 1992, "The response of the South Brazil Bight to the passage of wintertime cold fronts", *Journal of Geophysical Research: Oceans*, v. 97, n. C6, pp. 9507–9520.

[91] STEVENSON, M. R., DIAS-BRITO, D., STECH, J. L., et al., 1998, "How do cold water biota arrive in a tropical bay near Rio de Janeiro, Brazil?" *Continental Shelf Research*, v. 18, n. 13, pp. 1595–1612.

[92] SUURSAAR, U., KULLAS, T., 2006, "Influence of wind climate changes on the mean sea level and current regime in the coastal waters of west Estonia, Baltic Sea", *Oceanologia*, v. 48, n. 3.

[93] TODD, R. E., CHAVEZ, F. P., CLAYTON, S., et al., 2019, "Global perspectives on observing ocean boundary current systems", *Frontiers in Marine Science*, v. 6.

[94] TOMCZAK, 2018. "Coastal trapped waves and other oscillations". `https://www.mt-oceanography.info/ShelfCoast/chapter08.html`. [Online; accessed 05-March-2018].

[95] VALENTIM, S. S., BERNARDES, M. E. C., DOTTORI, M., et al., 2013, "Low-frequency physical variations in the coastal zone of Ubatuba, northern coast of São Paulo State, Brazil", *Brazilian Journal of Oceanography*, v. 61, n. 3, pp. 187–193.

[96] VALLE-LEVINSON, A., 1995, "Observations of barotropic and baroclinic exchanges in the lower Chesapeake Bay", *Continental Shelf Research*, v. 15, n. 13, pp. 1631–1647.

[97] VIANA, C. C. G., 2017, *A Assimetria da onda de maré na Baía de Guanabara - RJ.* Tese de Mestrado, Faculdade de Oceanografia, Universidade Estadual do Rio de Janeiro.

[98] WOODWORTH, P. L., MAQUEDA, M. Á. M., ROUSSENOV, V. M., et al., 2014, "Mean sea-level variability along the northeast American Atlantic coast and the roles of the wind and the overturning circulation", *Journal of Geophysical Research: Oceans*, v. 119, n. 12, pp. 8916–8935.

[99] WOODWORTH, P. L., MELET, A., MARCOS, M., et al., 2019, "Forcing factors affecting sea level changes at the coast", *Surveys in Geophysics*, pp. 1–47.

[100] YU, P., MOREY, S. L., O'BRIEN, J. J., 2006, *Development of new techniques for assimilating satellite altimetry data into ocean models.* Florida State University.